Microstructural evolution of iron meteorites

Candidate: Alessandro Colacino, s254227

Relator: Prof. Paolo Matteis

Co-relator: Prof. Giorgio Scavino

INDEX

***«L'acido nitrico distruggendo il lustro ch'era puro effetto dell'arte, mi svelò la tessitura»* - G. Thomson** G.Thomson. *Saggio di G.Thomson sul ferro Malleabile trovato da Pallas in Siberia*. Atti dell'Accademia Delle Scienze di Siena, 1808, Tomo 9, p37

1.INTRODUCTION

1.0 Generalities

The objective of this thesis is to give a panoramic of meteorites and asteroids, to understand the complexity of a pioneering subject with few certainties, since the first witnessed impact scientifically studied dates back in 1751, and to focus on the technical study of iron meteorites and, in particular, on two samples and the experiments done on them.

Meteorites, named after the place of discovery, are the fragments of what remains of meteoroids (small asteroids) after the atmosphere ablation and impact on Earth.

Meteoroids and asteroids come from the Solar system, mainly orbit between Mars and Jupiter and the biggest observed "Cerere" is 1000km in diameter (fig 1).

When the origin is not the Solar System extraterrestrial objects are called "comets".

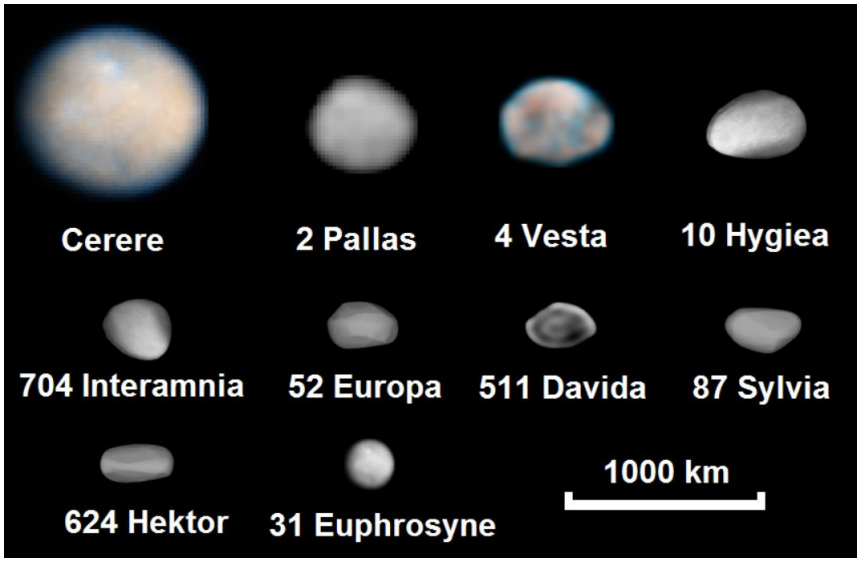

Figure 1 biggest asteroids (17)

The place of discovery may not be the place of impact, the fragments are found in an elliptical surface surrounding the impact point, but from a single meteoroid many fragments already divide in the atmosphere.

In total more than 30.000 fragments were retrieved and ~5.000 impacts were witnessed.

Meteorites can be classified as follows:

Chondrites, stony fragments that didn't undergo a process of fusion and/or differentiation, typical of planets/asteroids: they are most prevalent type, around 85%, of found meteorites and contain all the solar elements except for the volatile ones, and come from cold planetesimal formed from the protoplanetary disc, their age is around 4,6 By, so they date back to the formation of the Solar System.

Achondrites or differentiated meteorites, stony fragment, around 8%, some of them are have been proven to come from Mars and Moon.

Iron meteorites, the main argument of this thesis, are 5% of found fragments, composed of Iron-Nichel (95% total weight).

The iron meteorites have been estimated to come from collapsed protoplanets of relatively small size (~1000km), studying the cooling rates of meteorites of the same chemical group and assuming that the metallic material was at the center of them, like on Earth, and above the fusion temperature (1).

Stony-iron meteorites, 1% of found samples, that can have a metal Fe-Ni matrix and big stony crystals, generally of olivine or other silicates (Pallasites), or a stony silicate matrix with Fe and Ni (Mesosiderites)(2). They probably come from the interface between nucleus and mantle of a theoretical protoplanet.

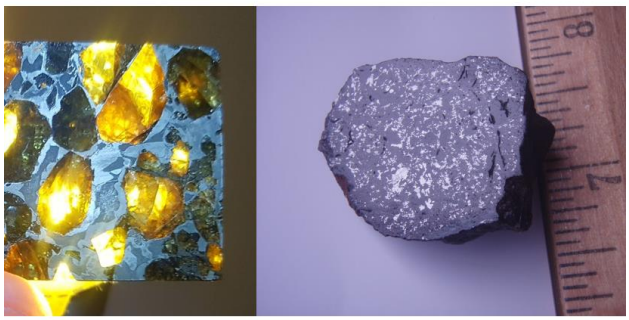

Figure 2 Stony-iron meteorites: pallasite(left) with olivine crystals and a mesosiderite (right)

Figure 3 iron meteorite "Campo del Cielo", London National History Museum, 635kg.

1.1 Iron Meteorites microstructure

This Thesis is about the study of two iron meteorites.

Externally is possible to recognize iron meteorites by their characteristic shape without bubbles, with bevels left from the impact and without sharp edges (see fig. 3).

Iron meteorites must be ferromagnetic.

Thanks to polishing on a plan and exposure to Nital (solution of ethanol and nitric acid), it is possible to see the microstructure of the iron meteorites, mainly composed by Ni and Fe that alloying forms a phase and a metallographic constituent, stable at environment temperatures, named respectively kamacite (ferrite, Ni%=5-7,5), and taenite (Earth environment temperature stabilized austenite, small ferrite lamellae, tetragonal FeNi, Ni%=15-60):

Groups division of iron meteorites by microstructure (3).

- Exaehdrites (H): low Ni, No Widmanstatten Structure, all kamacite.
- Octaehdrites (O): medium-high Ni, Widmanstatten Structure ferrite+taenite (mix of ferrite, retained austenite and other microstructure (e.g. tetragonal FeNi).
- Ataxites (D): High Ni, No Widmanstatten Structure, stabilized austenite with microscopic ferrite lamellae.

Exaehdrites, having a low Ni%, experience a complete nucleation of ferrite alpha at high temperatures.

Octaehdrites are at an intermedium stage and develops kamacite(ferrite) lamellae with band width negatively correlated to Ni%.

Ataxites instead, due to the high Ni%, would have the exsolution of kamacite from taenite at a temperature too low, so ferrite can't nucleate and diffuse on macroscopic level because in order for Ni to diffuse the temperature must be above 500-600° C, it is stabilized austenite. (3)

Ni% is the crucial factor in microstructural development, but not the only one, as will be demonstrated in the next chapters.

1.2-Widmanstatter structure

Octaehdrites are the kind of iron meteorites that shows the W.S. (Widmanstatten Structure), which is believed to form at temperatures of 700°C below the melting temperature for solid diffusion with conditions of extremely slow cooling, that's because in space heat transfer is possible only in the form of irradiation.

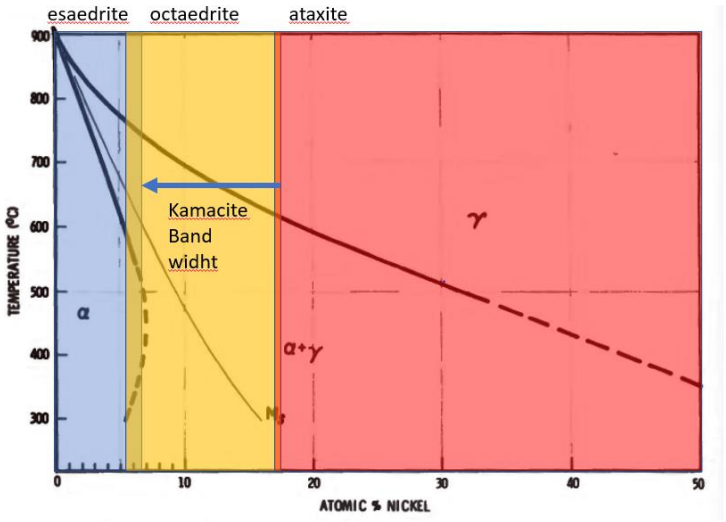

Figure 4 indicative microstructure prediction based on Ni%, shown on a detail of Fe-Ni diagram

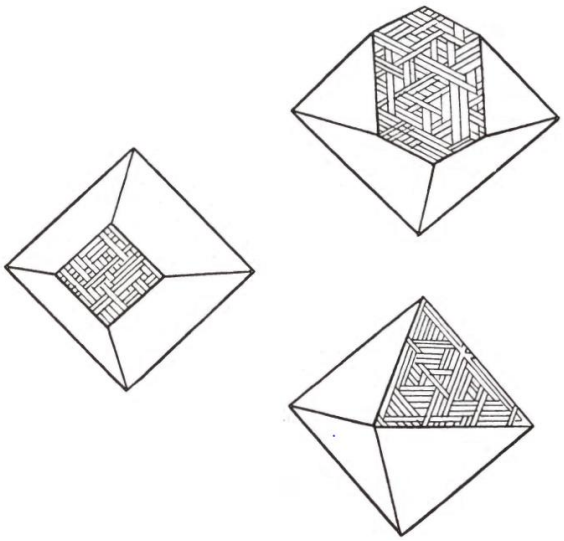

Figure 5 Sketch of W.S. by Tschermak (1894) on cristallographic planes <111>

Octaehdrites form in the range between 5-6 Ni% and 16-18 Ni%

The component of the structure are kamacite (α ferrite) and taenite (various mixture of ferrite and γ austenite); kamacite nucleates around octahedral planes of austenite and it is believed to form around the inclusions first, then along the octahedral planes.

$\{\bar{1}11\}_\gamma \parallel \{110\}_\alpha$ Cristallographic relation between taenite and kamacite in W.S. (Young, 1906).
$[110]_\gamma \parallel [\bar{1}11]_\alpha$

It was possible to obtain the W.S. experimentally with a synthetic solution of Fe-Ni-P, with P at 0,1-0,4%, obtaining kamacite lamellae of 1-10 µm thanks to P, that greatly increases the diffusion coefficient at austenite-ferrite transformation temperature, however it's not possible to artificially obtain a clear phase separation, (16).

Kamacite lamellae in the samples found on Earth have different band widths, we can define the kind of structure as such:

-Plessitic

-Very fine (vfO), b.w<0,2mm

-Fine (fO), 0,2<b.w.<0,5mm

-Medium (mO), 0,5<b.w.<1,3mm

-Coarse (cO), 1,3<b.w.<3,3mm

-Very coarse, b.w.>3,3mm

Plessite is a structure presenting Widmanstatten pattern, but visible at a microscopic level, kamacite lamellae are not fully developed (3).

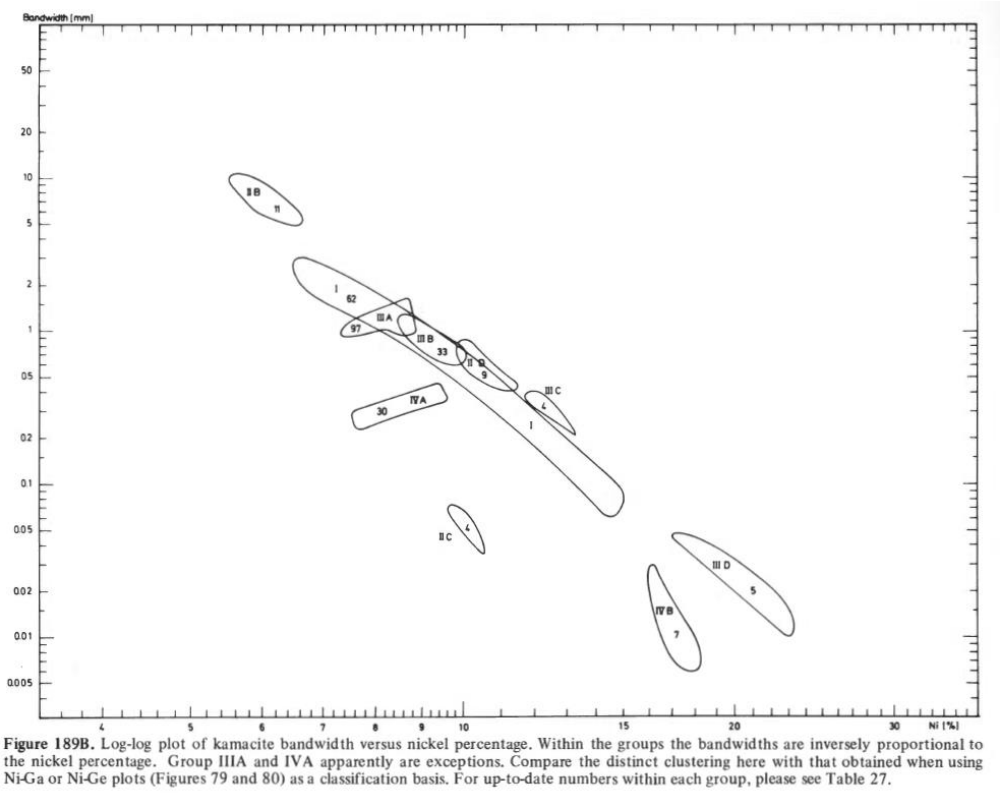

Figure 189B. Log-log plot of kamacite bandwidth versus nickel percentage. Within the groups the bandwidths are inversely proportional to the nickel percentage. Group IIIA and IVA apparently are exceptions. Compare the distinct clustering here with that obtained when using Ni-Ga or Ni-Ge plots (Figures 79 and 80) as a classification basis. For up-to-date numbers within each group, please see Table 27.

Figure 6 relations between kamacite band width, chemical groups and Ni% (3)

1.3 -Composition: main elements.

The main elements of the iron meteorites are:

Fe, composing the main part of the matrix.

Ni, between 5-35%, the avg is 8%, it is very rare to find meteorites with a Ni %>18%, 5 to 7,5% of Ni in kamacite, 25-40% in taenite.

Co, between 0,32 and 1%, average 0,4-0,6%. 0,3% is in solution with kamacite, 0,6% is in solution with taenite. There is a weak, positive correlation between Co and Ni.

P, between 0,01 and 2%, low concentrations in metallic phases, when the percentage is high is in schreibersite, a frequent inclusion in iron meteorites. It has a relevant role in the formation of W.S.

C, up to 2%, more abundant in taenite. In cohenite, the natural version of perlite, C is present.

Si, low in iron meteorites, very high in stony-iron meteorites, its percentage may give hints about the position of the meteorites in their original parent bodies.

There are many others, such as metallics Au, Cu, Cr, Zn, Mn, Mo, but they are seemingly less frequent and less important in the microstructural evolution, or volatile, that are hard to recognize (3).

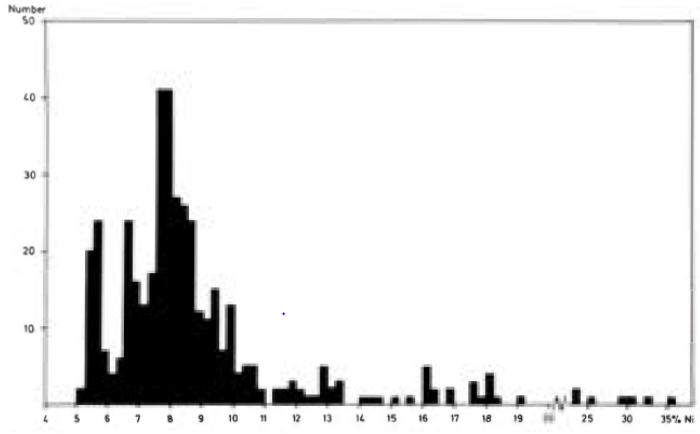

Figure 7 frequency of Ni percentages in iron meteorites samples(3)

Another way to classify iron meteorites, by chemicals *(2)*, partially used in the further studies of this thesis,

follows:

- IAB
    - IA: Medium and coarse octahedrites, 6.4-8.7% Ni, 55-100 ppm Ga, 190-520 ppm Ge, 0.6–5.5 ppm Ir, Ge-Ni correlation negative.
    - IB: Ataxites and medium octahedrites, 8.7–25% Ni, 11–55 ppm Ga, 25–190 ppm Ge, 0.3-2 ppm Ir, Ge-Ni correlation negative.
- IC
- IIAB
    - IIA: Hexahedrites, 5.3–5.7% Ni, 57–62 ppm Ga, 170–185 ppm Ge, 2-60ppm Ir.
    - IIB: Coarsest octahedrites, 5.7–6.4% Ni, 446-59 pm Ga, 107–183 ppm Ge, 0.01–0.5 ppm Ir, Ge-Ni correlation negative.

- IIC: Plessitic octahedrites, 9.3–11.5% Ni, 37–39 ppm Ga, 88–114 ppm Ge, 4–11 ppm Ir, Ge-Ni correlation positive
- IID: Fine to medium octahedrites, 9.8–11.3%Ni, 70–83 ppm Ga, 82–98 ppm Ge, 3.5–18 ppm Ir, Ge-Ni correlation positive
- IIE: octahedrites of various coarseness, 7.5–9.7% Ni, 21–28 ppm Ga, 60–75 ppm Ge, 1–8 ppm Ir, Ge-Ni correlation absent
- IIIAB: Medium octahedrites, 7.1–10.5% Ni, 16–23 ppm Ga, 27–47 ppm Ge, 0.01-19 ppm Ir
- IIICD: Ataxites to fine octahedrites, 10–23% Ni, 1.5–27 ppm Ga, 1.4–70 ppm Ge, 0.02–0.55 ppm Ir
- IIIE: Coarse octahedrites, 8.2–9.0% Ni, 17–19 ppm Ga, 3–37 ppm Ge, 0.05-6 ppm Ir, Ge-Ni correlation absent
- IIIF: Medium to coarse octahedrites, 6.8–7.8% Ni,6.3–7.2 ppm Ga, 0.7–1.1 ppm Ge, 1.3–7.9 ppm Ir, Ge-Ni correlation absent
- IVA: Fine octahedrites, 7.4–9.4% Ni, 1.6–2.4 ppm Ga, 0.09–0.14 ppm Ge, 0.4-4 ppm Ir, Ge-Ni correlation positive
- IVB: Ataxites, 16–26% Ni, 0.17–0.27 ppm Ga, 0,03–0,07 ppm Ge, 13–38 ppm Ir, Ge-Ni correlation positive
- Ungrouped meteorites. This is actually quite a large collection (about 15% of the total) of over 100 meteorites that do not fit into any of the larger classes above, and come from about 50 distinct parent bodies.

1.4 Inclusions

The main inclusions found in iron meteorites are:

-Cohenite, $(Fe,Ni,Co)_3C$, orthorhombic, the natural version of pearlite. It is hard and ductile (1100HV), brilliant white when reflects light, anisotropic.

-Schreibersite/Rhabdite, $(Fe,Ni)_3P$, it is brittle and its hardness is around 800HV, yellow. Ni% is higher the smaller the inclusion, from 15%Ni wt to 30%Ni wt. Small inclusions are microprismatic and are called “Rhabdite”.

-Haxonite, $(Fe,Ni,Co)_{23}C_6$, cubic, found in Taenite, hardness of 800 HV.

-Troilite, FeS, sensitive to shocks, so it can help to figure out the history of the samples where it’s found. It is almost in every iron meteorites. It is also the main inclusion present before the nucleation of kamacite, so it could provide informations about ancient shocks, that are estimated to be several kbar, to have an effect on metal matrix.

Many others may be present, like silicates, carbides, chromite, graphite, gold, diamond, ect. (3)

1.5 Cooling rate and microstructural evolution determination.

To determine the cooling rate is necessary firstly to understand how the microstructural evolution happens.

In an octaehdrite an important parameter is the Ni content in relation to the kamacite band width, that tends to raise in the taenite as the kamacite bands widen with nucleation because the temperature lowers. This effect is enhanced at the interface between kamacite and taenite.

Pressure is probably less influent, but other phenomena are likely to happen in space, like heat waves, pressure waves, or cosmic collisions, that contributes to microstructural evolution along with cooling rate.

Another important parameter is T_{Curie}=400-450°C, when taenite from paramagnetic becomes ferromagnetic. Some of the estimation methods - central Ni and cloudy zone - work respectively at 450°C and at 250-300°C, they usually agree but not in some samples (3), (4).

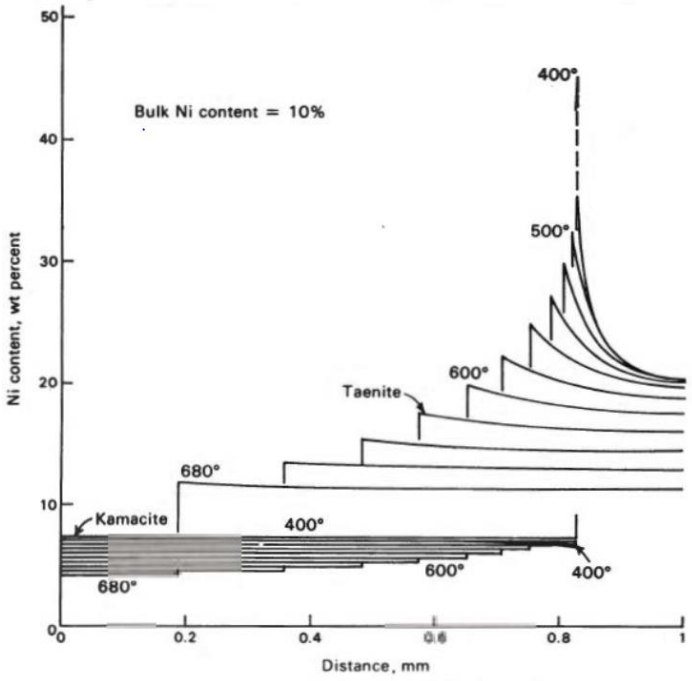

Figure 8 microstructural evolution rough estimate of octaehdrites, characteristic pattern of Ni% at progressively lower temperature, HIM.

1.6 Phosphorus role

It is experimentally determined that only above a certain P% W.S. forms from austenite with the mechanism Y+Ph→α+Y+Ph, where Ph is Phosphides forming when P is in supersaturated solution with Fe and Ni, generally schreibersite/ rhabdite is observed (see chap. 1.4), while below a certain P%, that is the case of many samples, the transformation should be Y→ α2 (martensite)+Y→ α +Y (plessite) for low Ni%, Y→α+Y(not nucleating)→α+Y+Ph for high Ni%.

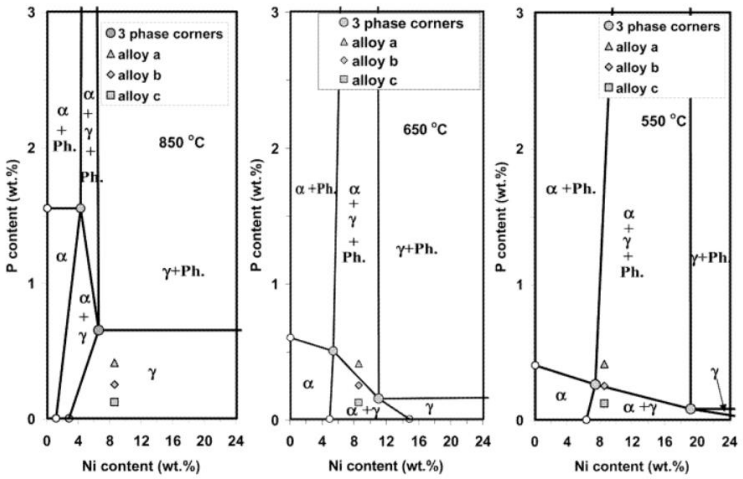

Figure 9 isothermal section of Fe-Ni-P diagram, Doan Goldstein (1970)

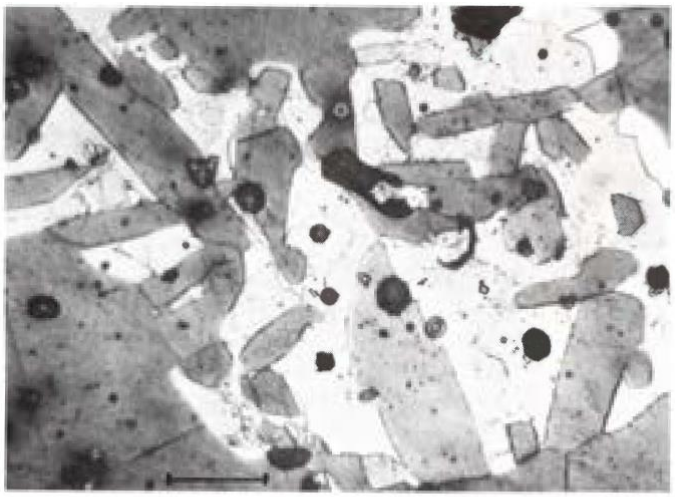

Figure 185A. Widmanstätten structure in a synthetic alloy with 3% Ni and 0.9% P. Upon cooling from homogenization at 1100° C (70 hours), the austenite started decomposition to ferrite lamellae (dark) and retained austenite (light) when kept for 71 hours at 760° C. Etched. Scale bar 30 μ.

Figure 10 from "The Handbook of Iron Meteorites", synthetical nucleation of ferrite in austenite following the W.S. orientation.

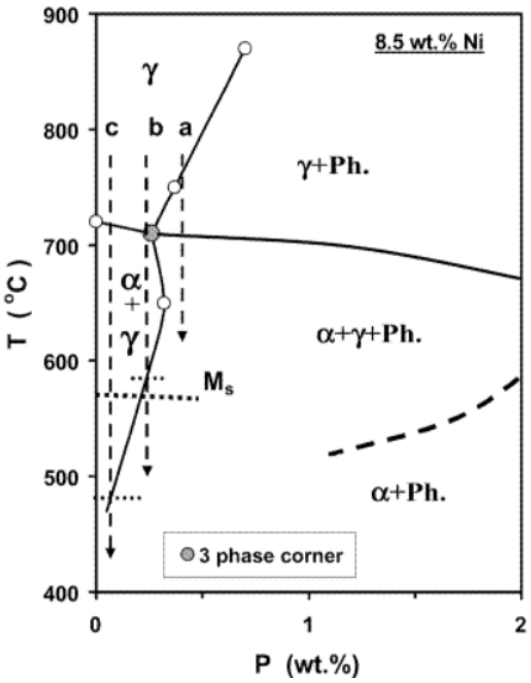

Figure 11 "b", "c" solutions can't nucleate kamacite, experimentally determined, "a" can due to P supersaturated solution.

Figures 9-11 show how under a certain P% the nucleation of ferrite must happen below Ms (martensitic temperature). In this thesis there won't be the details, it is just important to know that microstructural evolution is different depending on P%, and may or may not pass through metastable martensite: When P% and Ni% are low.

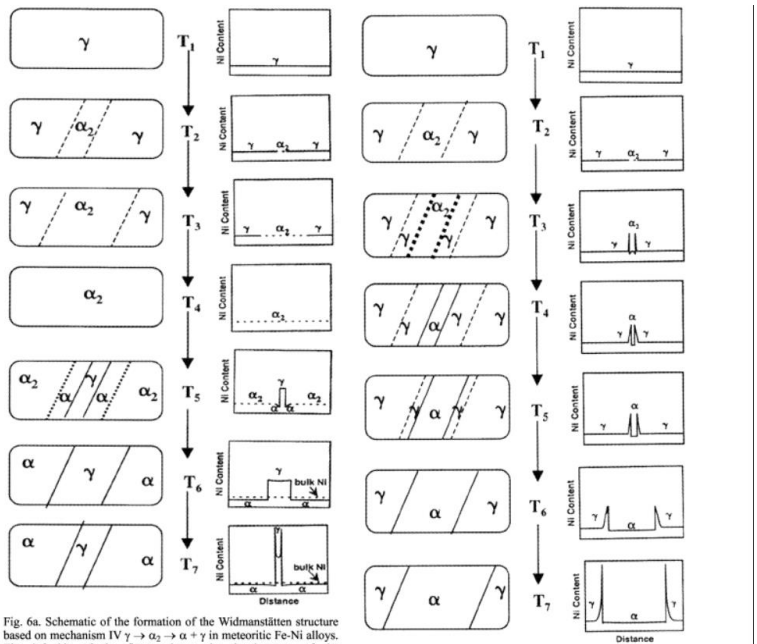

Fig. 6a. Schematic of the formation of the Widmanstätten structure based on mechanism IV $\gamma \rightarrow \alpha_2 \rightarrow \alpha + \gamma$ in meteoritic Fe-Ni alloys. The left-side of the figure shows the development of the microstructure and the right-side shows the development of the Ni profiles in taenite and kamacite as an alloy cools. T_1 through T_7 represent different temperatures during cooling.

Mechanism V

Fig. 6b. Schematic of the formation of the Widmanstätten structure based on mechanism V $\gamma \rightarrow \alpha_2 + \gamma \rightarrow \alpha + \gamma$ in meteoritic Fe-Ni alloys. The left-side of the figure shows the development of the microstructure and the right-side shows the Ni profiles in taenite and kamacite which develop as an alloy cools. T_1 through T_7 represent different temperatures during cooling.

Figure 12 two different paths for the transformation below Ms temperature

Keeping into account the different ways in which the iron meteorites microstructure is formed, to understand the limit of the methods and the complexity, it is possible to talk about the different methods to determine the cooling rates (4).

1.7 Method of Ni%.

Using the state diagrams plotted and the mass transport equation, this method has been proven by Goldstein to be valid above 450°C, the Curie temperature, where Ni diffusion happens, with many tests and interpolation.

We need to know Ni in central kamacite, Ni in central taenite, related to respective band width(taenite)/distance to nearest grain boundary(kamacite), Pwt% and Niwt%, and plots on iso cooling rates lines done by computer interpolating experimental data (5).

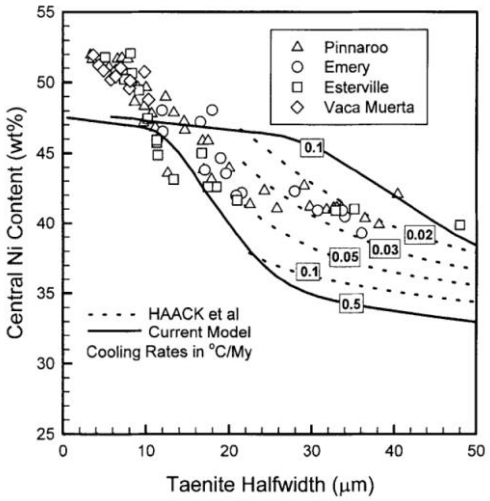

Figure 13 example by Yang Goldstein, "The formation of W.S. in meteorites."

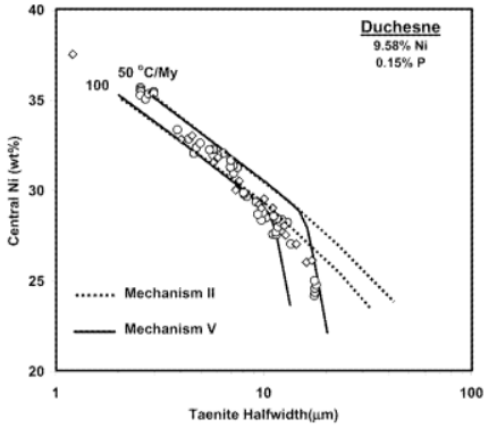

Fig. 9b. Comparison between the measured central Ni versus taenite half width data (open circle, Moren and Goldstein 1979; open diamond, Rasmussen et al. 1995) and the calculated Ni compositions based on mechanism II and V for the Duchesne IVA iron meteorite.

Figure 14 "The formation of W.S. in iron meteorites," Yang and Goldstein

1.8 Method of cloudy zone.

This empirical method evaluates, being valid at the end of diffusion process at 300-250°C, the relationship between the cooling rate and the size of island phase in the cloudy zone. The cloudy zone (Ni wt<=41%) is after the outer taenite ring (Ni wt>=48%).

The interface between OTR and CZ is presumably around 41% Ni, because of the formation mechanism, described by the state diagram:

400°C:γ→α(kamacite)+γ1

Below 350°C→γ1(where Ni is below 41%wt and keeps lowering)+γ"(where Ni is above 48% and is FeNi tetraenite)+Y2(OTR, Ni%=48%).

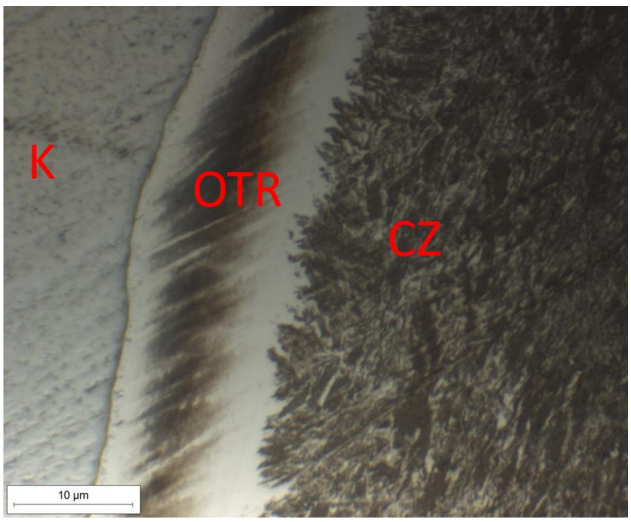

Figure 15 kamacite, outer taenite ring, cloudy zone in the sample "Carltown"

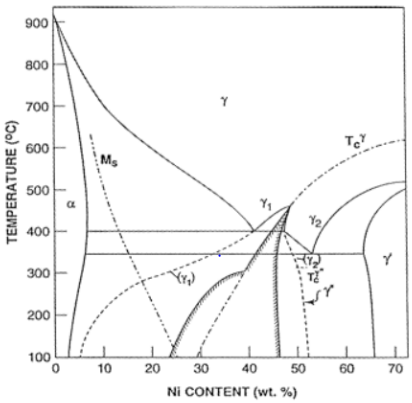

Fig. 1. Fe-Ni binary phase diagram (Yang et al. 1996): α is low Ni bcc phase; γ is a high Ni fcc phase; γ_1 is a low Ni paramagnetic fcc phase; γ_2 is a high Ni ferromagnetic fcc phase; γ′ is ordered Ni_3Fe; γ″ is ordered FeNi-tetrataenite; and M_s is the martensite starting temperature. T_c^{γ} is the Curie temperature of the γ phase. $T_c^{\gamma''}$ is the ordering temperature of FeNi, γ″.

Figure 16 Yang (1996) complete Fe-Ni phase diagram

Cloudy zone is formed by island phase, which are FeNi tetraenite, and a low Ni honeycomb phase, and their width, varying from 470-17 nm is in negative correlation with cooling rate, varying from 0,5-325 K/Mly.

Island size is also proportional to the Ni%, but confronting samples we know that near the interface with OTR the Ni% is always around 41%

To properly observe the island phase is necessary the SEM and a chemical treatment, in some groups (e.g. IVA) this correlation is absent, because other methods failed or because other cosmical events influencing the microstructural evolution(6).

1.9 distribution of Co at kamacite taenite interface

Data of Widge and Goldstein (1977) showed that the distribution is temperature dependent.

Plotting the logarithm of the double ratio [(Co/Ni)kamacite/(Co/Ni)taenite] (Rαγ) and inverse temperature yields a linear equation showing that the ratio ranges from ~2.5 at 1080 K to ~30 at 710 K. Thus, a measurement of Rαγ in the kamacite and taenite near the interface offers information about relative cooling rates; the higher Rαγ, the lower the cooling rate. This technique is mainly affected by the final cooling rate, before the sample cooled to the final temperature where there is no diffusion. (7)

Other methods include the study of isotope fractionation and the study of ferromagnetic-paramagnetic behaviour (8)(9).

These studies are still in experimental phase, a complete and extended use on every possible sample using all the possible methods to find the eventual relations between composition and cooling rate would be helpful.

1.10. Asteroids, types, mining perspectives

It's interesting to give information about what's going on in the world for asteroid nature and exploration.

We've seen that there are asteroids with good metal contents and we limit our consideration to these types.

Up to now the interest is for extracting materials from asteroids in the space; the goal is to obtain raw materials to be treated and used for construction in space or on satellites/planets.

In the last years we are facing a new period of "space colonization" finalized to use resources also of asteroids for extracting materials/metals.

New companies have been founded to use these materials and to optimize the systems for extracting metals from asteroids.

In USA: "Deep Space Industries", in California, and "Planetary Resources", in Washington, were built up some years ago but up to now we have no notices of launch or inspection on site made by these companies.

In Europe Luxembourg is trying to be the leader in the space resources extraction and use.

Before an extended use it will be necessary a deep examination of the rules and laws on the subject. Following the interpretation of some countries as Russia, Belgium, Brazil extracting any material from asteroids is forbidden by the OST (Outer Space Treaty), even if it is not explicit in the treaty, which allows the exploration and use of asteroids.

OST whatsoever excludes the possibility of "national appropriation" of asteroids and similar objects. Probably the treaty is applicable to space extraction activity, but on this point the treaty is not so clear, following the interpretation of Frans von der Dunk, space law professor in the University of Nebraska in Lincoln.

OST: Outer Space Treaty, established in 1967, has been -mainly- internationally recognized and do not permit space colonization. (12)

Economics perspectives are very attractive for investors, keeping in mind that even rare metals are available in asteroids.

With the NASA project, named Osiris-Rex the Osiris spacecraft, landed on 20 October 2020, on the so-called asteroid "Bennu" and through the three meters long robotic arm collected samples from the asteroid surface.

The following picture shows the aspect of the Bennu asteroid.

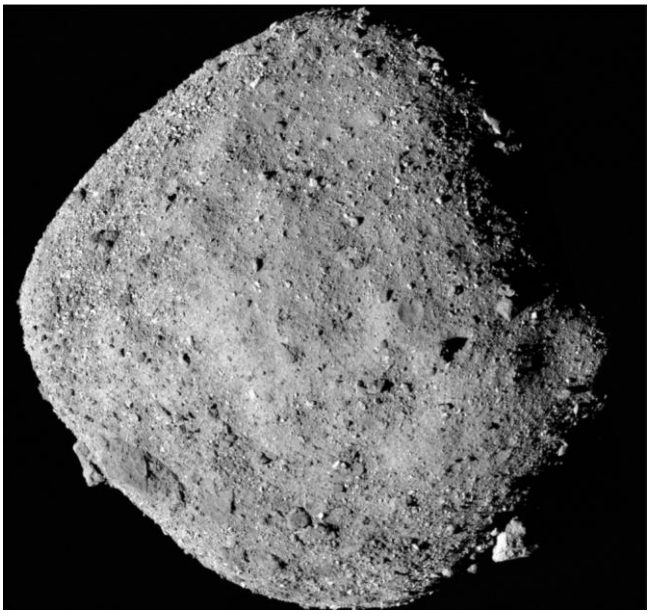

Figure 17 This mosaic image of asteroid Bennu is composed of 12 PolyCam images collected on Dec. 2, 2018 by the OSIRIS-REx spacecraft from a range of 15 miles (24 km). Credits: NASA/Goddard/University of Arizona

In order to demonstrate the importance of the extracting future activities on asteroids we notice the presence of different patents.

Some are dedicated to clamping systems, some others to inspecting and approaching systems to asteroids

Generally speaking, the main issue is to find the way to work in gravity absence, on small ground as the asteroids are.

One example (14):

"US 9339945 B2 - 2016-05-17 IL CALIFORNIA INSTITUTE OF TECHNOLOGY - SYSTEMS AND METHODS FOR GRAVITY-INDEPENDENT GRIPPING AND DRILLING.

Abstract

Systems and methods for gravity independent gripping and drilling are described. The gripping device can also comprise a drill or sampling devices for drilling and/or sampling in microgravity environments, or on vertical or inverted surfaces in environments where gravity is present. A robotic system can be connected with the gripping and drilling devices via an ankle interface adapted to distribute the forces realized from the robotic system.

Following pictures from patent."

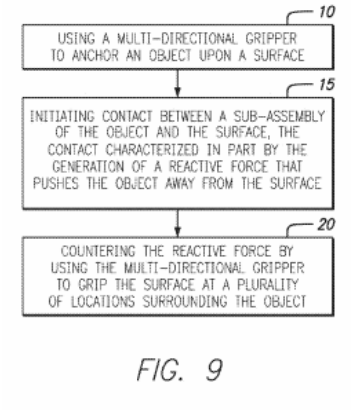

Figure 18 approaching and gripping on the ground from US 9339945 B2 - 2016-05-17

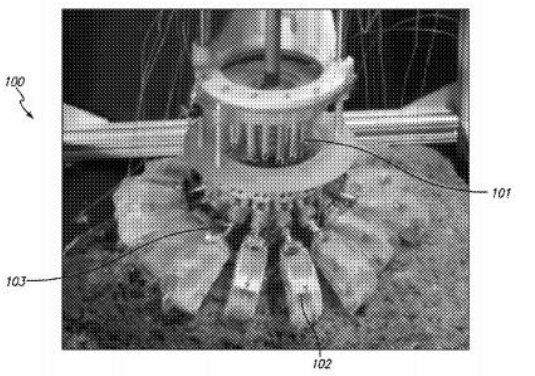

Figure 19 gripping unit from US 9339945 B2 - 2016-05-17

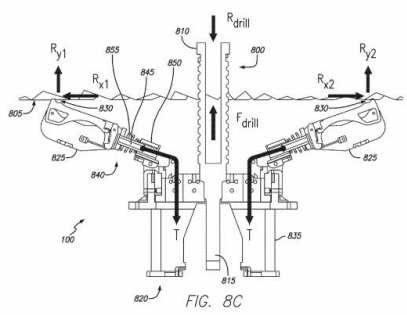

Figure 20 gripping unit drawing from US 9339945 B2 - 2016-05-17

2.METHODOLOGY USED

Choice of the samples: "Ava" and "Carltown". This samples are named after the place of finding and are conserved in the mineralogy museum of "Politecnico di Torino".

Figure 21 Carltown sample polished

Figure 22 Ava sample polished

Follows the procedure to polish the samples: they are grinded with a rotating plate, at first composed by metal grains gradually smaller and in the end with a diamond paste and lubricant to obtain a final precision of 1 μm. In the end is important to eliminate all traces of lubricant, water and paper before the microscope observation, so the samples are cleaned with ethanol.

Once the samples surface is plane is possible the microscopy observation. The microscope is linked to a camera and is possible to take pictures on the computer. The magnifying lens are 2x, 5x, 10x, 20x, 50x and 100x.

In this phase, without metallografic attack, we look mainly for impurities in the metal matrix and cracks propagations, even if it's possible to find some grain boundary of Windmanstatter structure.

The samples are divided in zones where the lens operate in order to track the impurities distributions. The zones are evidenced in following pictures.

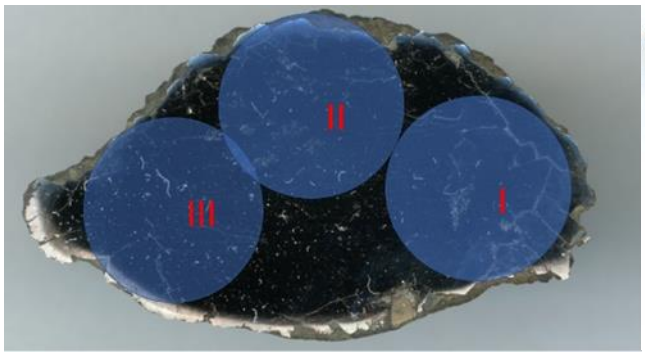

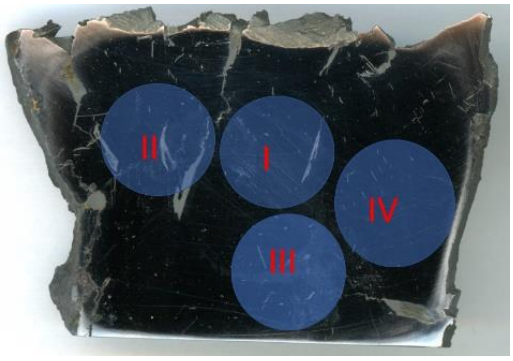

2.1 Optical microscopy after metallografic attack

After the first observations, it is possible to proceed with the Metallografic attack, that is done by submerging the samples in a solution of ethanol and 3% in concentration of HNO_3, called "Nital".

This was done for 1'20" for each sample; nital reacts with the metal matrix in different ways (e.g. kamacite is more attacked than taenite and most mineral inclusions), allowing a better observation of the grain borders and Widmanstatten structure, if present.

The same microscope as before is used after the attack, and the second observation is done.

2.2 Microhardness test.

Figure 23 microdurometer

The Vickers micro-hardness tester (in the picture on the side) is an instrument capable of imprinting a force with a punch that leaves an impression.

It is possible then to evaluate the hardness with the following empirical formula:

$$HV = \frac{F}{A} = 1{,}8544 * F/d^2$$

The force could be chosen between 0,001 and 1 kgf, The choice, after some controls to check if the results were similar with 0,1 and 0,3 kgf, was to proceed with 0,005 kgf for all the measurements.

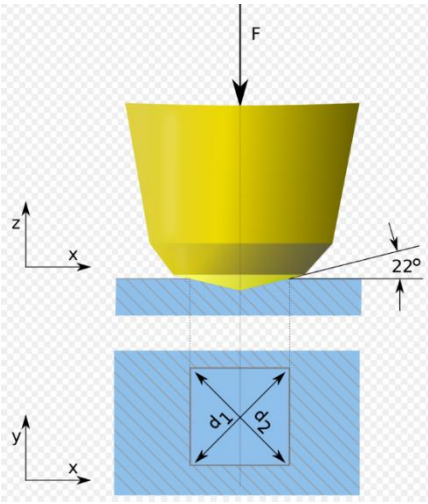

Figure 24 microdurometer parameters

On the display of the computer is possible to check the zone before and after the impression thanks to the camera in the microscope.

Then the Vickers hardness is automatically found by the computer selecting the points of measurement, which must be clearly seeable.

The measurements are taken in particular zones, sometimes sparse, computing the average value for a defined phase, sometimes tacking a serie of tests with equispaced impressions in order to see the gradient of hardness in specific zones.

Example in pictures below.

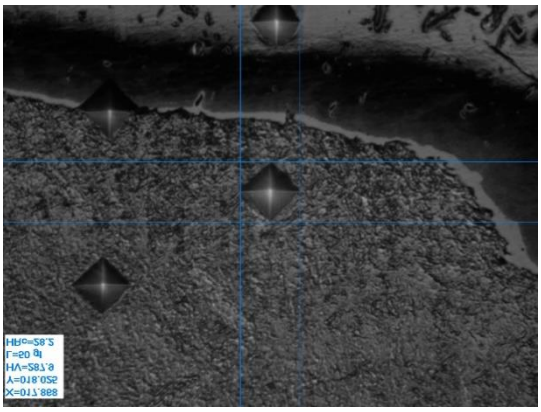

Figure 26 example of microdurometer test

Figure 25 example of microdurometer test

2.3Quantometer test

The quantometer is used to check the elements composing the samples.

Figure 27 quantometer

Functioning principles: a spark vaporizes part of the sample starting from the surface, it is a distructive test. Since atoms and the ions are excited, they emit a characteristic optical radiation.

This radiation in then decomposed and detected thanks to a CCD and an optical fiber.

The intensity of a single wavelength is proportional to the elements concentrations that in the end are represented on the monitor.

2.4 X-Rays Diffractometer

XRD technique is a branch of X-rays crystallography, which studies the atomic-molecular structure of a crystal thanks to diffraction and electrons elastic scattering.
From the angle and intensity of the rays diffracted it is possible to determine the lattice structure, eventual strains and the possible presence of defects.

Figure 28 The X-Rays Diffractometer

Atoms scatter X-rays primarily by electrons, the X-rays scattered in such a way interact destructively. At certain wavelength they interact constructively according to Bragg's law:

$$2d * \sin\theta = n * \lambda$$

Where n is an integer number, λ is the wavelength, d is the distance between two lattice plans and θ is the angle of diffraction.
The instrument has 3 main components:

- X-Ray tube, that produces X-Ray by mean of a cathodic ray tube at 30 mA and 40 kV, in the instrument used.
- X-Ray detector, that sends the signal to be printed on screen of angle and intensity of radiation.
- Sample holder

The final result is a graph of angle (x) and intensity (y) of the signal, which has to be interpreted according to Bragg's law.

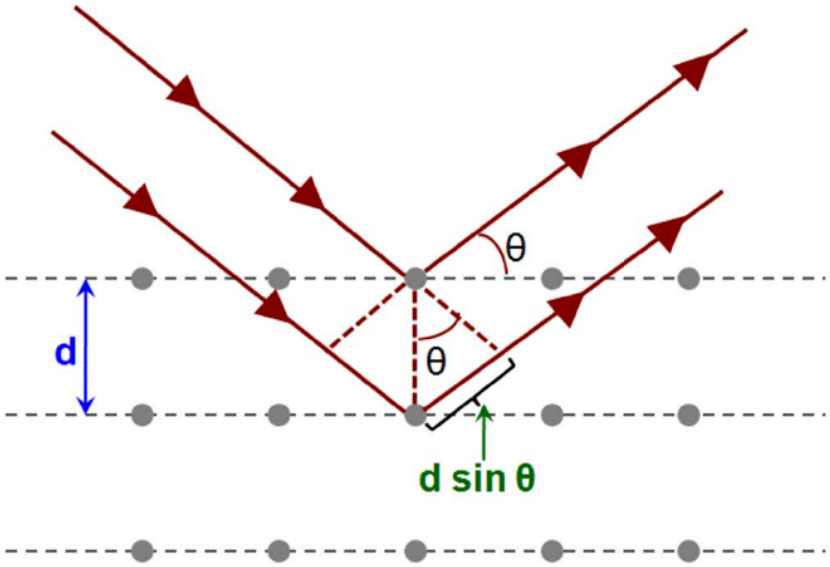

Figure 29 XRD, Bragg's law, graphical explanation.

3.RESULTS

3.1 Ava

3.1.1 Pre-nital observation.

In this first observation is not possible to see the grain borders. Is already possible to see a change in color in the metal matrix that distinguish kamacite from taenite, this phenomenon can be explained by considering the difference in hardness between the 2 phases.

Taenite is very rare and Widmanstatten Structure is absent, it is an exahedrite and the inclusions are already clearly seeable and it is possible to distinguish various typologies.

In the picture below it is possible to see a big inclusion and a cream yellow stripe, probably taenite.

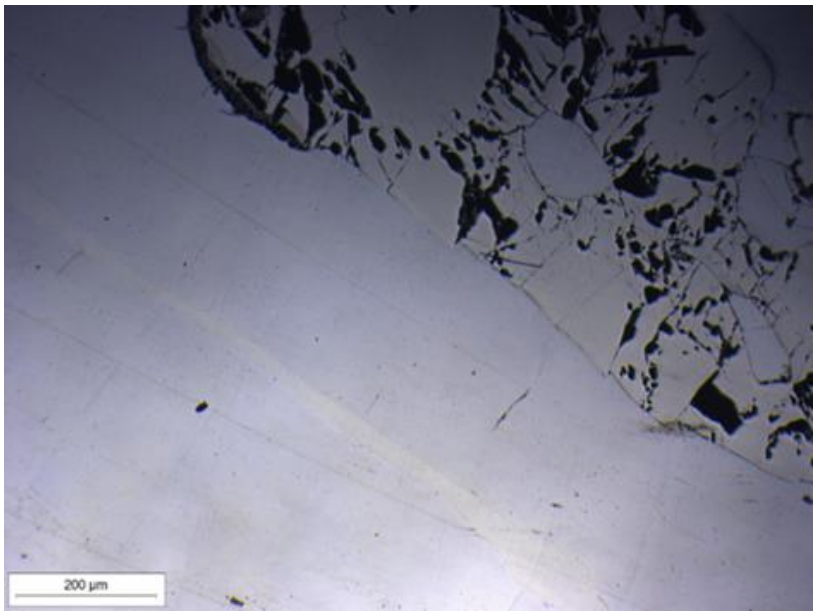

Figure 30 inclusion type "A" kamacite, plessite

There are 4 types of inclusions:

- Inclusions type “A”, With an extended surface, sometimes two phases and many small dark inclusions and/or withdrawal cavities. It is possible to see by eyes this inclusion, as they are around 2 mm long.

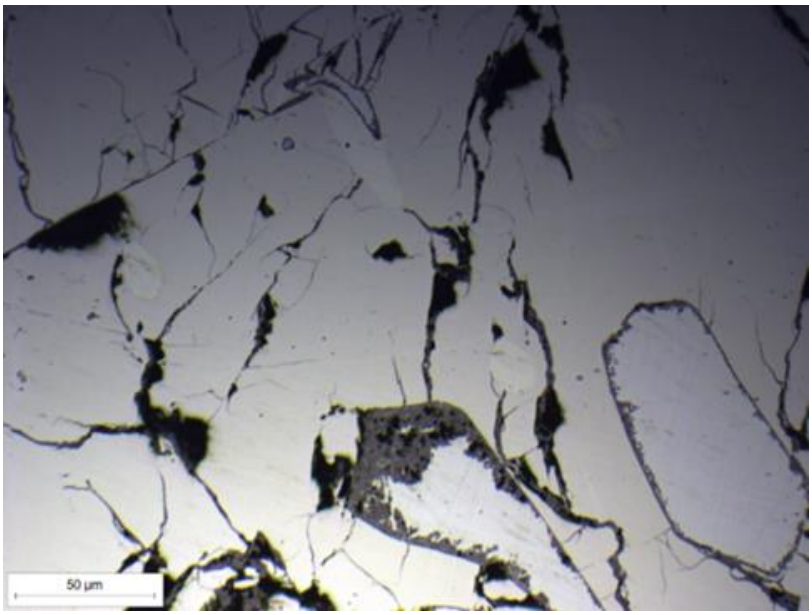

Figure 31 inclusion type "A" detail with cohenite white, troilite dark, schreibersite yellow and chromite, small blue crystal, ZONE II

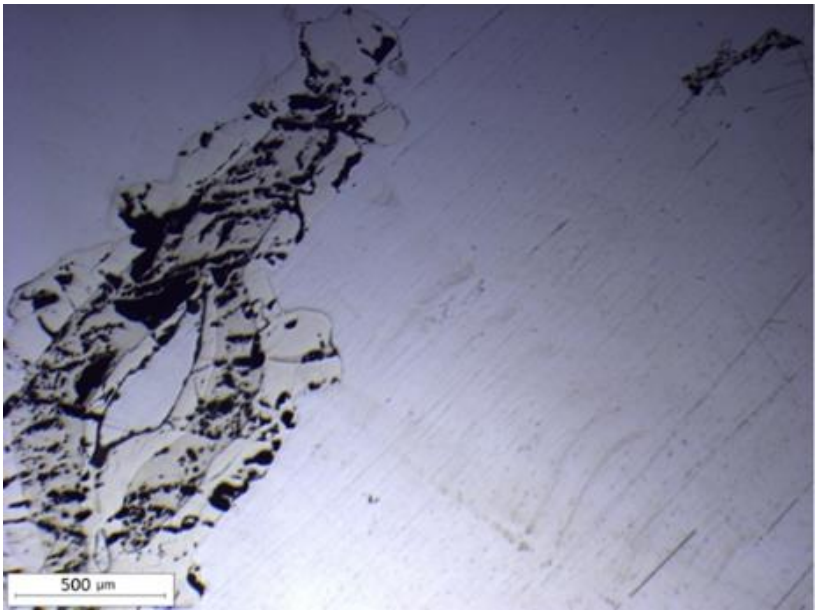

Figure 32 inclusioni type "A" ZONE I

Figure 33 ZONE II schreibersite, cracks due to fragility

- Inclusions type "B", With a smaller surface, less dark inclusions and/or withdrawal cavities, different shapes and dimensions. The presence of cracks propagating in some inclusions may suggest that the dark spots are withdrawal cavities.

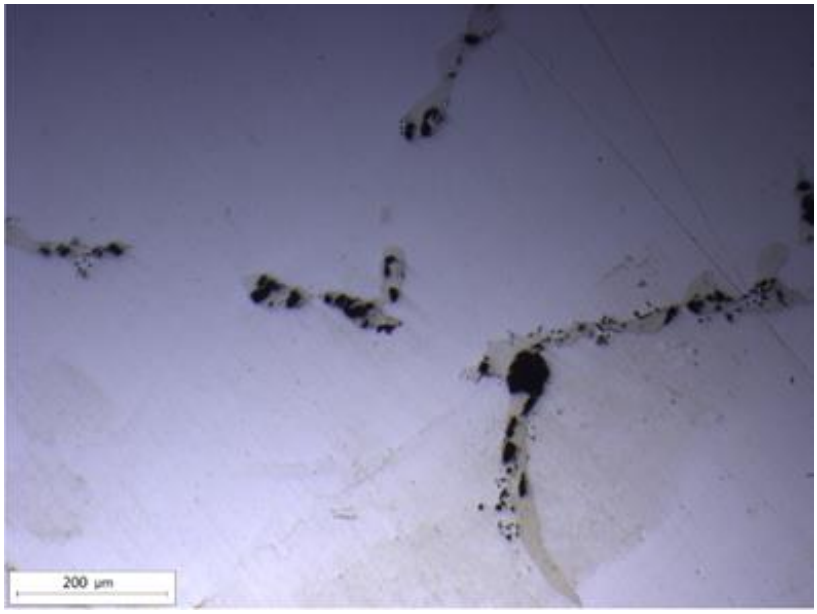

Figure 34 zone III, schreibersite

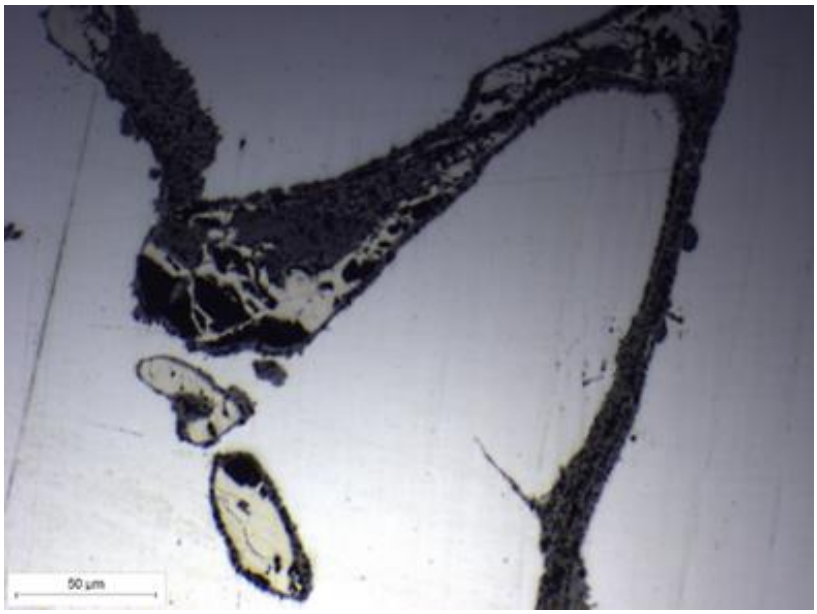

Figure 35 zone I schriebersite and troilite

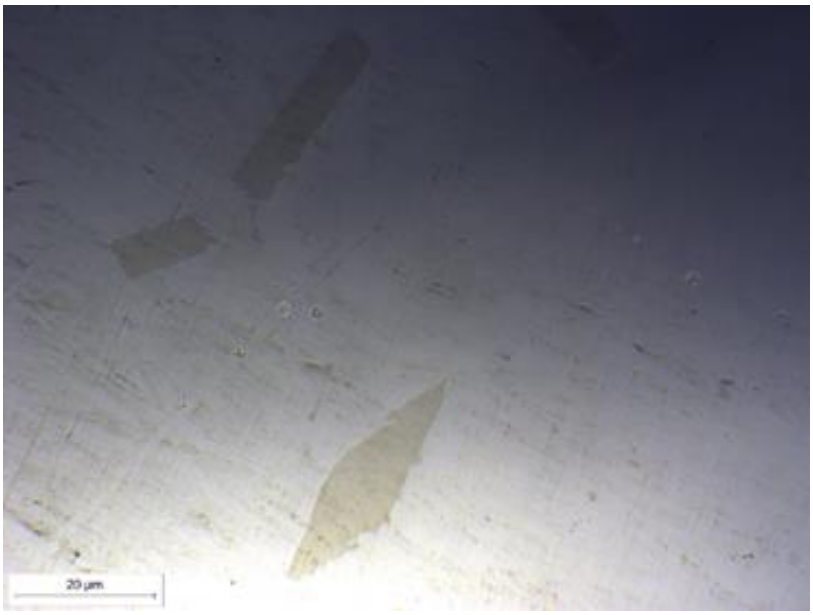

Figure 36 zona II rhabdite

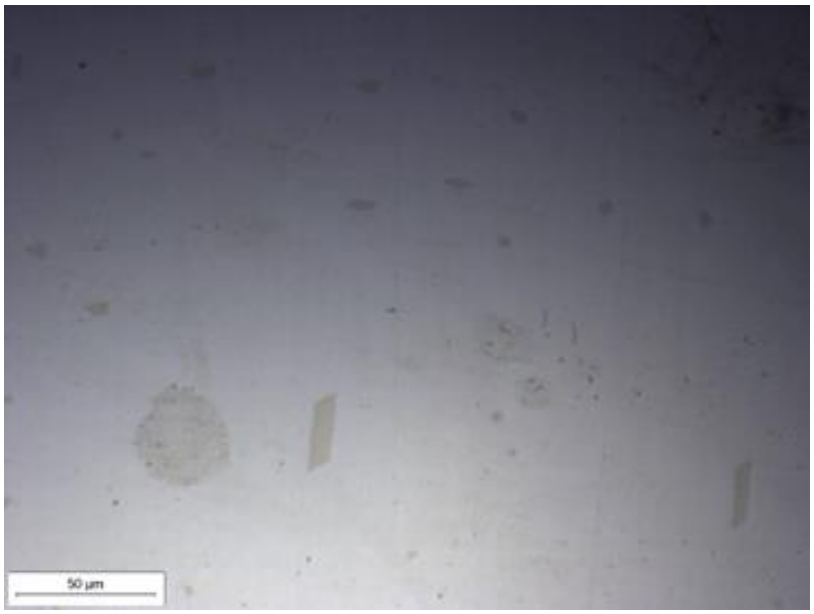

Figure 37 zone II rhabdite

- Inclusions type “C”, really small change of phase in the metal matrix, generally regularly shaped as a parallelepiped. They are sparse in all the metal matrix, without a clear pattern, but as previously said generally not near type “A” and “B” inclusions.
- Inclusions type “D”, dark and with many withdrawal cavities, sometimes conglomerated in type “A” inclusions, sometimes alone.

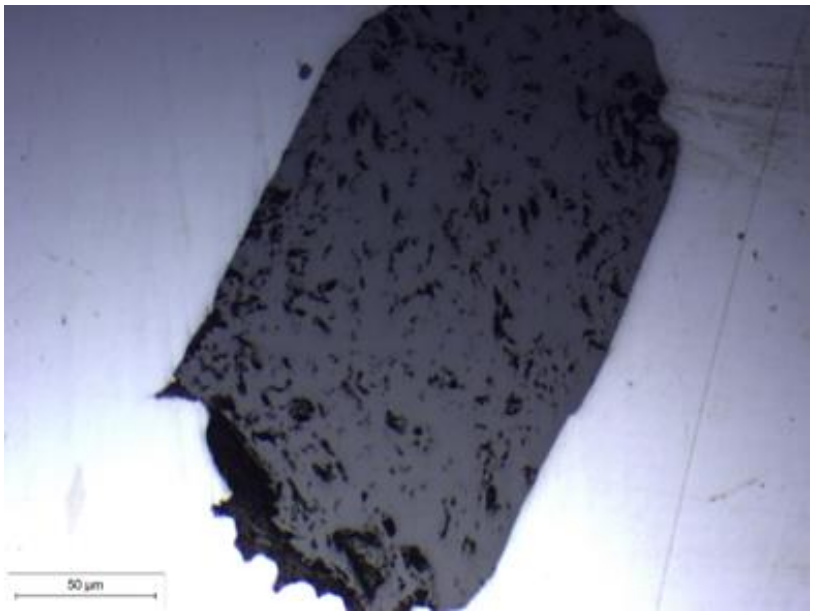

Figure 38 zone II probably troilite

It is interesting to notice that for 1 type “A” there are around 10-15 type “B” and 100-150 type “C”. Also near types “A” and “B” there are less type “C”, suggesting that the material of the inclusions is the same and it tends to conglomerate.

The grain borders of the metal matrix are not visible without metallografic attack.

3.1.2 Observation after metallographic attack

Figure 39 AVA after nital attack

After metallographic attack grain borders and the difference between kamacite and taenite are clearly visible.

At a first observation, without the microscope, we see some inclusions (type “A”) and grain borders. This is clearly an exahedrite.

Metal matrix: the metal matrix is composed by kamacite (mainly) and taenite, which is very rare and sometimes presents plessite inside.

In the images on the side is possible to see the taenite (darker on the borders, white inside) inside the kamacite.

In particular the first image has a plessitic phase with the W.S. inside the taenite, and could be interesting to study for the microstructural evolution.

This is the only case noticed in this sample.

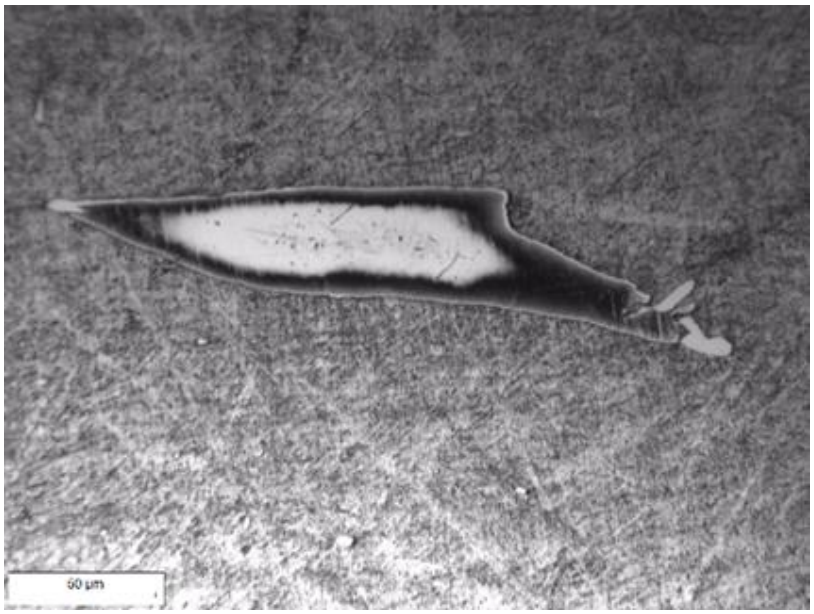

Figure 40 rare, central plessite

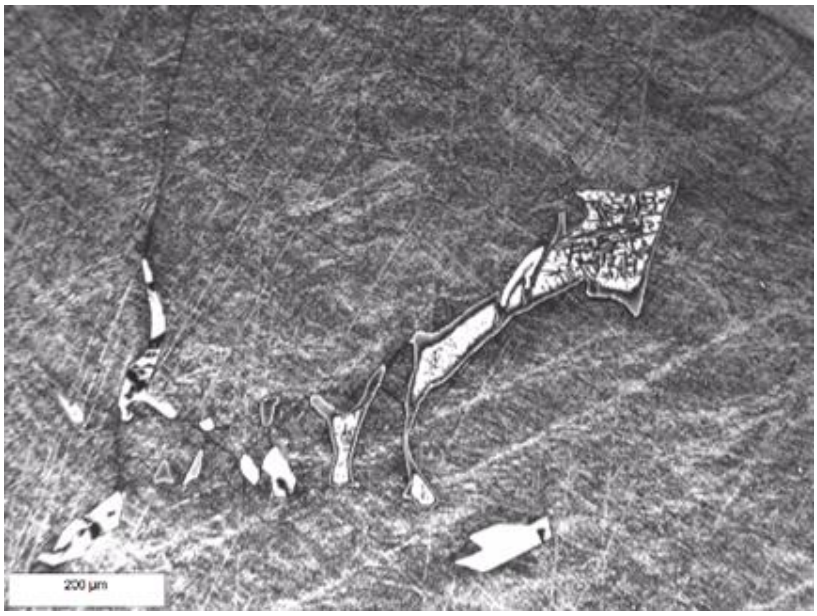

Figure 41 rare, central plessite

Inclusions: with the grain borders clearly visible now is possible to do some further considerations, in fact now is clearly visible that inclusion type "B" are always lie on the grain borders, while inclusion type "C" are always inside the grain, never on the border.

This can indicate something about the nature of the inclusions. Also all the inclusions are in kamacite, but this could be due to the fact that kamacite is much more than taenite.

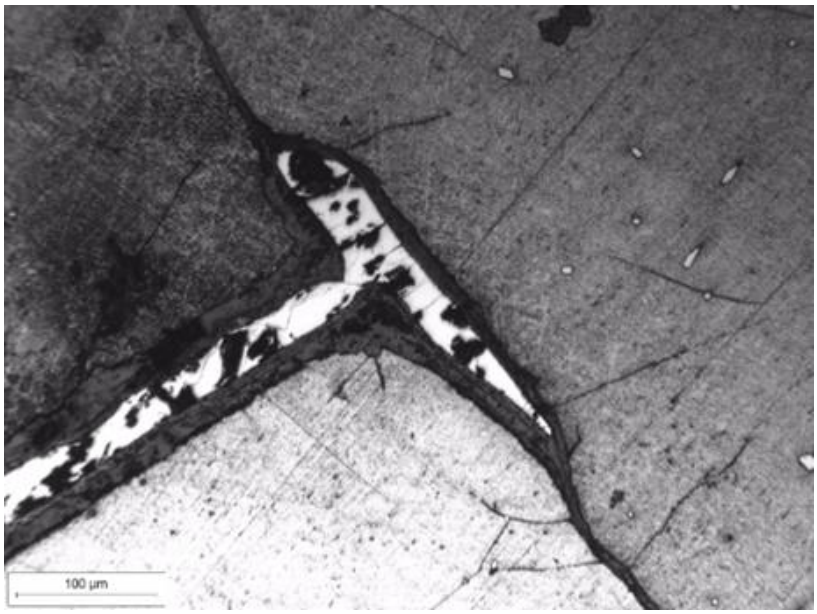

Figure 42 schreibersite, troilite on the grain border-crack, microprismatic rhabdite

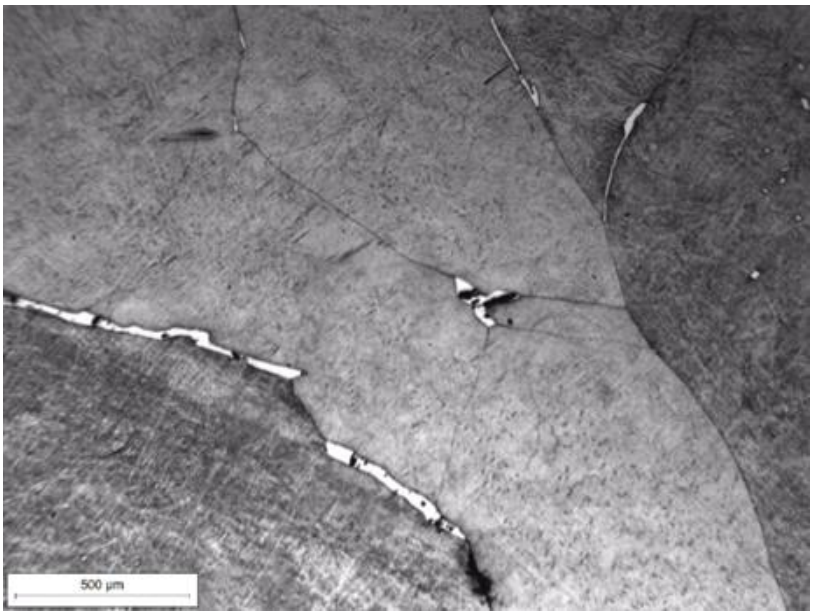

Figure 43 grain border schreibersite

Figure 44 Zone II, near the extreme border. Rhabdite here is not present and the reason may be the presence of the inclusion, that seems to generate a sort of white river

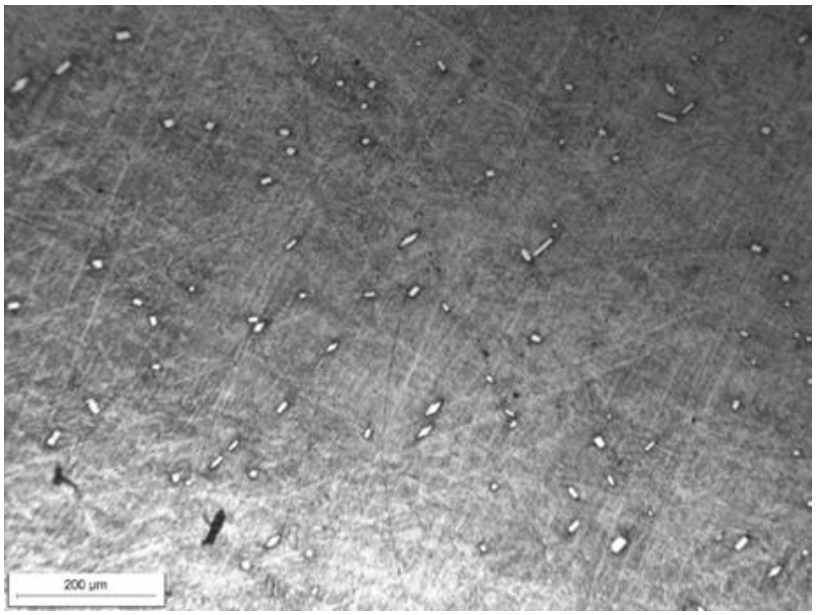

Figure 45 rhabdite il always intergranular, generally far from grain borders around 100 mn

3.1.3. Micro-hardness Vickers test

-matrix

When referring to the metal matrix is important to test both kamacite and taenite.

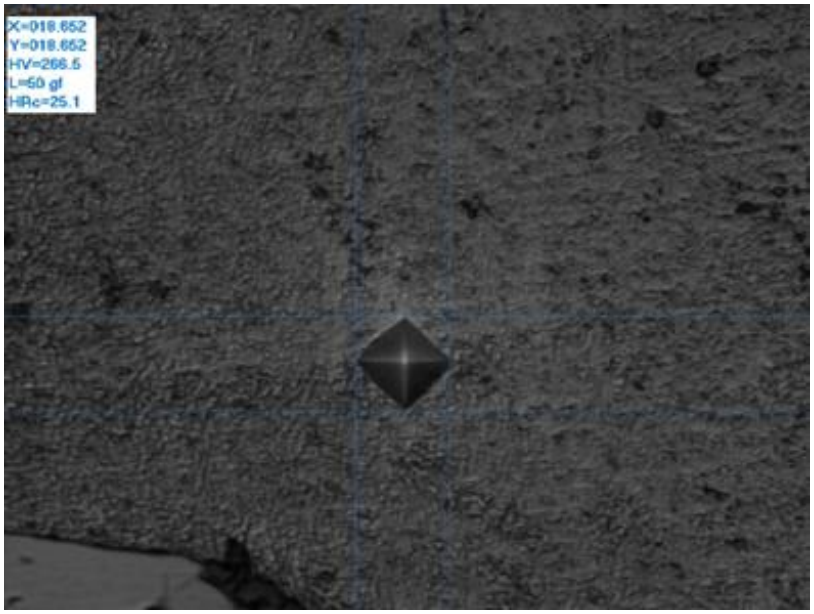

Figure 46 micro-hardness test example

As expected, kamacite has a steady hardness profile, without much variations in values, while taenite is very variable, even when two tests are done next to each other.

The middle Vickers value of kamacite is 302HV, obtained computing the average on a total of 14 tests in 4 different zones of the sample. It is a high value for kamacite, probably due to its microstructural evolution, that is further demonstrated to have passed through martensitic transformation.

Taenite hardness is more complex to study because it presents a clear gradient in hardness.

In order to solve this problem in the case shown in the picture below a series of tests is done and the hardness is finally plot with space, to show the hardness gradient in taenite, which as expected tends to be harder in its borders, and to decrease inside the band.

In fact in this case there is even a plessitic phase, so kamacite is present together with taenite.

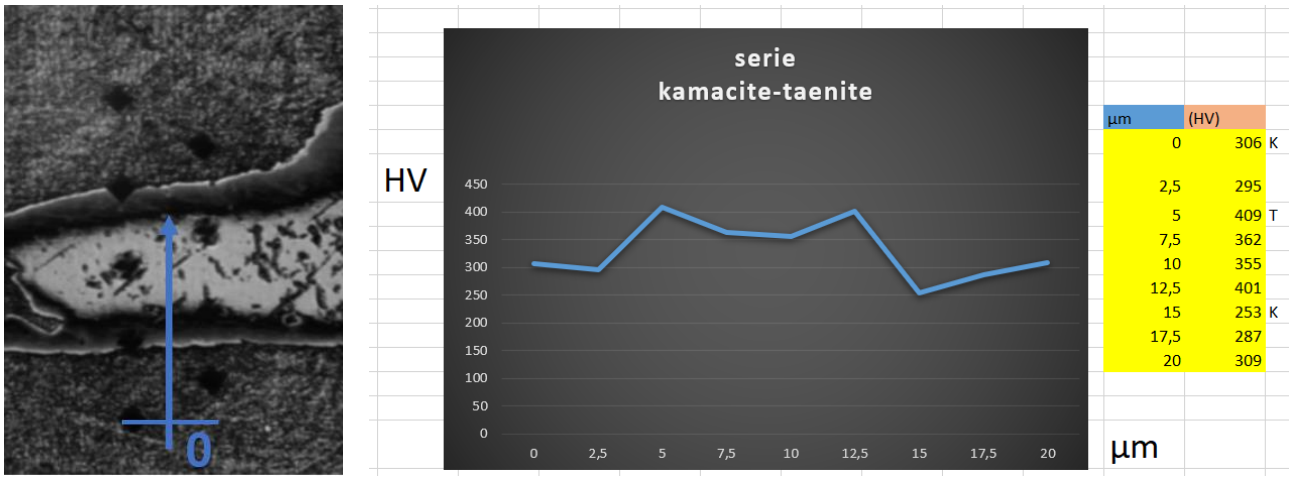

Another test is done, to confirm the previous pattern, even if the big taenitic phases, interesting to study, are not much.

Also in this case the dark, external phase is harder than the white, internal, plessitic phase.

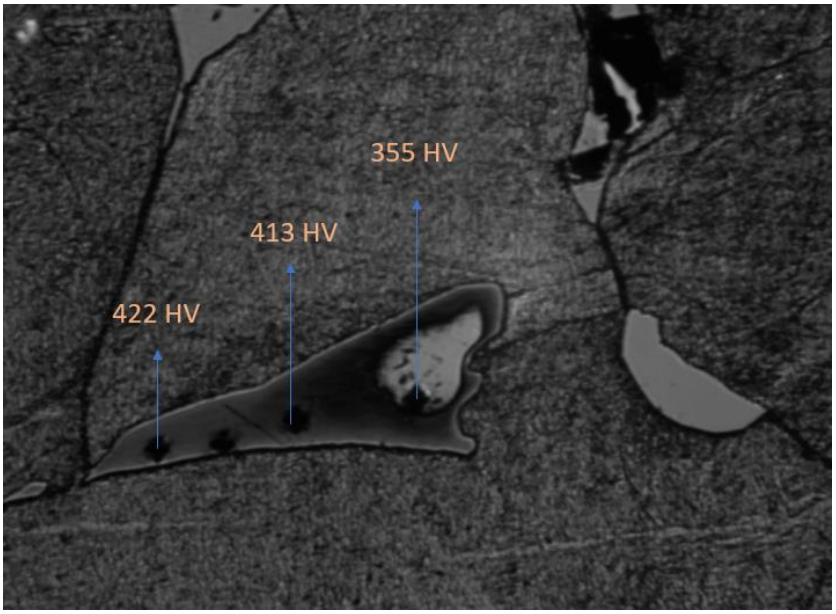

Figure 47 micro hardness tesst on a taenite-plessite field

There is an anomaly tough, in fact there is a taenitical phase where this pattern seems not to be respected.

There is a possible explanation: this taenitic phase is in the external part of the sample, and as can be seen in the picture the phase is martensitic, so it is almost certainly the result of the impact with the terrestrial atmosphere.

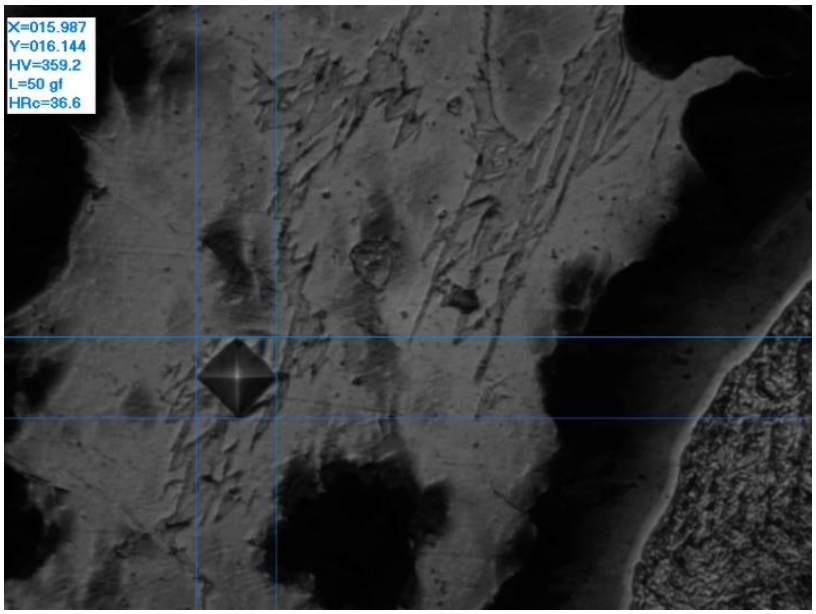

Figure 48 tests on Taenite-martensite field

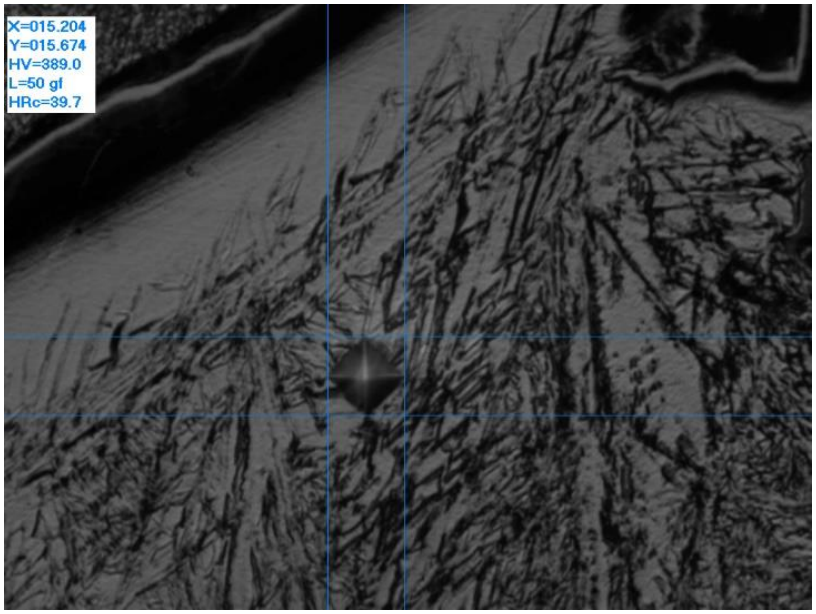

Figure 49 tests on Taenite-martensite field

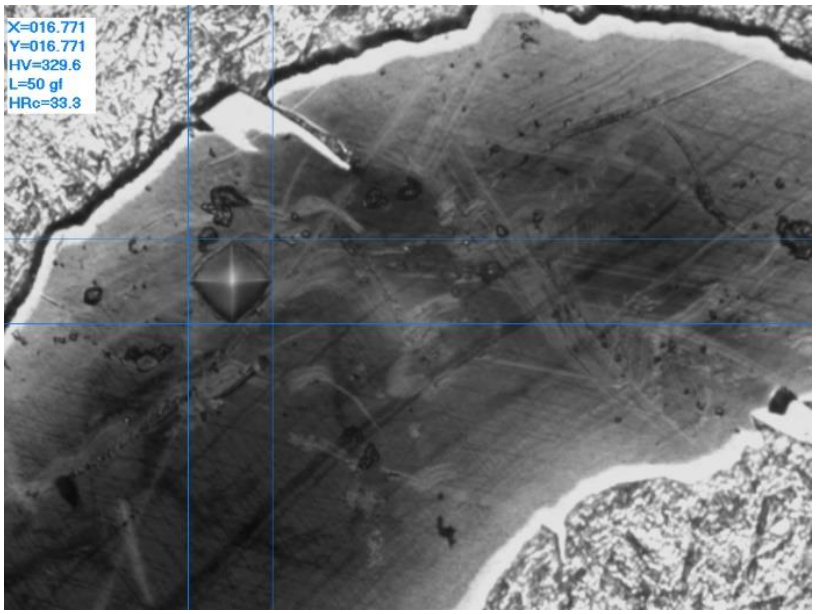

Figure 50 tests on Taenite-martensite field

inclusions

Regarding the inclusions, it was possible to establish an average of 1091 HV for the lighter phase, clearly cohenite, of the inclusion type "A" and of 782 HV for the darker phase, clearly schreibersite.

For the small inclusions at the grain borders (type "B") the average is 739 HV and for the intergranular type "C" inclusions 490 HV, with some execution difficulty, since their width in similar to the microdurometer'.

Type "D" inclusions hardness were impossible to establish due to too many withdrawal cavities.

Based on empirical method it is possible to conclude that type "A" are a mix mainly of schreibersite yellow, brittle and cohenite white, ductile, hard.

Grain borders inclusions is schreibersite as well, while the intergranular, microprismatic inclusions are rhabdite, which is a form of schreibersite, as shown by hardness and brittleness.

3.1.4 Quantometer test.

In the quantometer we can look at the percentage of each elements with a certain precision, but the really rare elements that should be estimated in ppm, such as V, Ge, Ir, are not detectable.

C is present but only in one test. It could be due to cohenite inclusions or due to small contaminations, that are generally carbonium-rich.

Ni is in average percentage of 6,41% in concentration, with small variations, as expected by an hexahedrite.

Co as expected is present with a constant percentage slightly above 0,4% and P slightly above 0,1%.

Zn is present in relatively high percentage (0,038%), but no studies were done on this element in iron meteorites.

None of the 3 tests were done on a big inclusion, so the way to determine their nature cannot be by composition.

Canale	1	2	3	MEDIA
C	<0,001	0,114	<0,001	0,038
Si	0,028	0,028	0,029	0,028333
Mn	0,007	0,01	0,009	0,008667
P	0,171	0,112	0,122	0,135
S	<0,001	<0,001	0,003	0,001
Cr	0,012	0,024	0,03	0,022
Mo	<0,001	<0,001	0,001	0,001
Ni	6,672	6,227	6,335	6,411333
Al	0,003	0,009	0,01	0,007333
Cu	0,018	0,117	0,065	0,066667
Co	0,431	0,434	0,44	0,435
Nb	0,009	0,01	0,009	0,009333
Ti	0,003	0,005	0,005	0,004333
V	0	0	0	0
W	0,012	0,009	0,013	0,011333
B	0,0006	0,0008	0,0006	0,000667
Pb	0,003	0,014	0,007	0,008
Sn	0,004	0,014	0,012	0,01
Zn	0,037	0,041	0,036	0,038
Zr	<0,001	<0,001	<0,001	<0,001
Ca	<0,0010	<0,0010	<0,0010	<0,0010
As	<0,002	<0,002	<0,002	<0,002
Bi	0,002	0,002	0,008	0,004
Fe	92,585	92,828	92,862	92,75833

Figure 51 elements concentration according to quantometer test.

3.1.5 XRD test.

On this sample the XRD confirms the presence of kamacite (ferrite bcc, strongly oriented), there are other peaks but taenite, surely present, is in a percentage too low, while the crystals are either too small or too composite to be identified clearly with this test.

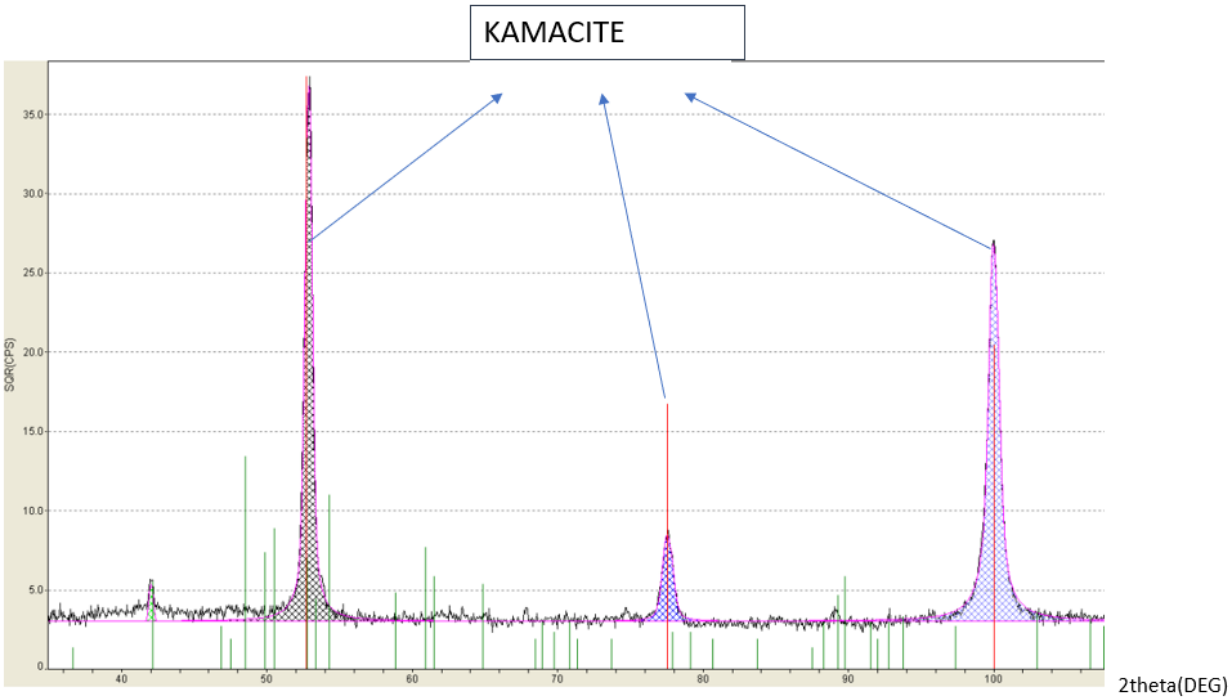

Figure 52 Black line: acquisitions; red straight lines: theoretical kamacite peak intensities.

3.2. Carltown.

In this sample the inclusions are less interesting, they are mostly small and yellow, except for one really big. There are some cracks and in this case is already clearly visible, even by naked eyes, the W.S.

The structure is homogeneous, as it is possible to notice in the pictures below, taken in 4 different zones of the sample.

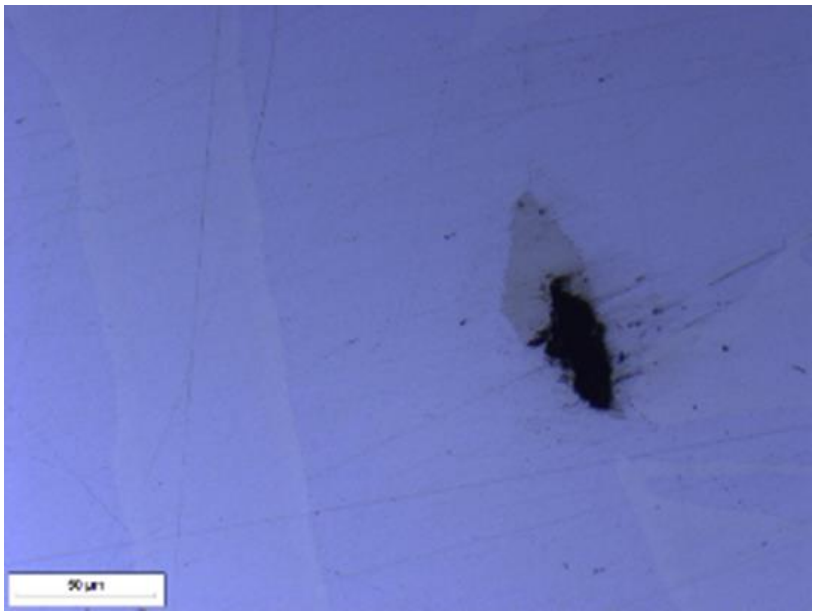

Figure 53 Zone II inclusion detail

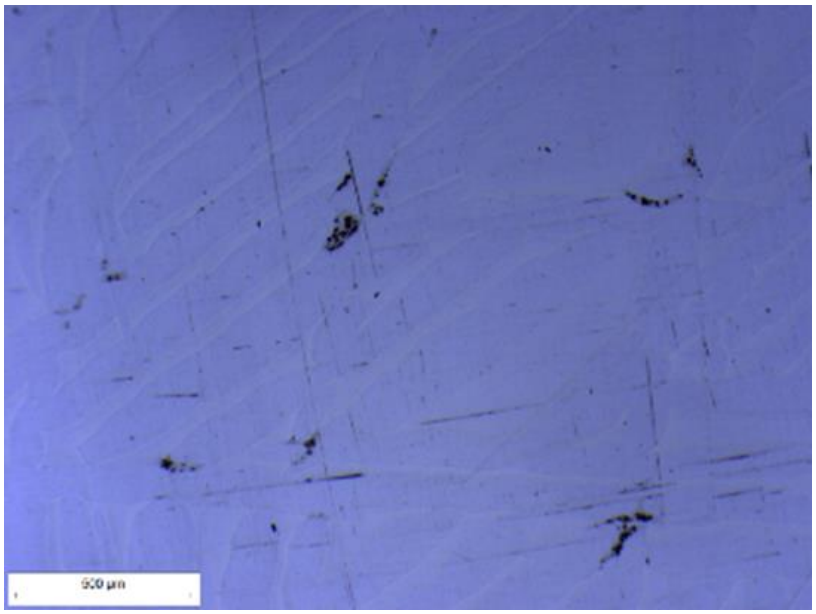

Figure 54 Zone I

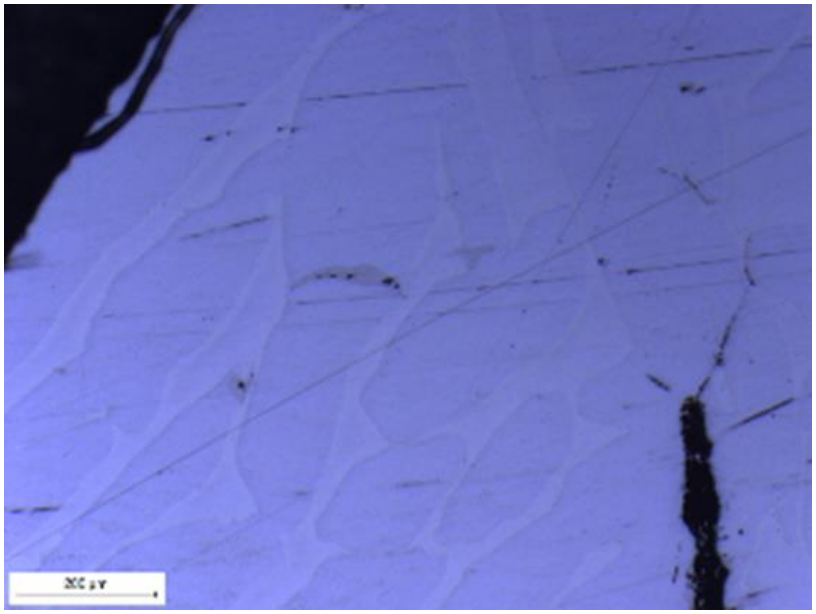

Figure 55 Zone IV

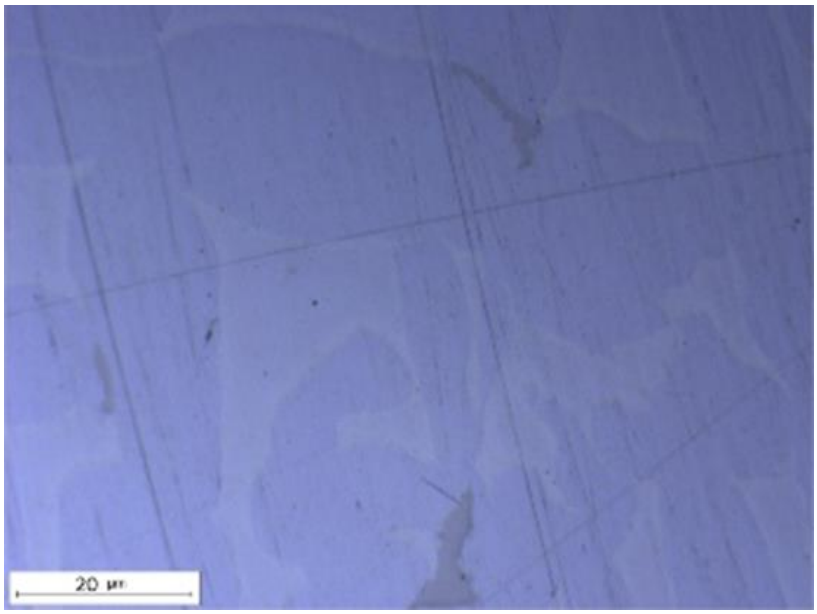

Figure 56 Zone III

3.2.1 Optical microscopy post-metallografic attack.

The Widmanstatter structure here is clearly present and it's fine and regular. So this is an octahedrite.

Figure 57 Carltown after nital

We can already notice that kamacite tends to develop around the big inclusions, impossible to observe through the microscope, because, being more fragile, they are ruined by the polishing procedure (fig 53, black circles).

Ferritic lamellae have all a similar band-width around 0,2mm (Off-Of W.S.).

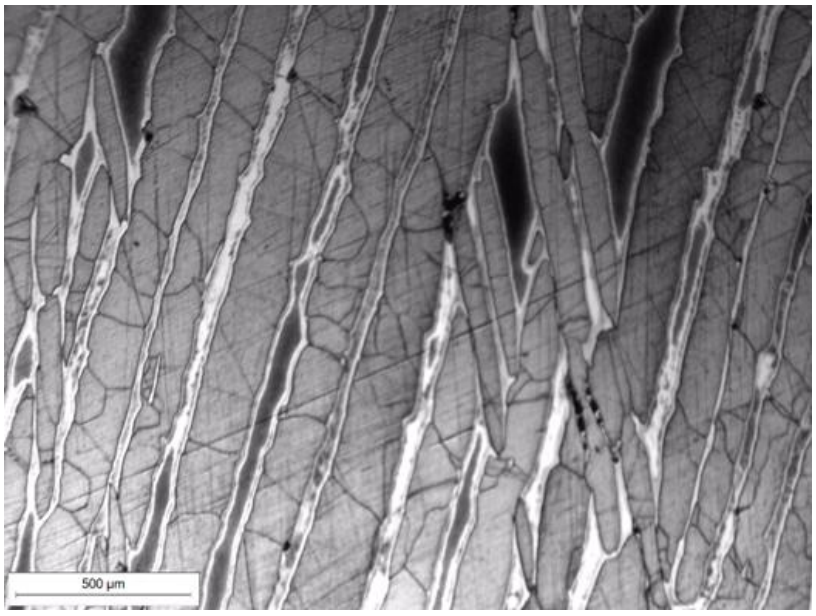

Figure 58 W.S. pattern Zone II

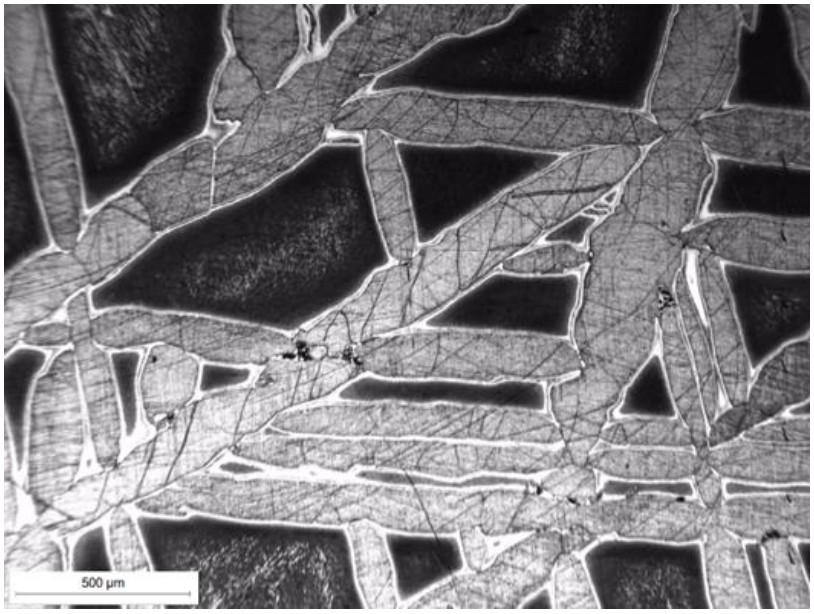

Figure 59 W.S. pattern Zone I

Metallic matrix

In the images above it is possible to see microstructure, some inclusions surrounded by kamacite (lighter), taenite (darker inside, lighter at the borders) and the grain borders that are present only in the ferritic phase.

In the picture below is possible to see details of taenite in a thin band, and in an alternance of extra thin-extra big bands; an inclusion (I), kamacite (III) and taenite (II), which has a complex structure and it's lighter on the border or completely light when the band is thin, and it's darker inside but presenting a "nebula" zone, where ferrite and austenite are mixed.

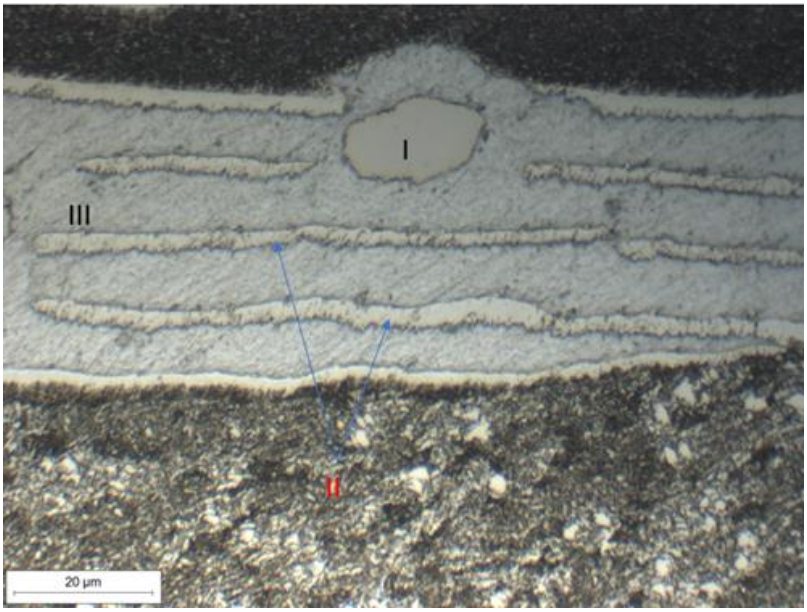

Figure 60 kamacite and taenite large bands

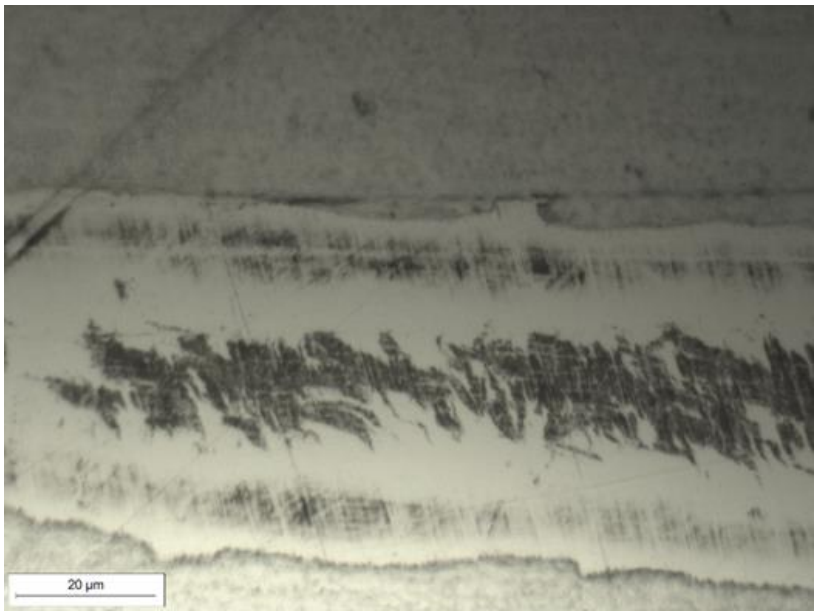

Figure 61 taenite thin band detail

Inclusions

Inclusions are extremely rare in taenite, while really common in kamacite. It is probably haxonite, due to its hardness and location.

Interesting to notice how the only inclusion is in the biggest taenitic phase and is next to a ferritic phase in formation; there are two kind of interpretation for this phenomenon:

1-ferrite, always tending to surround the inclusions, didn't have enough time for diffusion, without forming the kamacite band

2-ferrite in this case is a result of the heating of the meteorite, for cosmic/terrestrial heat. This is more likely due to the form and because is near to the border of the sample. Photo below.

The fact that the phase is ferritic is demonstrated by its hardness.

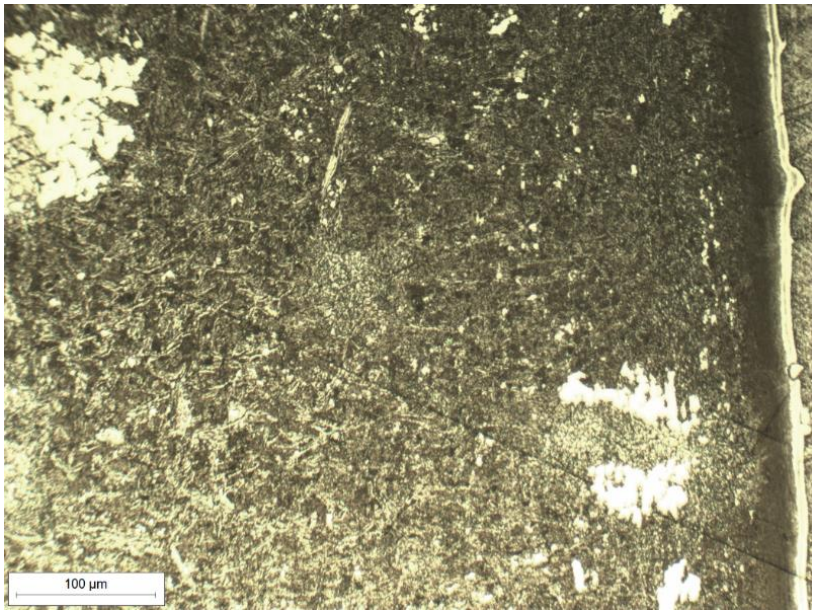

Figure 62 detail of bigger taenite band

In kamacite there are small to big inclusions, seemingly all of the same nature.

They are not so different by the inclusion type "B" seen in AVA, so it is probably schreibersite.

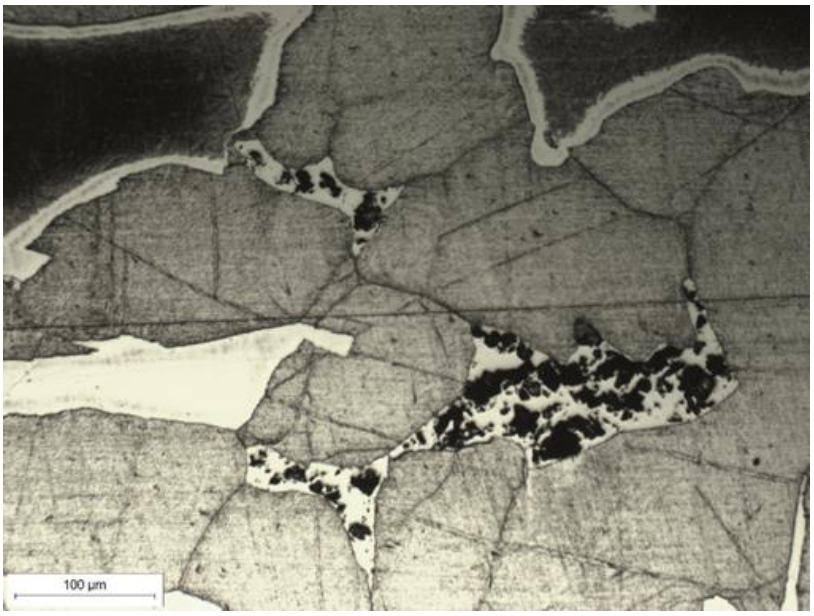

Figure 63 schreibersite inclusion surrounded by kamacite, pattern of grain borders starting from it

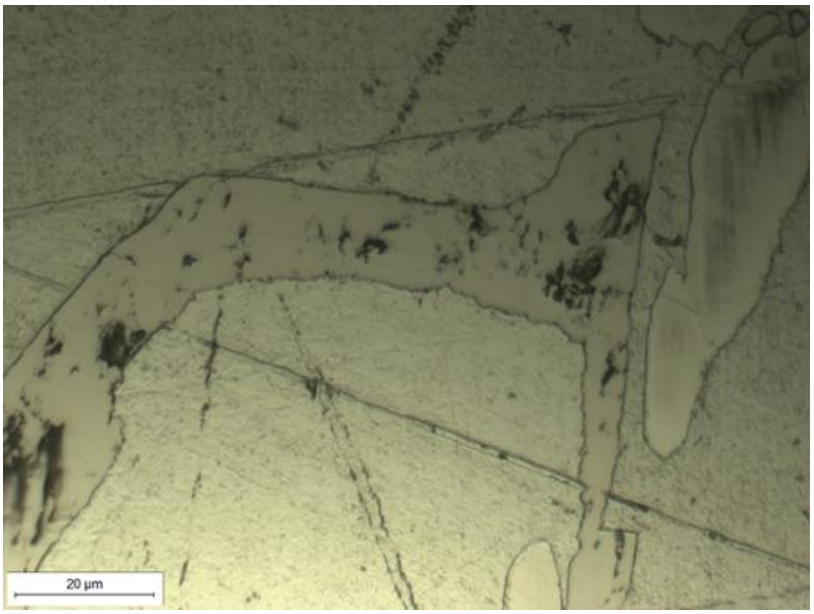

Figure 64 schreibersite inclusion

3.2.2 Vickers hardness tests

Matrix

In this case the approach used is to do some series of tests to check the ferritic and taenitic phase.

The average hardness of ferrite is far inferior to Ava sample, it is in fact of 186HV, the reason is probably a slower diffusion at lower temperatures.

Taenite instead has almost the same peak hardness, it would be pointless to do the avg value due to its variability, dependance on position in the band, and band-width.

Also in this case kamacite is less variable than taenite: kamacite stays mostly between 170HV and 200HV, while taenite can go from 250 HV to slightly more than 400 HV and tends to be harder on the borders and softer in the center, as the graphs below show; the small, white taenitic lamellae tend to have a middle value between the external and the internal part of the big taenitic phases: 325 HV. In the picture: tests on white, thin, taenitic lamellae.

Serie 1: test on a thin taenitic lamella, kamacite band and a medium taenite band.
Notice the homogeneity of kamacite hardness and the characteristic hardness profile of taenite.

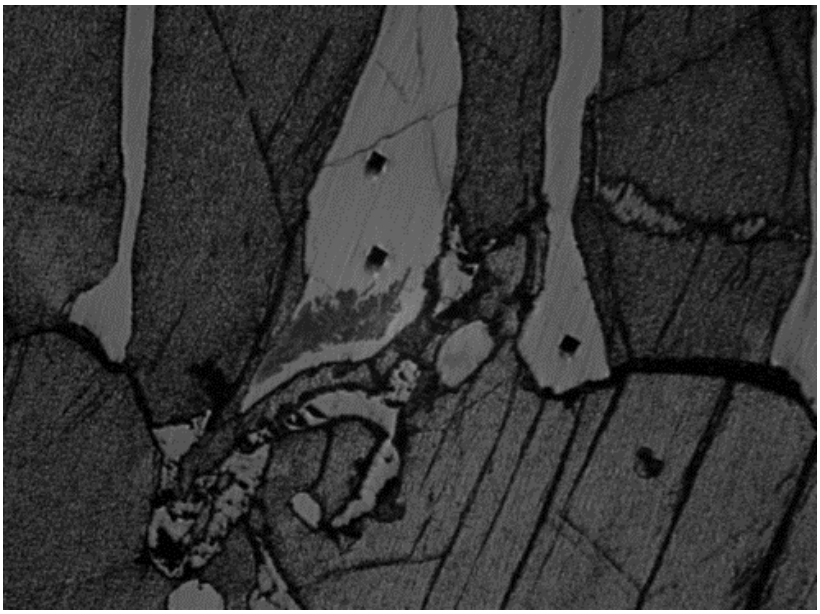

Figure 65 serie 1

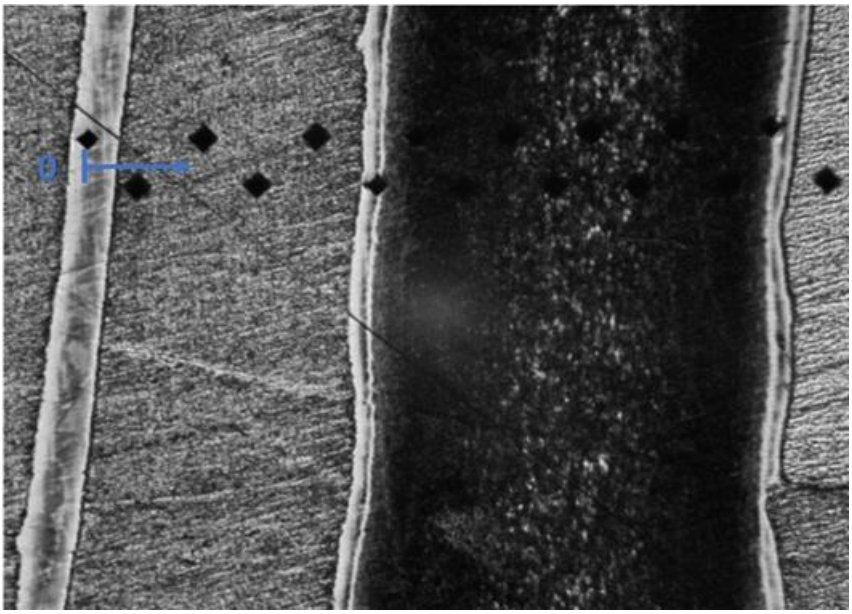

Figure 66 serie 1

serie 1 kamacite-taenite		µm	HV
	T	0	349
	K	3	187
		6	188
		9	184
		12	184
	T	15	311
		17,5	332
		20	311
		22,5	271
		25	271
		27,5	241
		30	298
		32,5	323
		35	332
		37,5	362
	K	40	192

HV

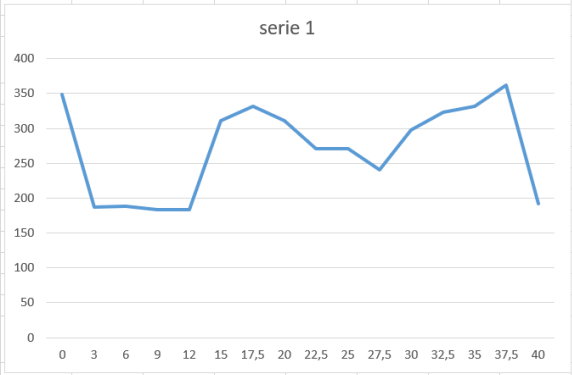

µm

Serie 2: test on a large taenite band. The pattern is the same, interesting to notice that in white zone is harder than full dark zone.

In the center there is a half ferritic-half taenitic phase softer, and high hardness variability.

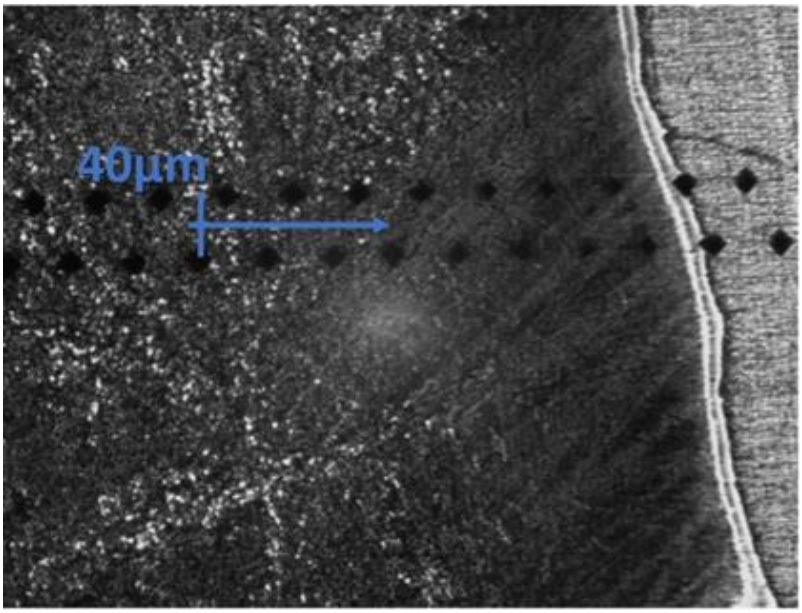

Figure 67 serie 2

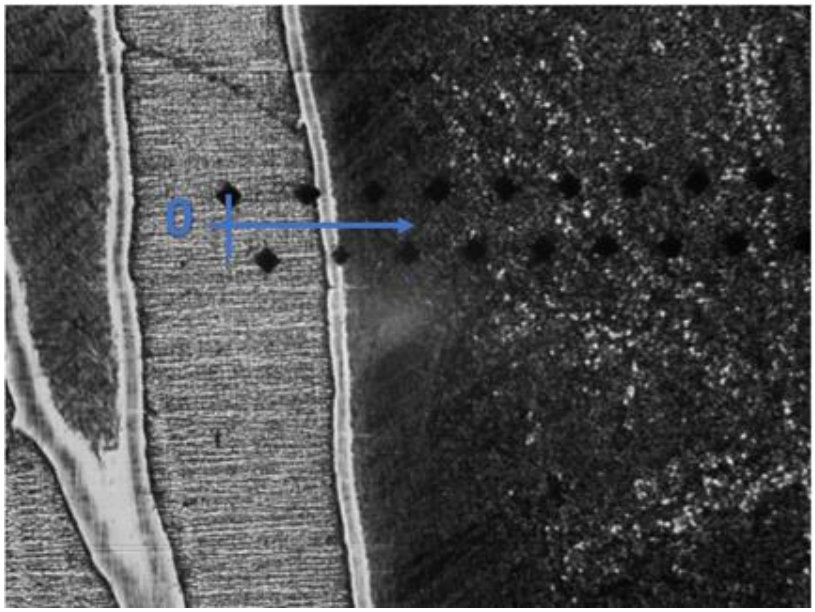

Figure 68 serie 2

serie 2 camacite taenite		µm	HV
	K	0	202
		2,5	198
		5	234
	T	7,5	381
		10	329
		12,5	271
		15	256
		17,5	268
		20	269
		22,5	251
		25	280
		27,5	295
		30	251
		32,5	290
		35	271
		37,5	280
		40	278
		42,5	278
		45	295
		47,5	282
		50	287
		52,5	290
		55	298
		57,5	339
		60	355
		62,5	366
		65	363
		67,5	359
		70	389
		72,5	405
		75	218
	K	77,5	216
		80	201
		82,5	189

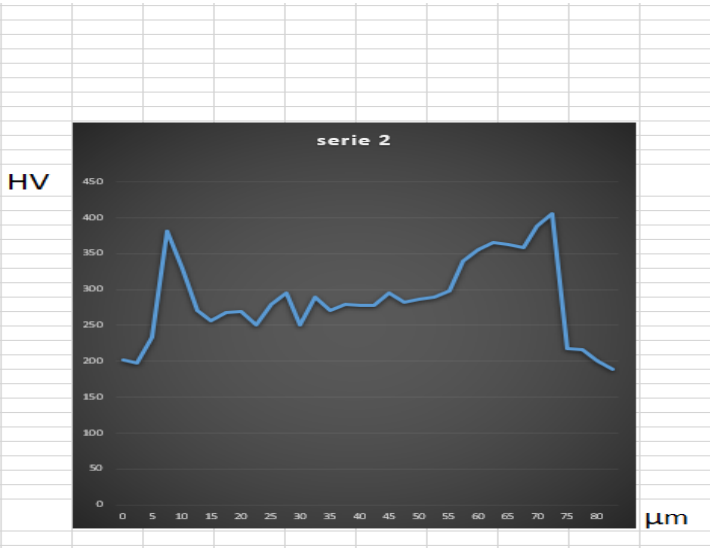

Serie 3: kamacite-small taenite band-kamacite-medium taenite band.

This test shows that if taenite is thin (5-20 µm) its hardness doesn't have a drop in the middle, but a peak, the drop is generally proportional to the band dimension.

serie 3 kamacite taenite		µm	HV
	K	0	192
		2,5	171
		5	202
		7,5	192
	T	10	320
		12,5	306
		15	401
		17,5	385
		20	323
		22,5	273
		25	170
		27,5	174
		30	184
		32,5	187
		35	179
		37,5	168
		40	180
		42,5	298
		45	352
		47,5	385
		50	332
		52,5	335
		55	345
		57,5	335
		60	355
		62,5	359
		65	393

HV

µm

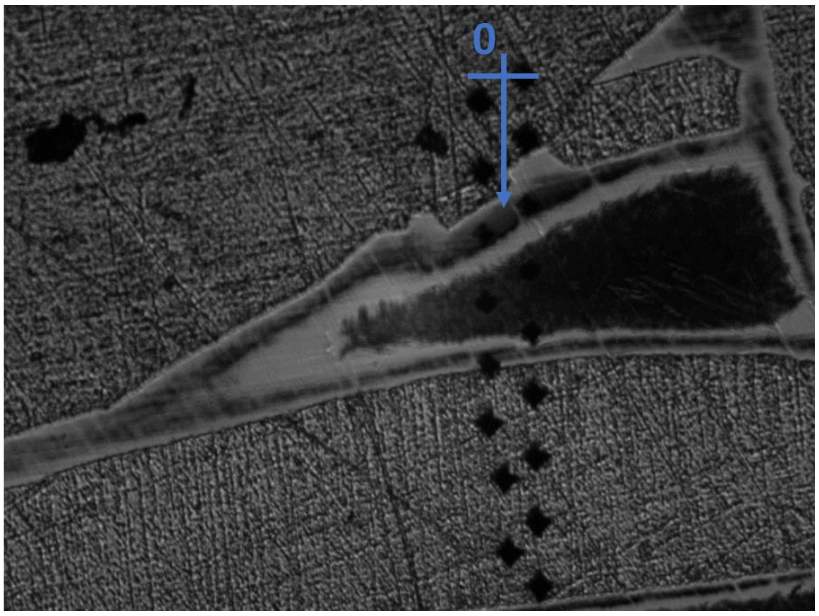

Figure 69 serie 3,1

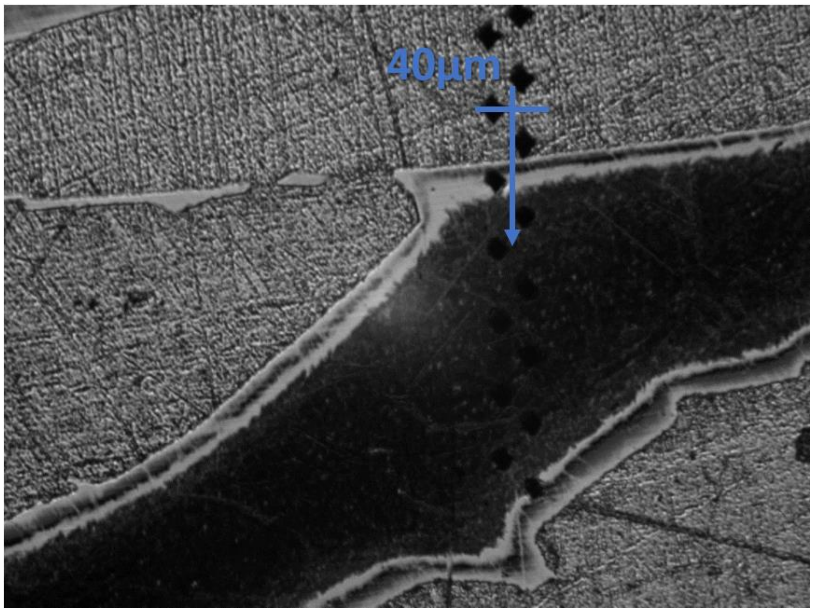

Figure 70 serie 3,2

Serie 4: this test is done on kamacite only.

We have a grain boundary and the dark part, which surrounds an inclusion, is harder of around 25-30 HV.

This could be because of the orientation, or because kamacite around the big inclusions forms before kamacite in the matrix.

The lighter grain tested near taenite is below avg of ~20 HV.

Further study on the subject would be useful also to figure out the cooling rate.

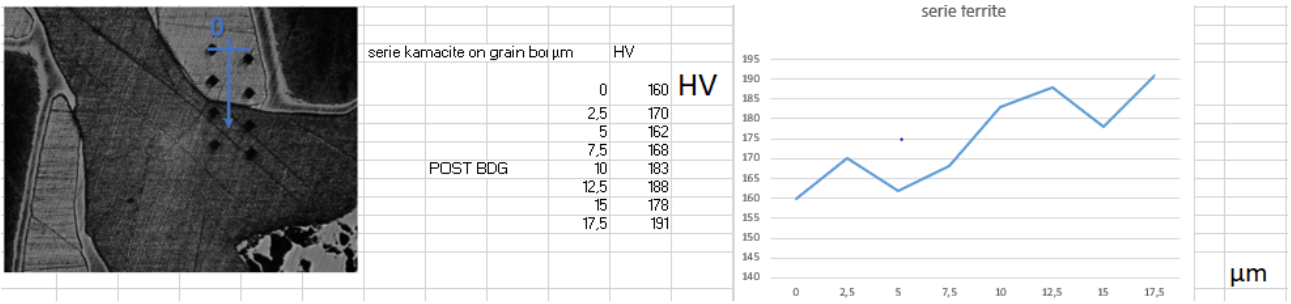

Inclusions

In kamacite there are many small-medium inclusions, of irregular form, with an average hardness of 735 HV, not so variable, fragile, so it is schreibersite.

The inclusion in taenite is more variable, probably because it is half melted haxonite, as is possible to see in the photo.

It is in a really big grain of taenite .

inclusion in taenite		
HV	avg	
644	616,5	HV
568		
450		
804		

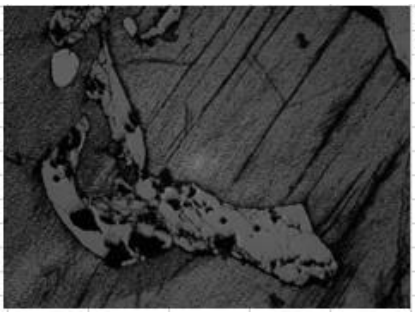

inclusions in kamacite		
HV	avg	
718	734,6	HV
816		
738		
653		
748		

3.3.3 Quantometer test

Out of 12 tests evenly distributed on the sample' surface, 2 were not considered.

The test number five because it was done partially (40%) on a big inclusion, which has a lot of Ni, doing a weighted avg around 24%. Considering a relatively high S concentration, a really high P concentration we can conclude that almost certainly the inclusion contains schreibersite and troilite. The high C percentage may be due to contamination or due to carbides. It can even be Ataxite stabilized by P.

Test number seven instead was done on a crack.

As expected from a medium-coarse octaedrite Ni is more than 13%.

Co and P are in the expected range.

This sample could be in the group IIICD/IB, or it could be without a group. It is impossible to know without knowing the concentrations of Ga, Ge and Ir in ppm.

Zn (>0,05%, in all tests) high percentage is to signal, there are no studies about the presence and influence on iron meteorites of this element.

MATRIX											Big INCLUSION		CRACK
Canale	1	2	3	4	6	8	9	11	12	MEDIA		5	7
C	0,417	<0,001	<0,001	0,015	<0,001	0,457	0,066	<0,001	0,521	0,3102		>2,300	1.600
Si	0,065	0,026	0,031	0,026	0,026	0,054	0,026	0,026	0,173	0,050333		0,075	1.682
Mn	0,009	0,007	0,007	0,007	0,007	0,014	0,007	0,007	0,007	0,008		0,045	0,007
P	0,135	0,062	0,112	0,071	0,074	0,236	0,053	0,049	0,141	0,103667		>1,500	0,598
S	0,025	0,004	0,004	0,004	0,004	0,021	0,004	0,002	0,03	0,010889		0,272	0,082
Cr	0,012	0,012	0,011	0,011	0,016	0,05	0,016	0,016	0,011	0,017222		0,177	0,011
Mo	<0,001	<0,001	<0,001	<0,001	<0,001	0,006	<0,001	<0,001	<0,001	0,001		0,028	0,001
Ni	13,409	13,542	13,312	13,382	13,128	13,639	13,115	13,202	14,089	13,42422		17.697	16.861
Al	0,045	0,004	0,005	0,004	0,008	0,017	0,006	0,008	0,036	0,014778		0,107	0,217
Cu	0,037	0,028	0,029	0,028	0,036	0,068	0,03	0,035	0,056	0,038556		0,461	0,071
Co	0,49	0,498	0,501	0,501	0,508	0,504	0,505	0,505	0,479	0,499		0,37	0,403
Nb	0,01	0,008	0,008	0,008	0,009	0,009	0,008	0,008	0,008	0,008444		0,008	0,007
Ti	0,005	0,003	0,003	0,003	0,004	0,008	0,003	0,003	0,004	0,004		0,023	0,007
V	0	0	0	0	0	0	0	0	0	0		0	0
W	0,01	0,005	0,003	0,014	0,008	0,016	0,006	0,004	<0,001	0,00825		0,056	0,015
B	<0,0005	0,0006	<0,0005	0,0006	0,0006	<0,0005	0,0006	0,0007	<0,0005	0,00062		0,0142	<0,0005
Pb	0,107	0,016	0,014	0,015	0,015	0,015	0,016	0,015	>0,200	0,026625		0,117	0,098
Sn	0,008	0,005	0,005	0,004	0,009	0,011	0,006	0,009	0,009	0,007333		0,089	0,02
Zn	>0,050	>0,050	>0,050	>0,050	>0,050	>0,050	>0,050	>0,050	>0,050	>0,050		>0,050	>0,050
Zr	<0,001	<0,001	<0,001	<0,001	<0,001	<0,001	<0,001	<0,001	<0,001	<0,001		<0,001	<0,001
Ca	0,0362	<0,0010	0,0023	0,0011	<0,0010	0,007	0,0015	0,0012	>0,0500	0,008217		>0,0500	>0,0500
As	<0,002	<0,002	<0,002	<0,002	<0,002	<0,002	<0,002	<0,002	<0,002	<0,002		<0,002	<0,002
Bi	0,001	0,009	0,011	0,01	0,01	0,002	0,009	0,007	0,002	0,006778		<0,001	<0,001
Fe	85,075	85,688	85,861	85,816	86,057	84,766	86,044	86,021	83,710	85,44867		68.542	77.656

Figure 71 Carltown, quantometer test, concentrations of the different alloy elements.

3.3.4 Carltown XRD.

The XRD test on this sample shows clearly peaks referring to strongly oriented kamacite, and taenite. The peaks referring to austenite are not clearly centered, this can be due to the fact that taenite is not only retained austenite, but also a mix of FeNi tetragonal, small kamacite grains, etc.

As in the previous case the nature of some small peaks are unclear, the reason is probably that the big inclusion are composite of many types of crystals, while the small are too small to be detected in this way.

There may be FeNi3, unexpected in literature for the meteorites. Further investigation are suggested.

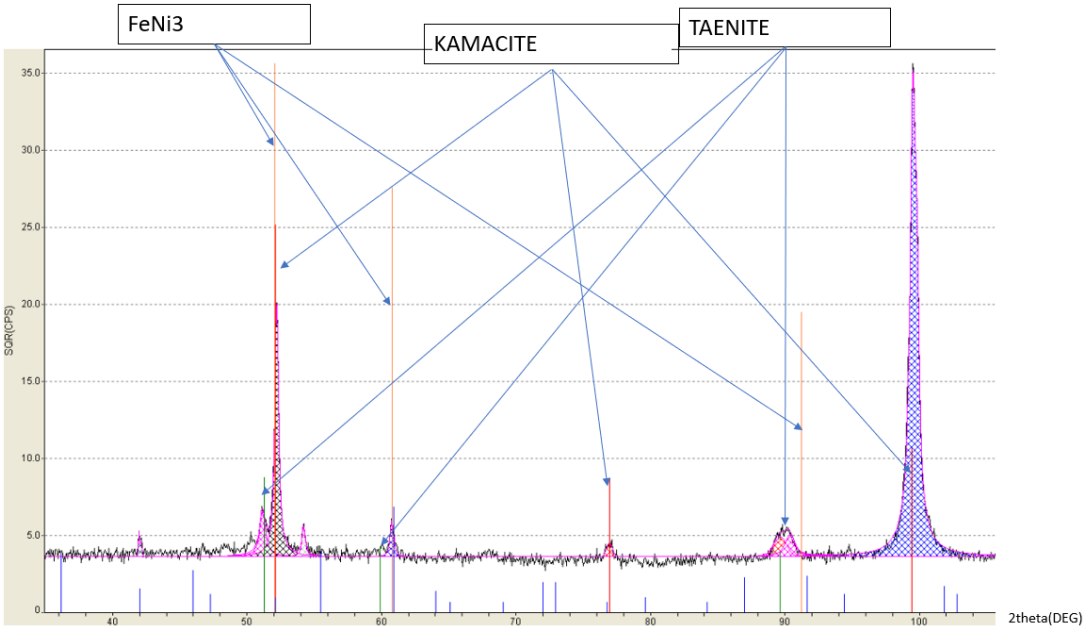

Figure 72 XRD output results, source: POLITO library.

4. FINAL MICROSTRUCTURAL CONSIDERATIONS

4.1Metal matrix

Experimental graphs are used to establish the microstructural evolution:

-Ava→Y→[T>640°C]α(not nucleating)+Y→[T<640°C]α2(martensitic)+Y→[T<570°C]α(mainly)+Y (see fig. 6, on the right, there are 2 possible mechanism, the one proposed is more likely according to Yang and Goldstein)

Probably taenite is residual but shrinks between 640°C and 360°C, then widens below 360°C, not for sure, **should be investigated experimentally**, as it is possible to see in the picture below. Ferritic part of plessite probably nucleates below 570°C in taenite.

-Carltown→Y→ [T<630°C]α(not nucleating)+Y→[T<460°C]α+Y+Ph.

By its big, even if not clearly visible, cloudy zones islands, its cooling rate seems to be tens-hundreds°C/My.

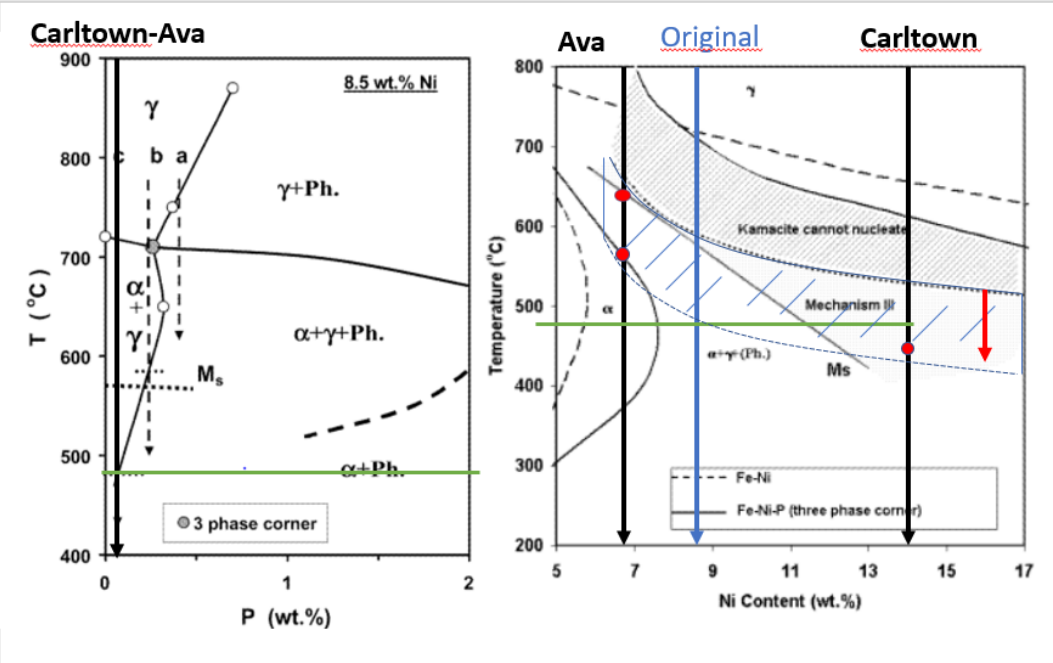

Figure 73 showing the method to establish the structural evolution of the samples, on the left the graph was done by Doan, Goldstein (1970) on the right is from "the formation of W.S. in meteorites" by Yang, Goldstein (4)

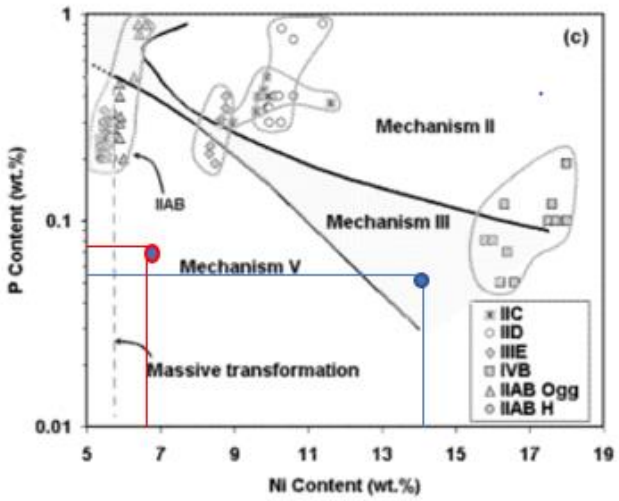

carltown

ava

Figure 74 Yang, Goldstein, "the formation of W.S. in meteorites"(4)

4.2 Inclusions

Inclusions follow characteristic patterns:

-Ava:

-Few Inclusions (7-8) with many grain borders around tend to conglomerate in big (~1-2mm width) clusters, composed mainly by schreibersite and cohenite, some troilite and few Chromite (small, cubic crystals).

-Some Schreibersite (~100 inclusion of various size) and more rarely Troilite is crushed between grain borders, up to 100μm long but 3-4 μm width for schreibersite, in big dark nodules for troilite.

-A lot of small prismatic Rhabdite (~1000 inclusion around 20-50 μm widht), same composition of schreibersite but with 50%Ni, few chromite.

-Many small inclusions not clearly observed.

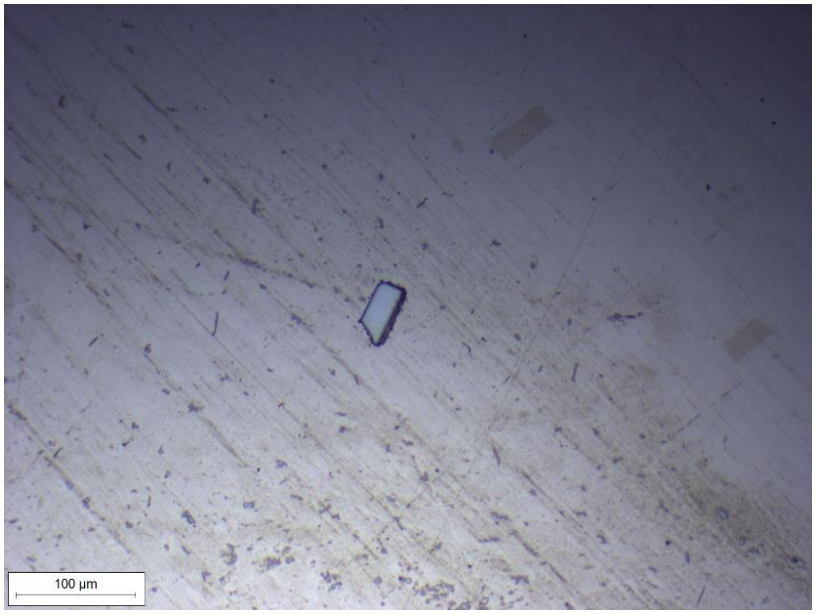

Figure 75 Ava a rare chromite inclusion, probably due to the nature of the polishing procedure one of the rare survivor.

Carltown:

-4 really big (3-15 mm surface area) inclusion, unobservable because crushen in big grain borders-cracks, but according to spectrometer analysis, with schreibersite, troilite, cohenite.

-Few hexaenite, similar to cohenite medium (0,5 mm width) in big taenite residuals.

-many grain borders and small (up to 0,01mm^2) schreibersite inclusions.

In my opinion, meteoroid original size is a further parameter that deserves to be investigated with physical equations for its influence on microstructural evolution and cooling rate of the available samples. Schreibersite inclusions are interesting given their omnipresence and the proved role of Phosphides in the transition process of the austenite.

5.CONCLUSIONS

General conclusions

The samples studied in this thesis follows 2 different microstructural evolutions, the difference it is due to their composition and microstructure <"Ava"→esaehdrite><"Carltown"→octaehdrite>.

To study their cooling rates an accurate investigation with "central taenite Ni% and band width method" and "cloudy zone method", using respectively "microprobing technology" and "SEM technology" is required to interpolate the methods to find out cooling rates. This is a suggestion for possible further analysis.

The theory of protoplanet seems to be confirmed by the fact that meteorites estimated cooling rates are 0,5-325K/My (5)(6).

Assuming:

- the samples are at low T before the fall on Earth; a fact up to now, as confirmed by observing the samples and reading the main studies(3).
- a uniform cooling rate; as suggested and proven by Goldstein and others studies(5)(6), that had compared different cooling rate methods that work at 2 different temperatures <250°C Cloudy zone method-400°C Ni% method>, assumed but yet to be certainly demonstrated, because there could be unknown factors altering heat release in space,
- that the upper limit is 900°C and lower limit is 400°C, which is the interval of the transformations studied in order to find the cooling rates.

Now we can compute roughly:

T[K] /CR(Cooling Rate)[K/My]=MAOC(Age of Collapsing, minimum)[years ago]=400-900[K]/~300=1,3-3 My.
T[K] /CR(Cooling Rate)[K/My]=MAOC(Age of Collapsing, maximum)[years ago]=400-900[K]/~0,5=800-1800 My.

the most far away event of collapsing protoplanets in time is hundreds of millions-billions years ago, so the event is cyclical and may date back to the Solar System formation, considering that we don't know the cooling rates above 900 K and if the case occurred, but not recent (at least 1,3My ago, see calculations above).

Inclusions-chemicals

The inclusions follows a characteristic pattern, with a correlation in size ratios in the 2 samples analyzed but with slightly different order of magnitude, almost equal in composition: summarizing big clusters of carbides and phosphides alloying with Ni and Fe in ordinate crystalline structure, hard and brittle.

This big Cohenite and Schreibersite inclusions are at the conjunction of many grain boundary or, when they are really big, cracks. a lot of small Schreibersite inclusions are intergranular. Troilite is omnipresent but in lower percentage and mostly in dark nodules(3).

This inclusions of Carbides and Phosphides have both been proven to melt at austenitic temperatures, and to be unstable in standard terrestrial conditions(3).

Troilite (FeS) is unstable at terrestrial environment conditions but is already present at austenitic temperatures.

P, the main element in matrix inclusions has been proven to be critical for the microstructural evolution, together with Ni, so it is possible to assume that clusters forms before than small inclusions that are mainly schreibersite (phosphide) and have a role in transport of Ni in Fe to kamacite-taenite interface.

The smaller the inclusions the bigger the Ni%. Almost all inclusions , except for some rare carbonic haxonite, likely caused by terrestrial impact pressure, are in kamacite according to the observations.

"Ava", which nucleates ferrite at higher temperatures than "Carltown", has more regular inclusions in general (**e.g. intergranular microprismatic rhabdites inclusions, that may be a leftover of taenite, since they contain high Ni%(3) and have a rhomboidal form, according to growth model of kamacite in taenite,** according to the observations).

It is important to consider that this 2 samples have low P%(~0,06%wt), which means that the nucleations of kamacite from austenite starts late, in particular if the Ni% is high (Carltown), so it would be interesting to study the patterns of inclusions in samples that have medium-high amount of P.

In both the samples there is an high % of Zn, it is probably substitutional in the metal matrix, according to the small variance in the spectrometer tests.

Metal matrix and suggestions for possible studies

The microdurometer tests proves that hardness is in solid positive correlation to Ni%, in particular in taenite. The pattern in taenite is lower Ni-lower hardness at the band center, higher Ni-higher hardness at the interface with kamacite while kamacite is mostly uniform both in hardness and in Ni%.

Microprobing for Ni% wasn't done in the experimental phase, but the pattern is surely similar according to many studies (3)(5). If correlation will be formalized mathematically, the cooling rates could be possibly estimated more simply by hardness in kamacite-taenite.

It would be interesting to study the effect of terrestrial-atmosphere impact more in detail, examining the slightly altered borders of the samples and imposing the right border conditions, e.g. temperature reached, dynamic pressure, speed, metallic alloy thermal conductivity to study the complex dynamic-kinematic-thermodynamic problem of the seconds before the impact on the crust.

An experiment that would be interesting would be to slowly (e.g. 1-10 years) cool down different Iron-Nichel-Phosphorus synthetic alloys, to check if the cooling rate estimation methods are reliable or if other parameters are to keep into account for the thermal diffusion theory.

In my opinion, observing the slightly altered samples borders and considering thermal conductivity, most Fe-Ni parts of meteorites, together with other non-metallic elements, are not significantly affected by air dynamic pressure, while other elements may -or may not- evaporate. A quantic study of light emitted by falling meteorites in relation to size would clarify, but it's extremely difficult to apply.
To study the eventual presence of other elements and the size of the asteroids we must explore and/or observe space.

6.BIBLIOGRAPHY

- *(1) J. Yang, J. I. Goldstein, E. R. D. Scott, 2007. "Iron meteorite evidence for early formation and catastrophic disruption of protoplanets", Nature 446, 888-891.*
- *(1) J. I. Goldstein, E. R. D. Scott, N. L. Chabot, 2009. "Iron meteorites: Crystallization, thermal history, parent bodies, and origin", Chemie der Erde 69, 293-325.*
- *(2) M. K. Weisberg; T. J. McCoy, A. N. Krot (2006). "Systematics and Evaluation of Meteorite Classification).*
- *(3) W. F. Buchwald, 1975 "Handbook of Iron Meteorites", University of California Press.*

- *(4) J. Yang, J. I. Goldstein, 2004. "The formation of the Widmanstätten structure in meteorites", -NASA-Meteoritics & Planetary Science 40, 239–253.*
- *(5)W. D. Hopfe, J. I. Goldstein, 2000. "The metallographic cooling rate method revised: application to iron meteorites and mesosiderites", Meteoritics & Planetary Science 36, 135-154.*
- *(6)C. W. Yang, D. B. Williams, J. I. Goldstein, 1997. "A new empirical cooling rate indicator for meteorites based on the size of the cloudy zone of the metallic phases", -NASA-Meteoritics & Planetary Science 32, 423-429.*
- *(7)J. I. Goldstein, J. Yang, E. R. D. Scott, 2014. "Determining cooling rates of iron and stony-iron meteorites from measurements of Ni and Co at kamacite-taeinite interfaces", Geochimica et Cosmochimica Acta 140, 297-320.*
- *(8)John T. Wasson, Peter Hoppe, 2012. "Co/Ni ratios at taenite/kamacite interfaces and relative cooling rates in iron meteorites", Geochimica et Cosmochimica Acta 84, 508-524.*
- *(9)* Heather C. Watson, Frank Richter, Ankun Liu, Gary R. Huss, 2016. "Iron and nickel isotope fractionation by diffusion, with applications to iron meteorites", Earth and Planetary Science Letters 451, 159-167.
- *(10)C. R. Chapman, D. Morrison, and B. Zellner, Surface properties of asteroids: A synthesis of polarimetry, radiometry, and spectrophotometry, Icarus, Vol. 25, pp. 104 (1975).*
- *(11) Article by Andrew Zaleski in the Fortune Italy magazine - January 2019.*

- *(12) "Scientific American" August 28th 2017.*
- *(13)S. J. Bus, F. Vilas, and M. A. Barucci, Visible-wavelength spectroscopy of asteroids, in Asteroids III, pp. 169, University of Arizona Press (2002).*
- *(14)Google Patent search +*
- *(15) (Geothermal gradient adapted from Boehler,R.(1996). Melting Temperature on the Earth's Mantle and Core: Earth's thermal structure. Annual review of Earth and planetary science,24-(1),15-40,estimated)*
- *(16) Determination of the interdiffusion coefficients in the Fe-Ni and Fe-Ni-P Systems Below 900 °C,D. C. Dean & J. I. Goldstein*
- *(17) Creative commons*

Ringraziamenti e auspici:

Ringrazio I Professori Paolo Matteis e Giorgio Scavino per avermi dato l'opportunità di studiare questi campioni dallo spazio, sperando che presto potremo adattarci senza paura a quelle condizioni con la tecnologia e l'ingegno e capire pezzo dopo pezzo la sua complessità enorme, come si evince da queste pagine che ne studiano solo dei piccoli frammenti.

APPENDIX

AVA

Pre-M.A. observation

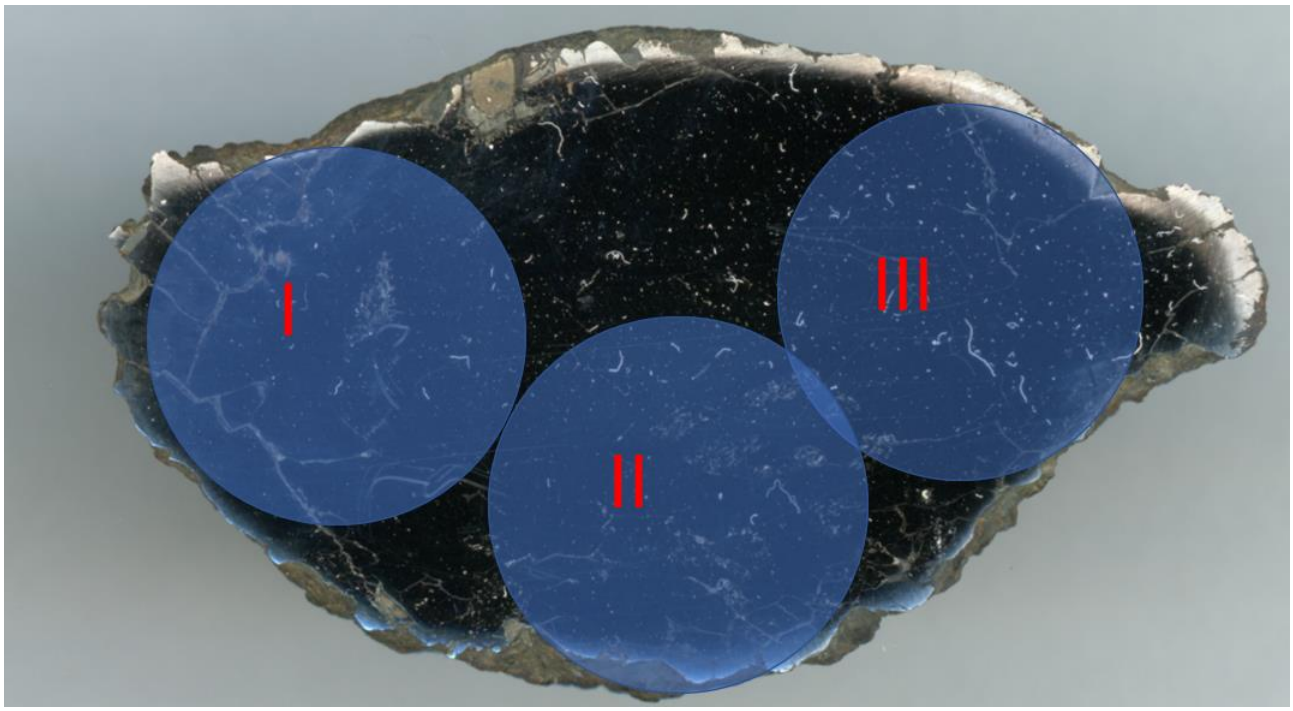

Zone I

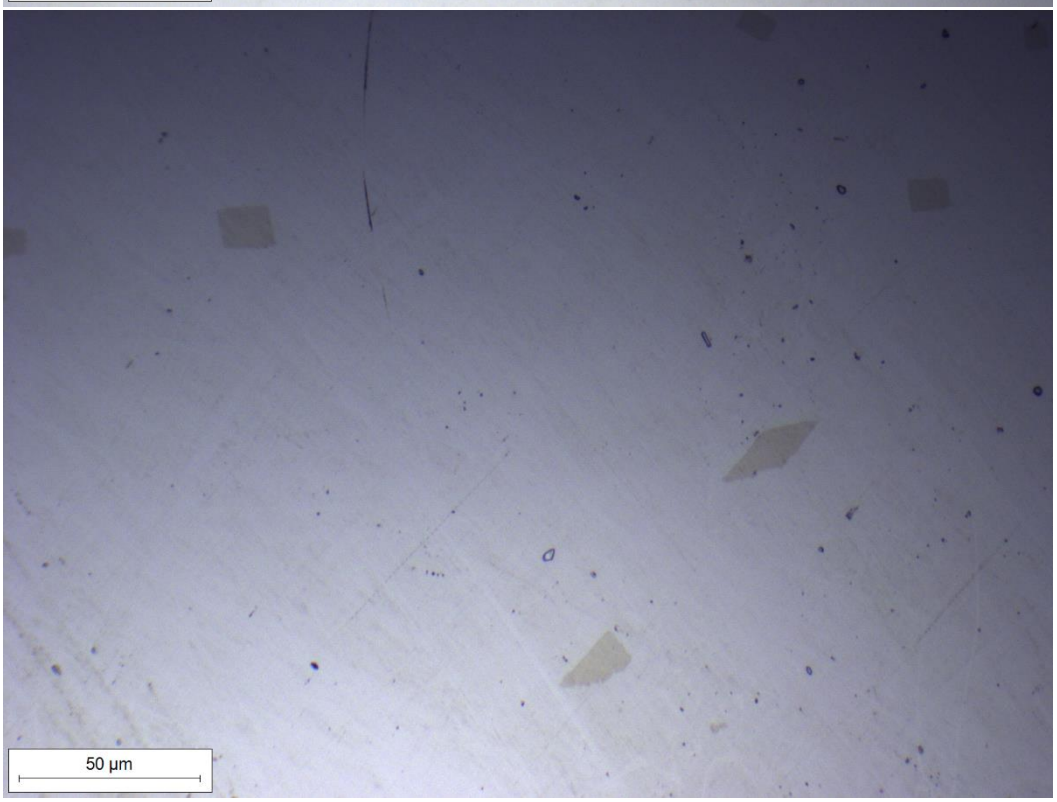

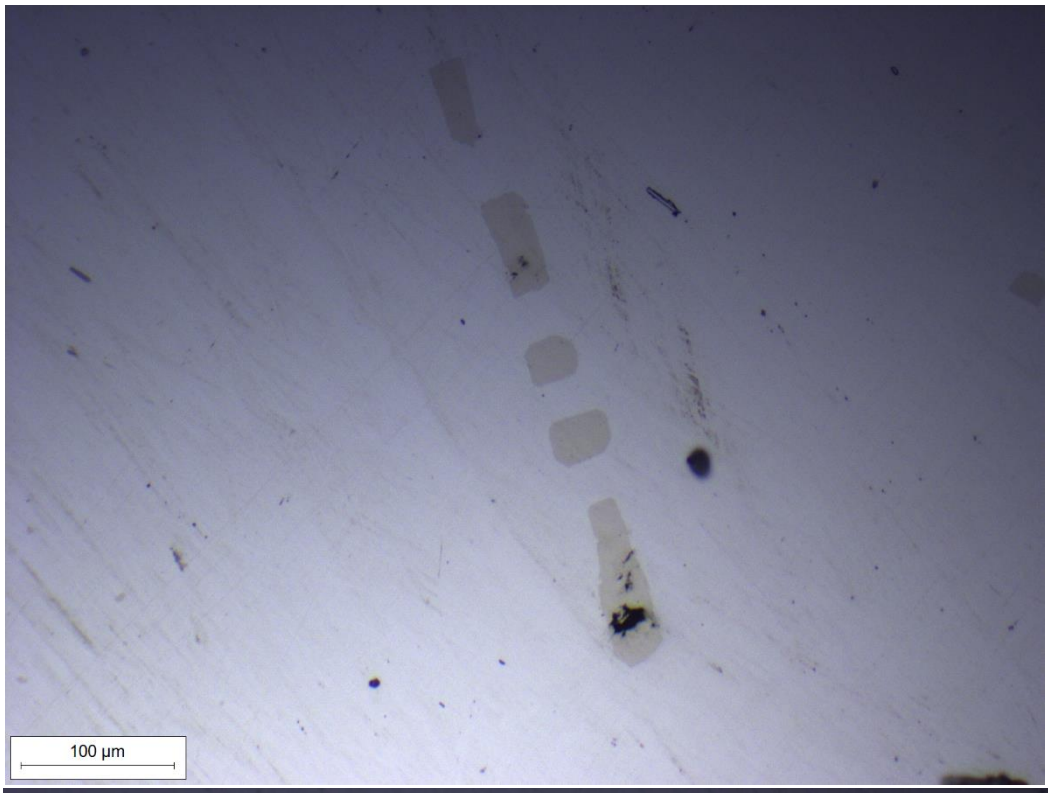
100 µm


100 µm

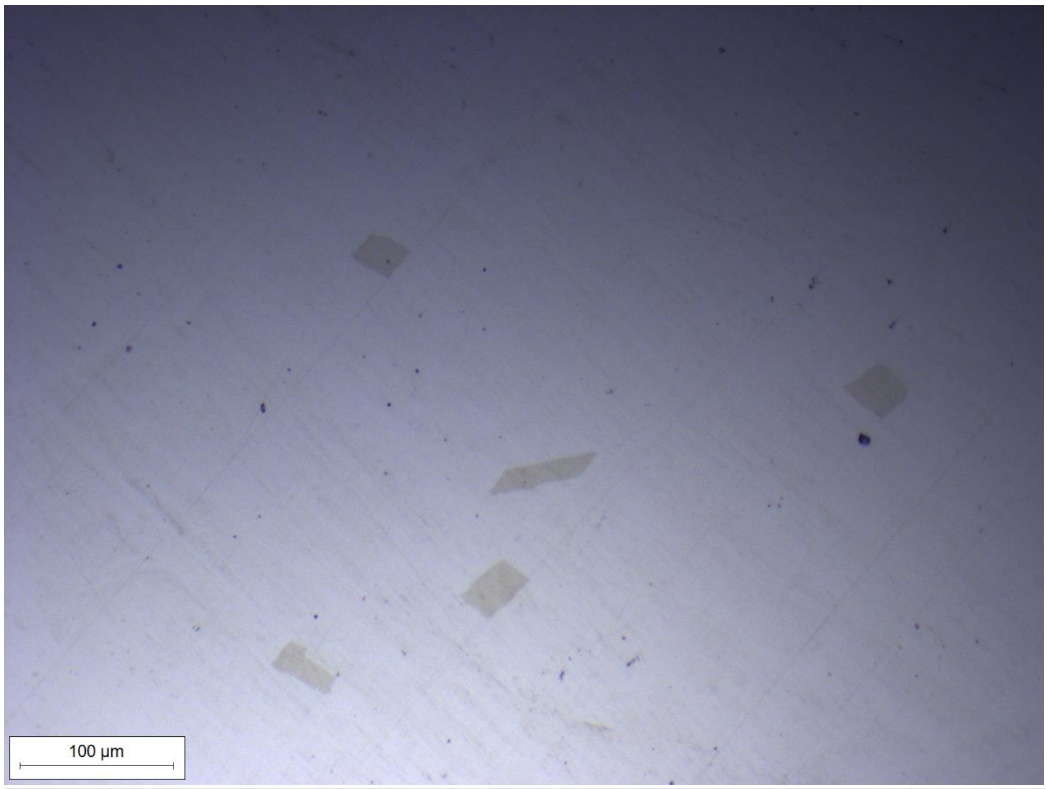
100 µm

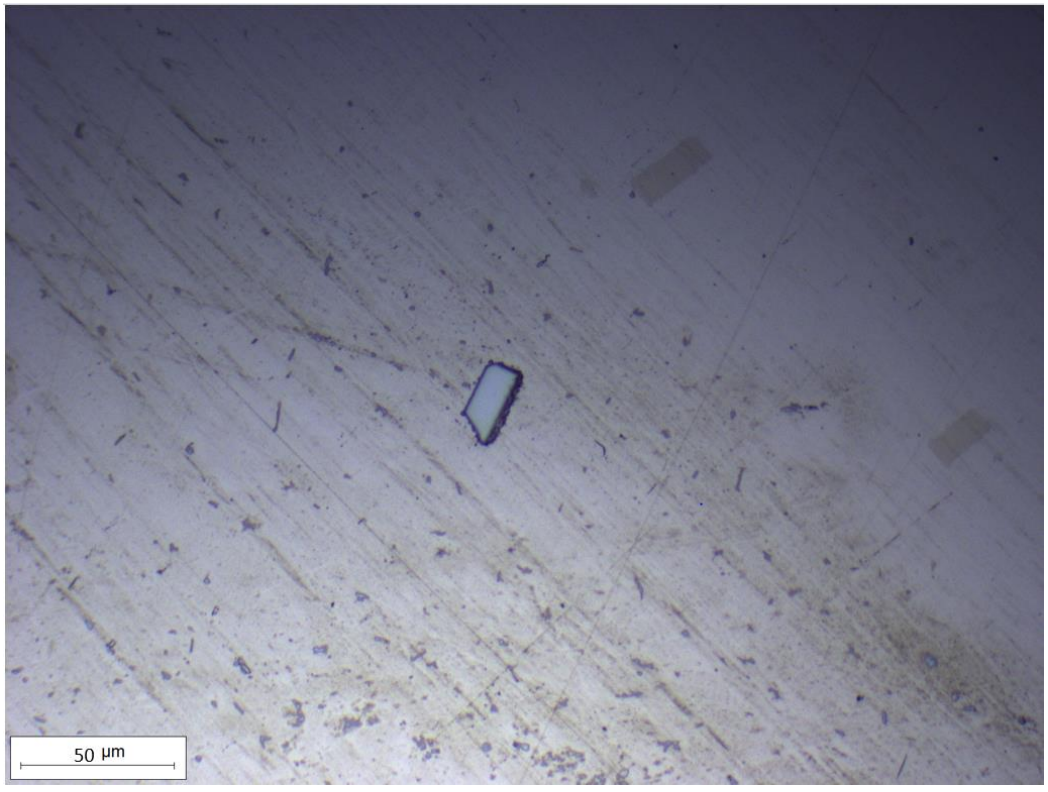
50 µm

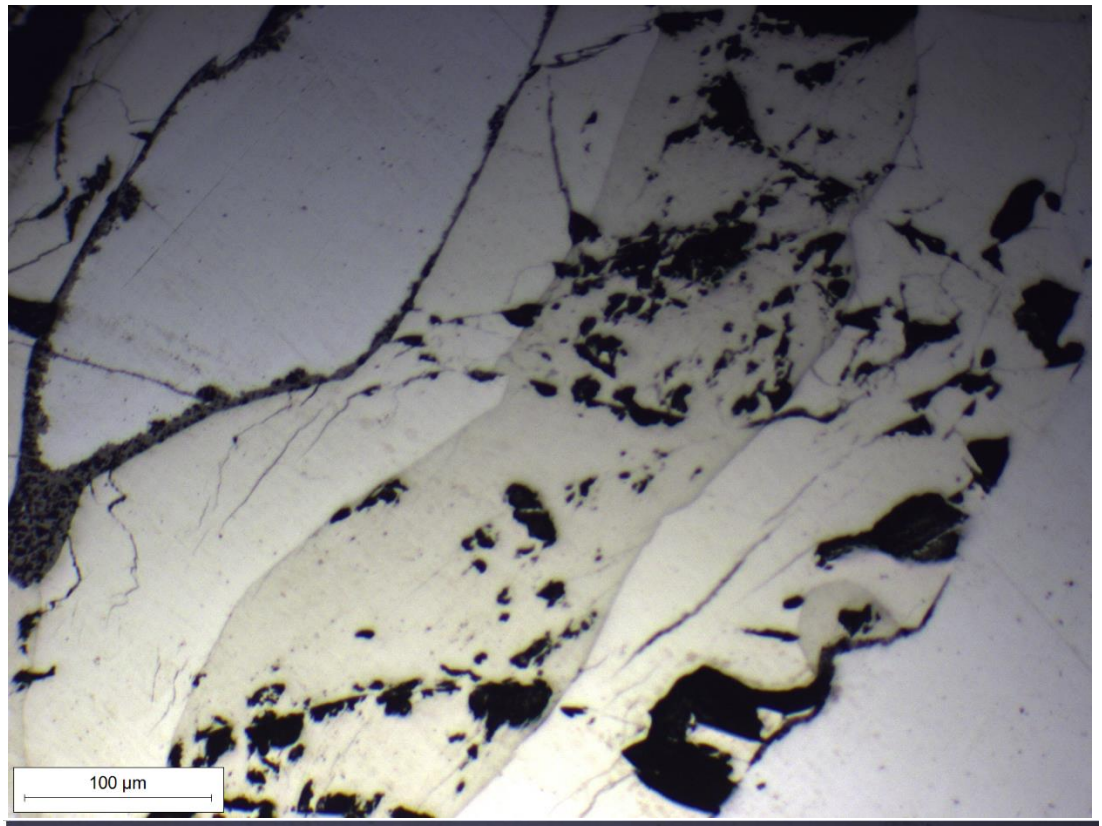
100 µm


200 µm

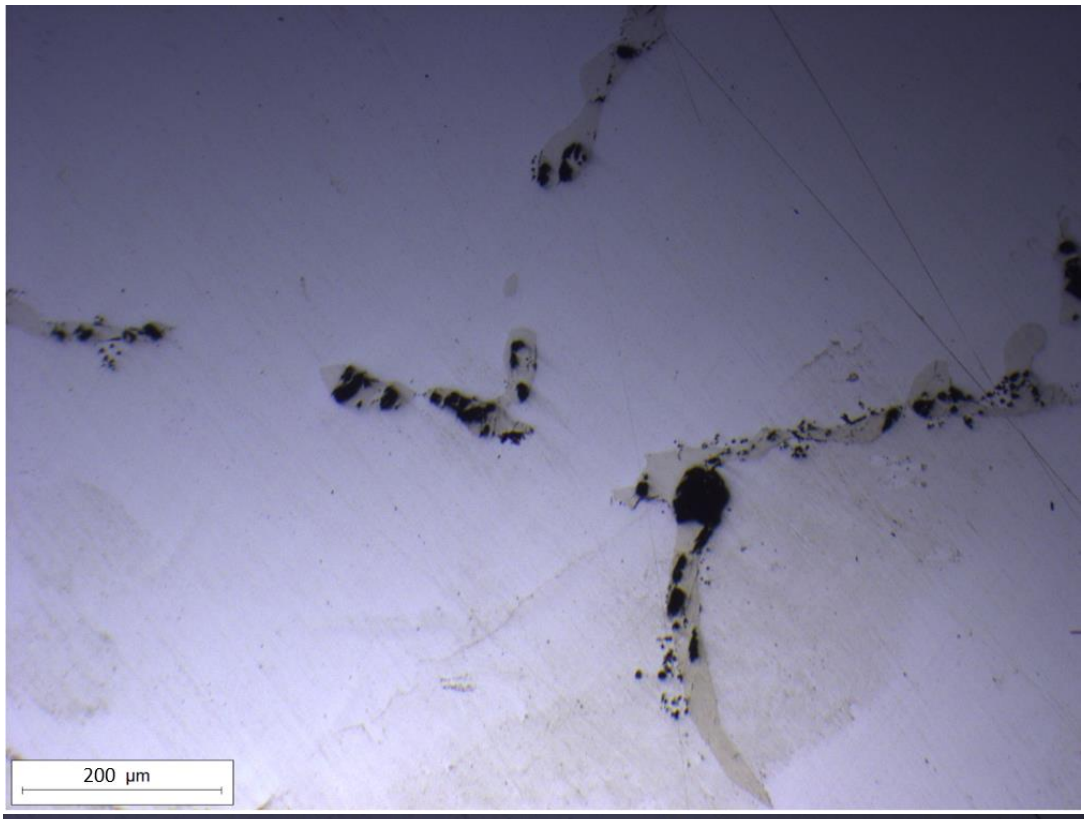
200 µm

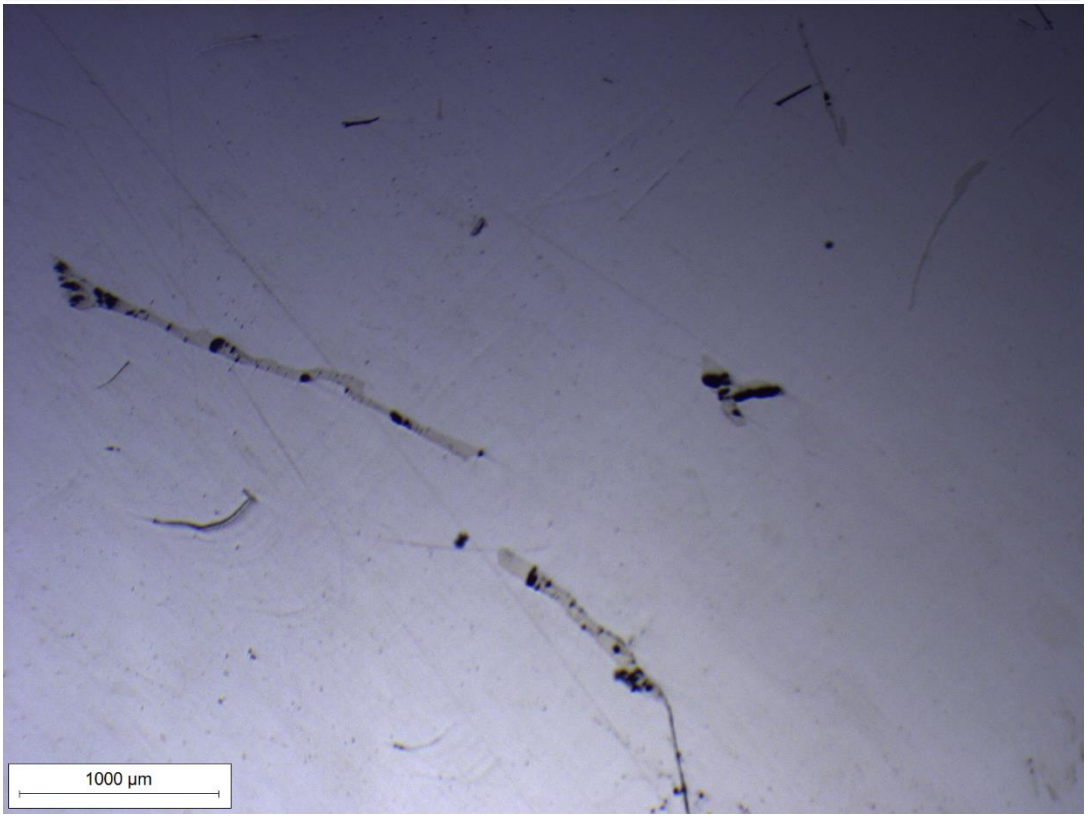
1000 µm

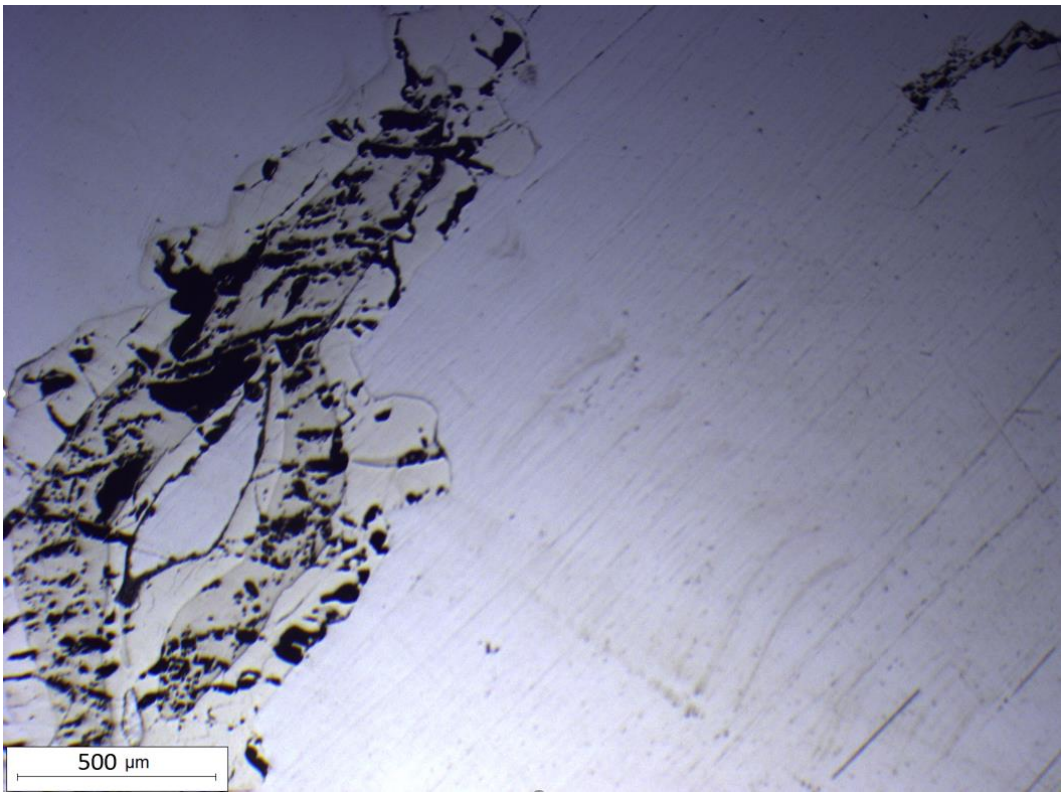
500 µm

Zone II

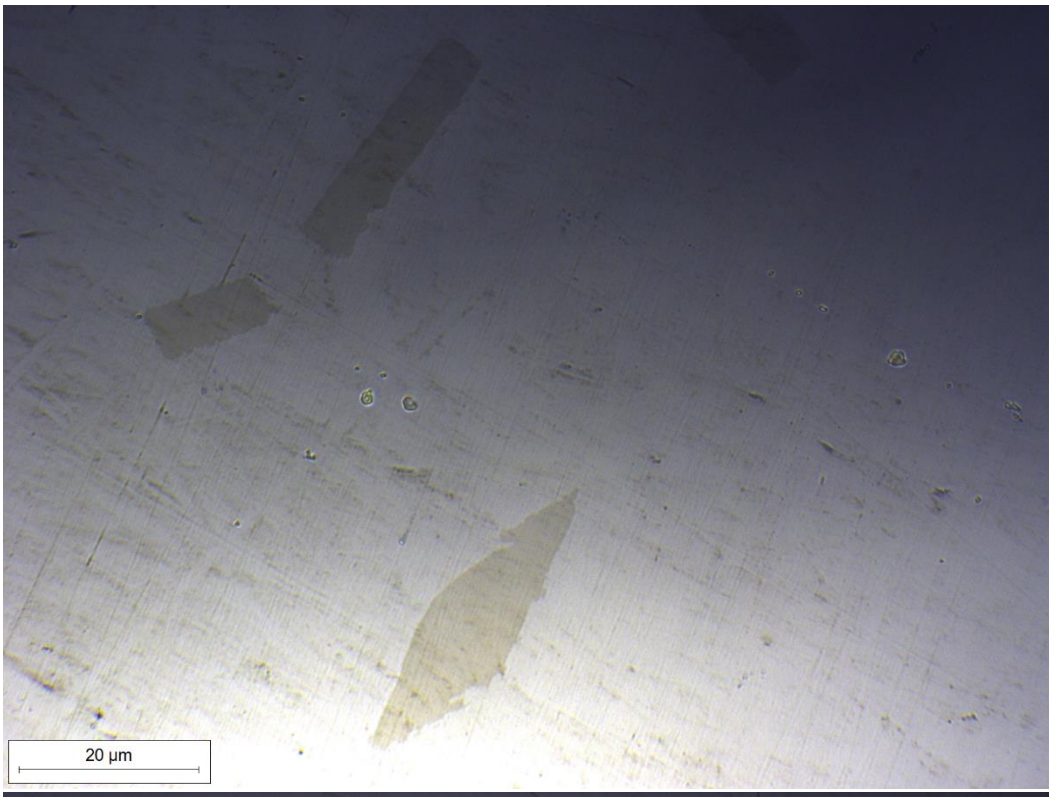

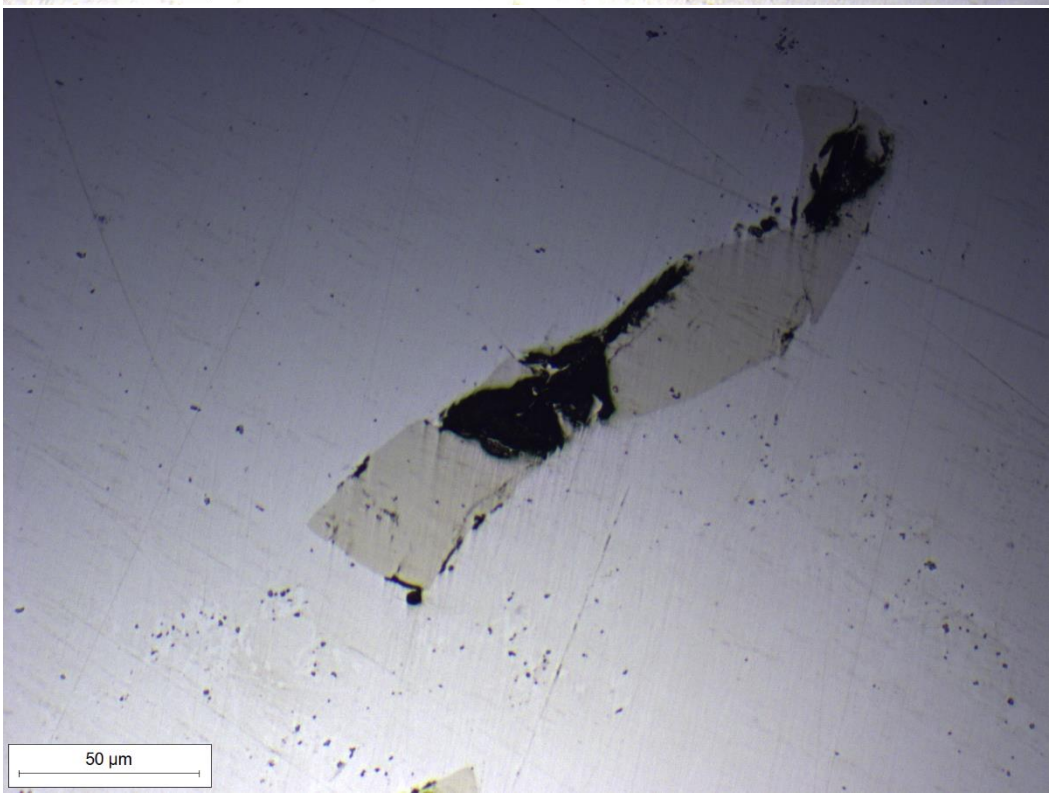

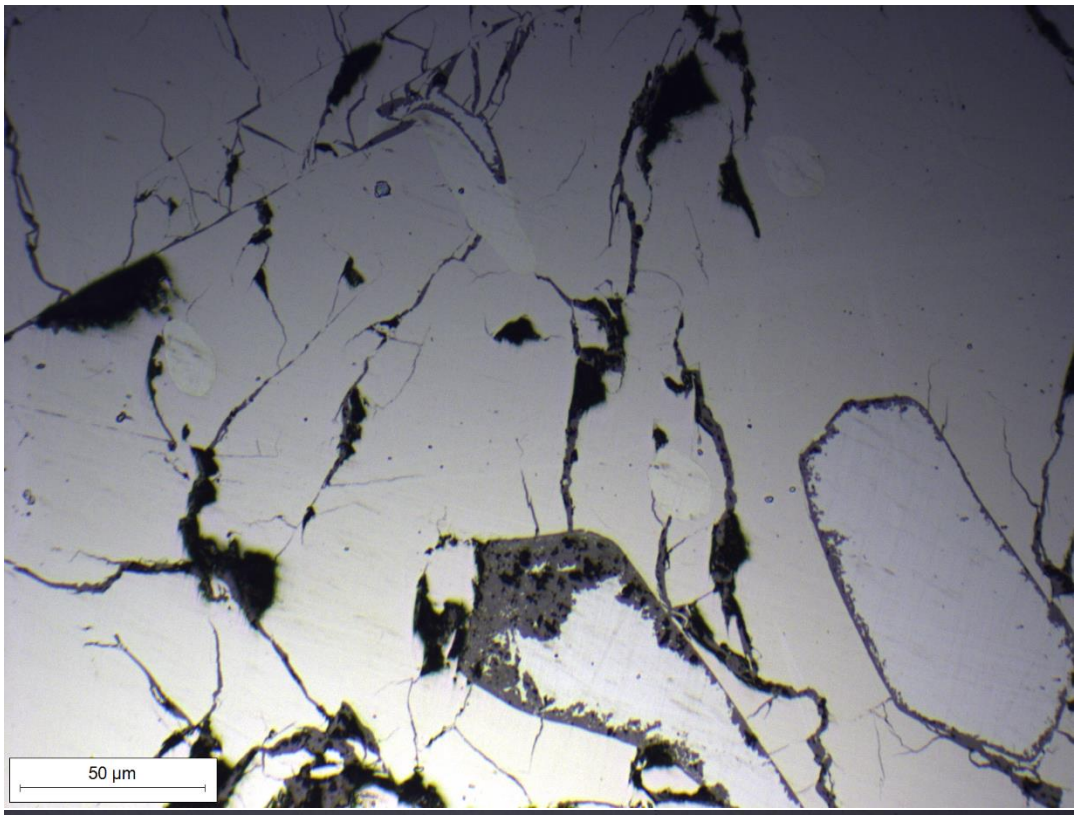
50 µm

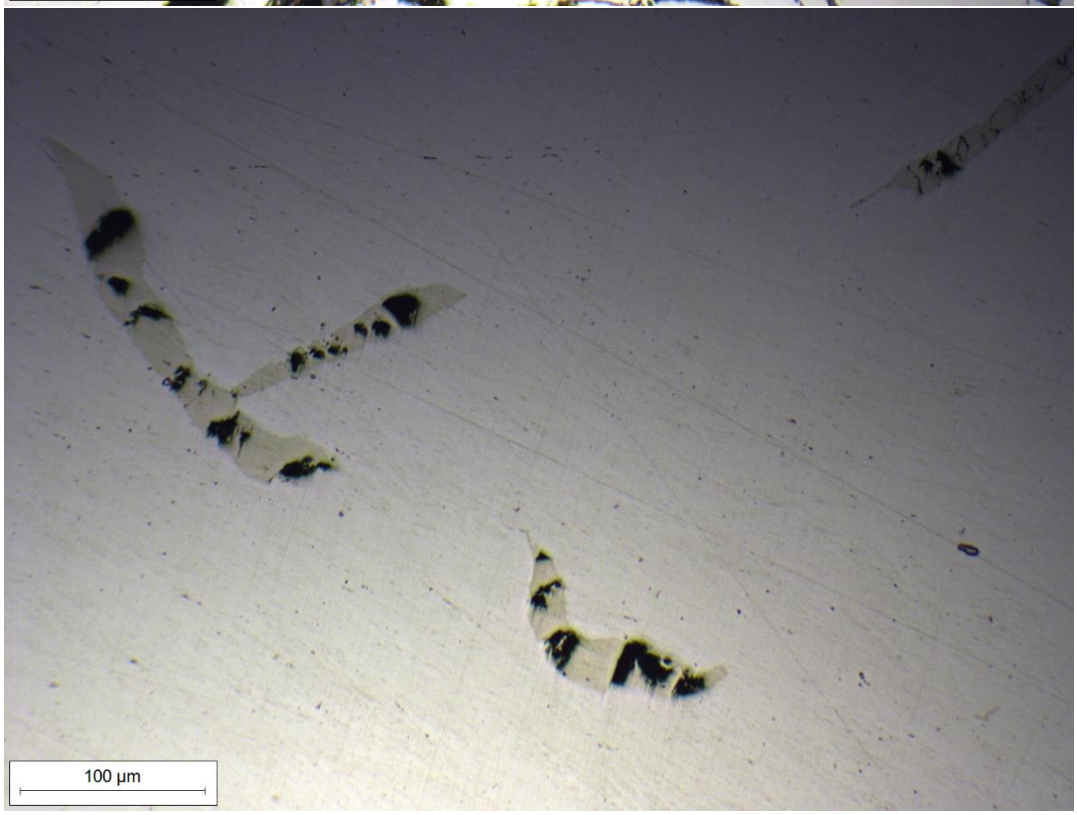
100 µm

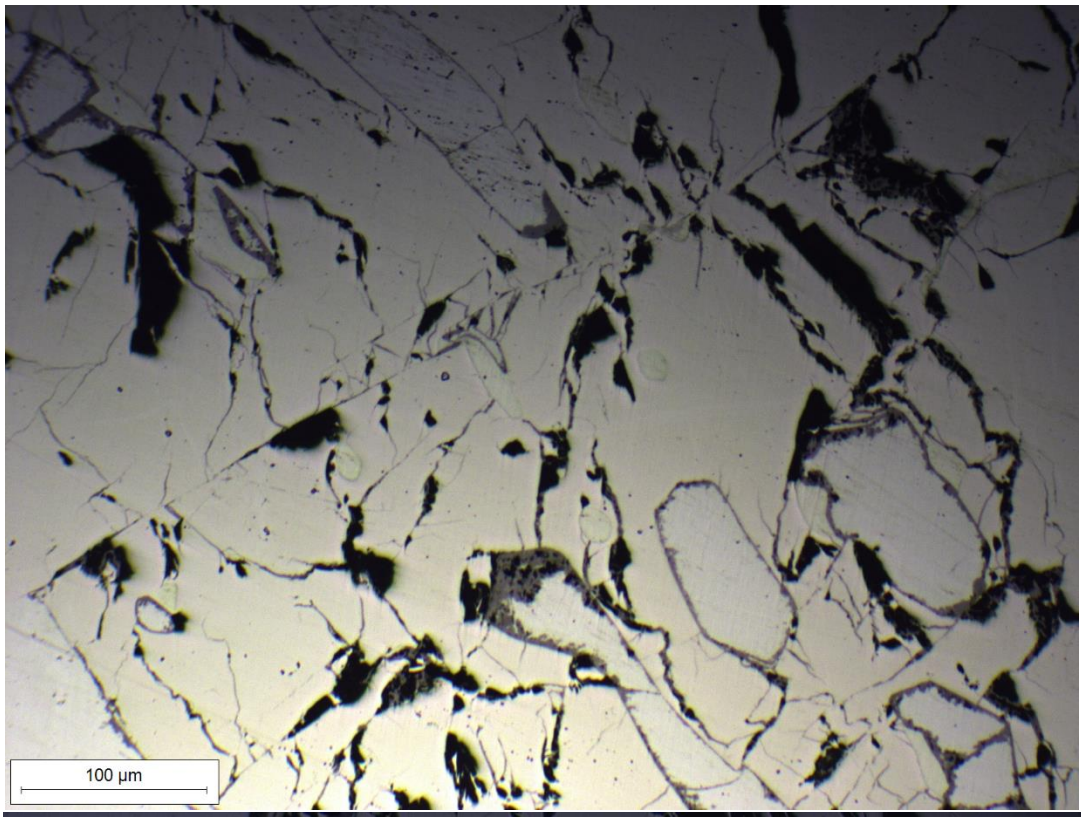
100 µm

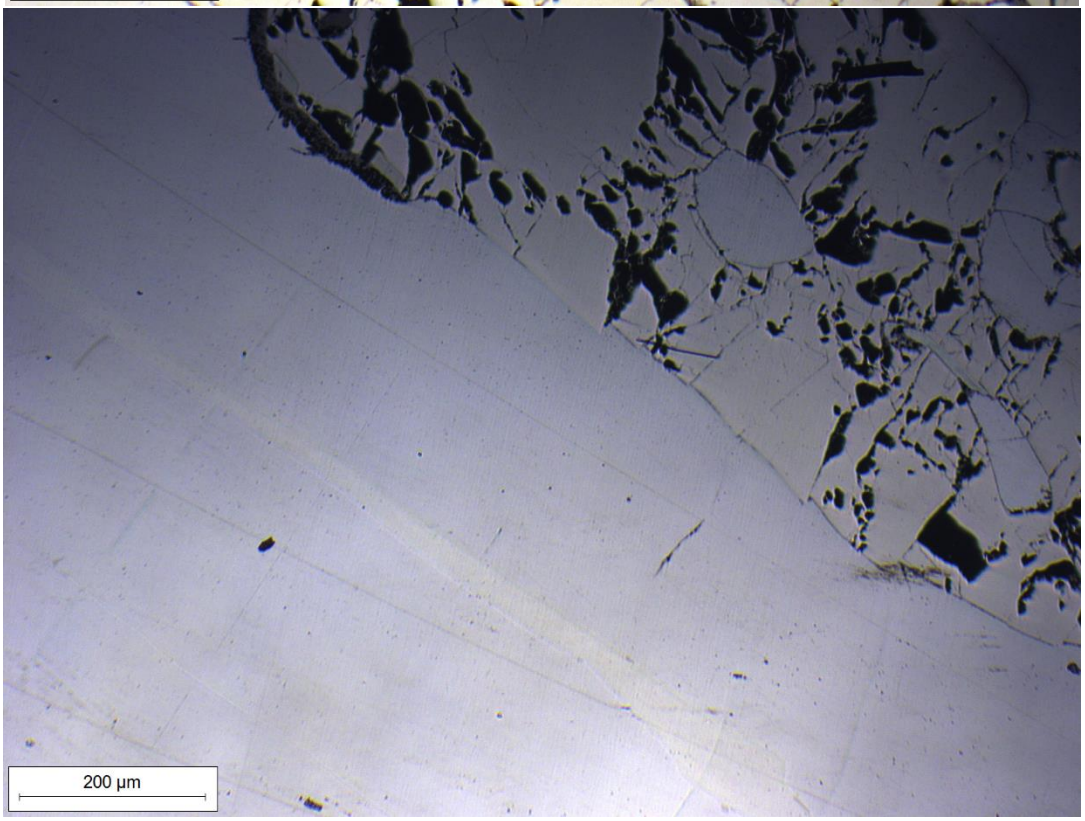
200 µm

Zone III

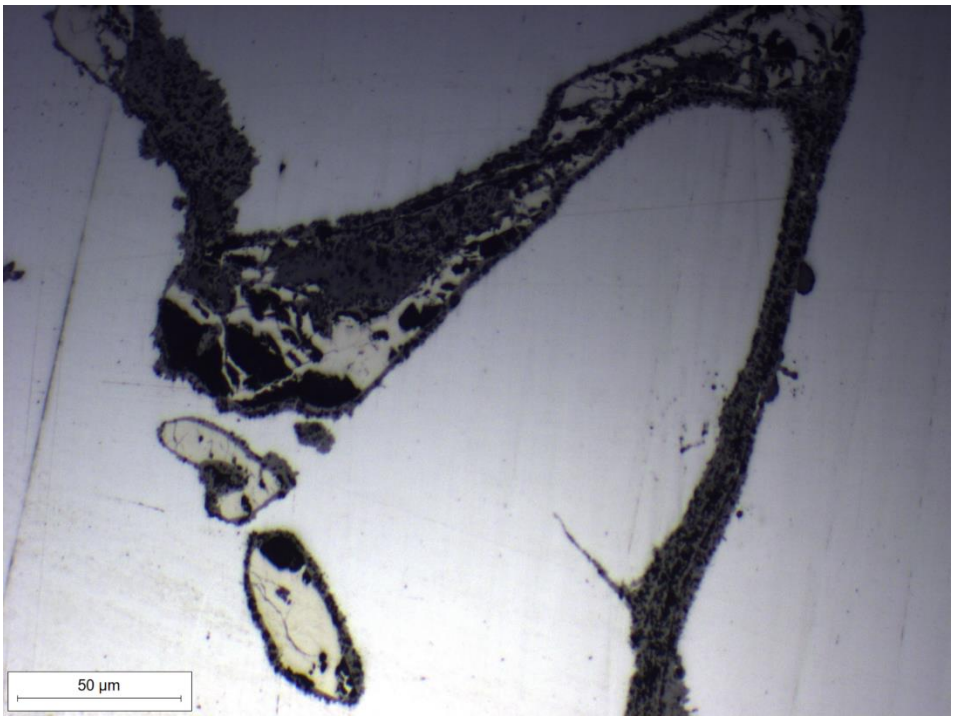

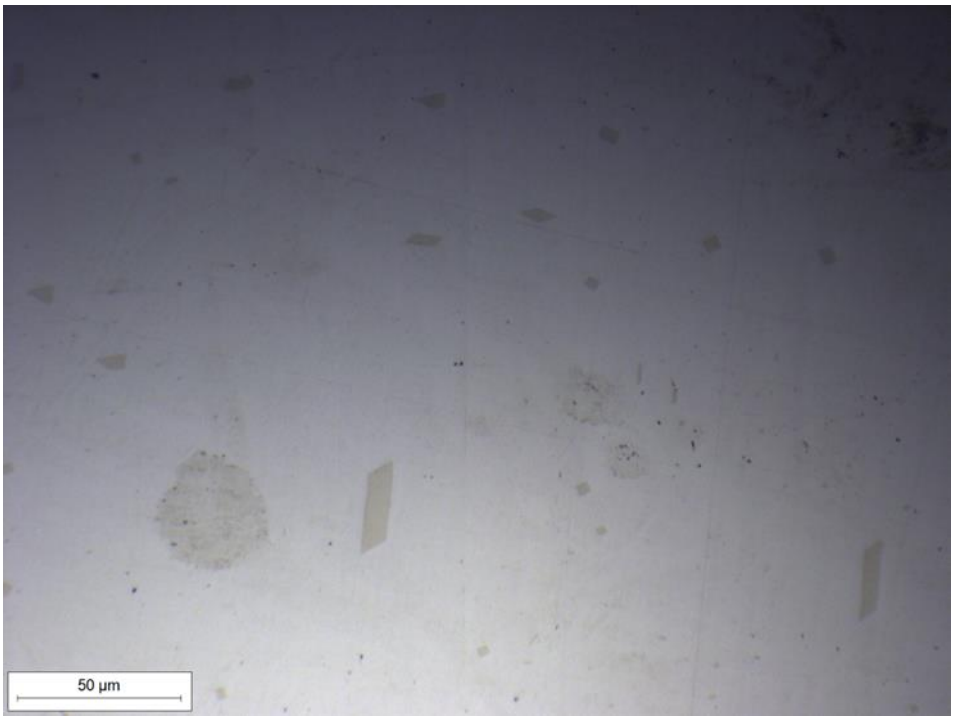

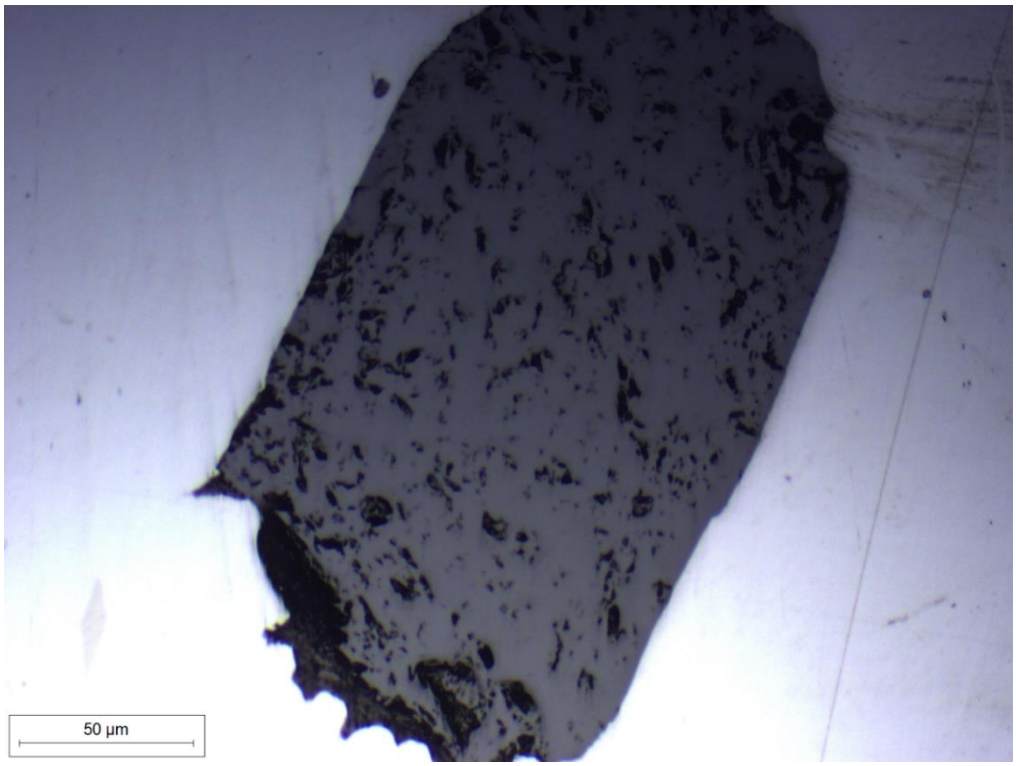
50 µm

Post-M.A. observation

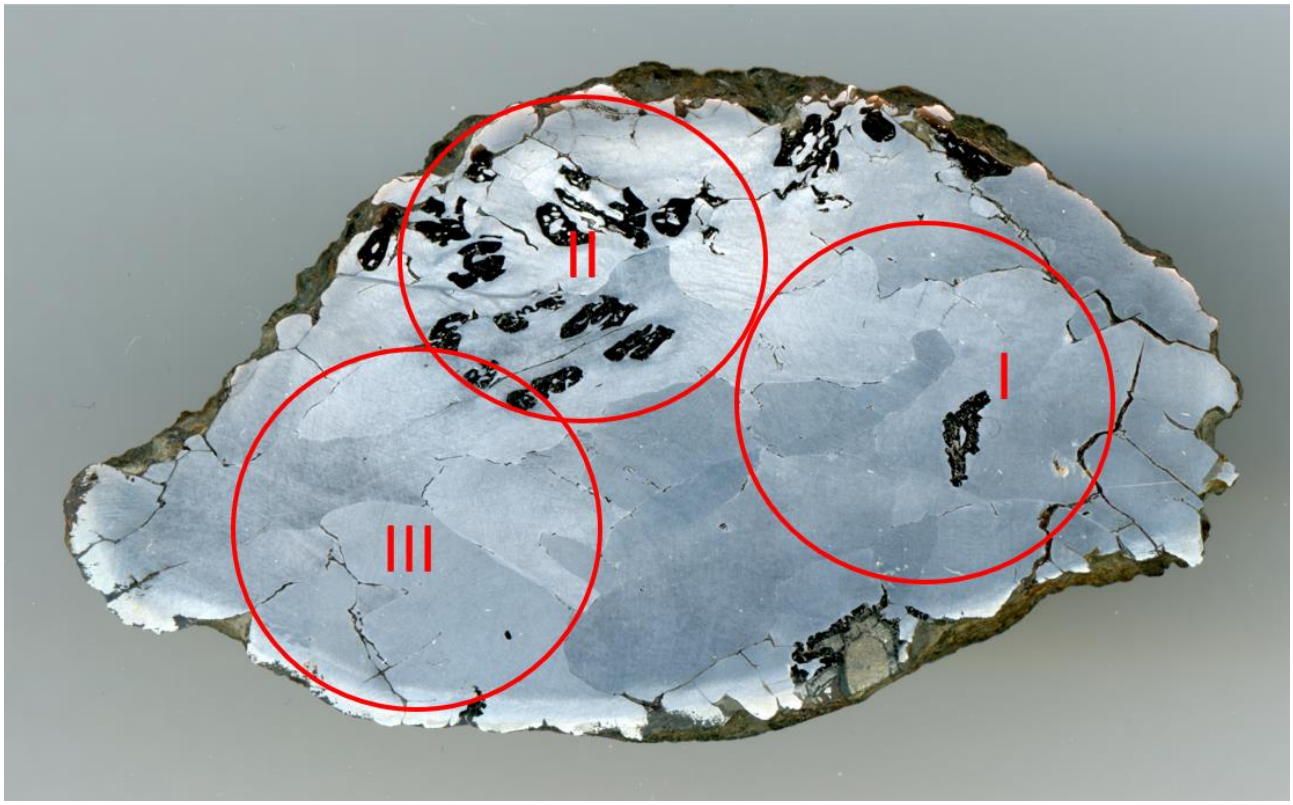

Zone I

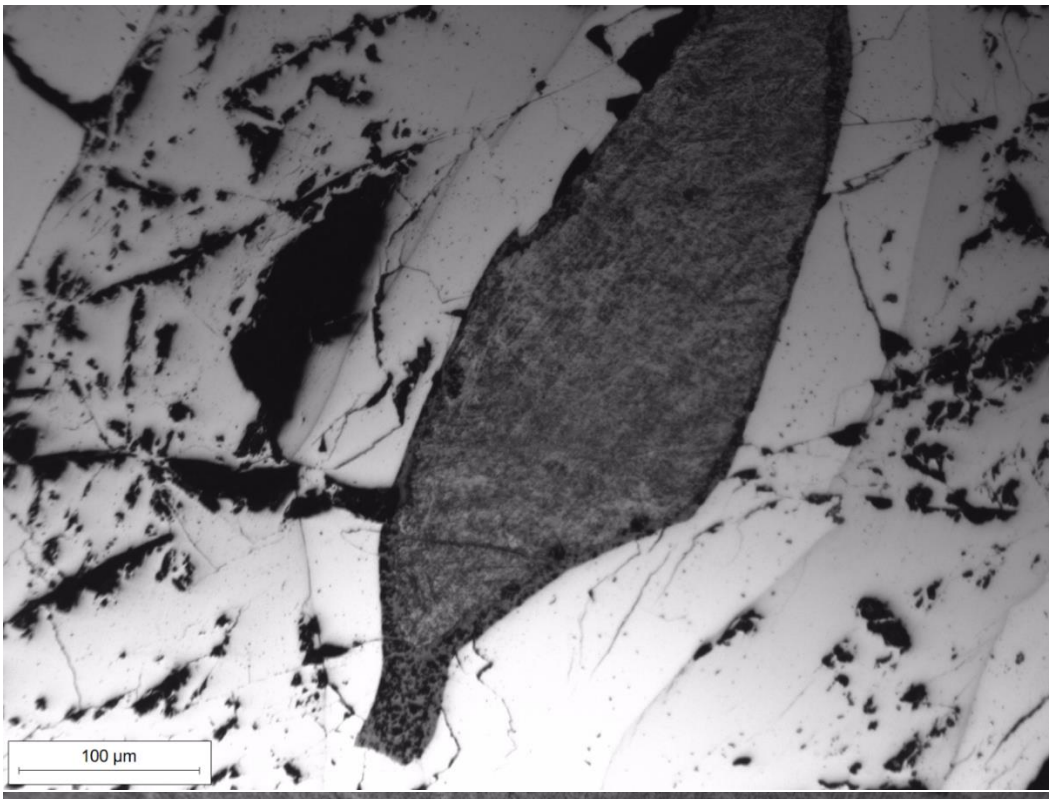

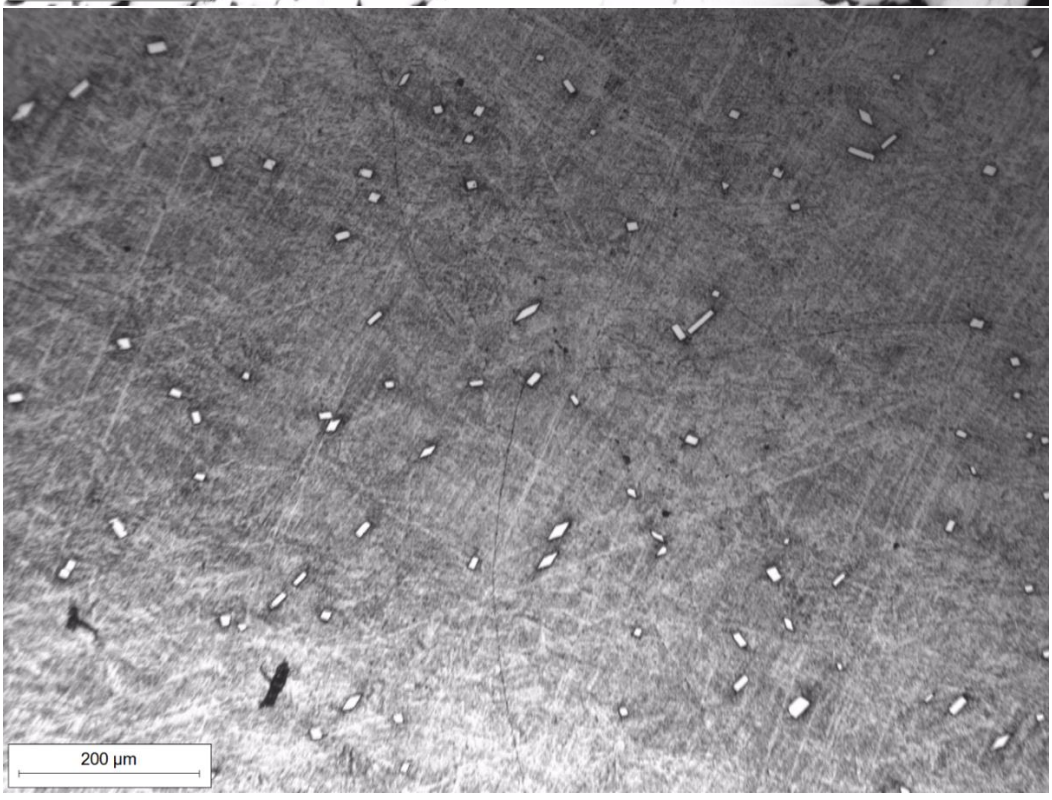

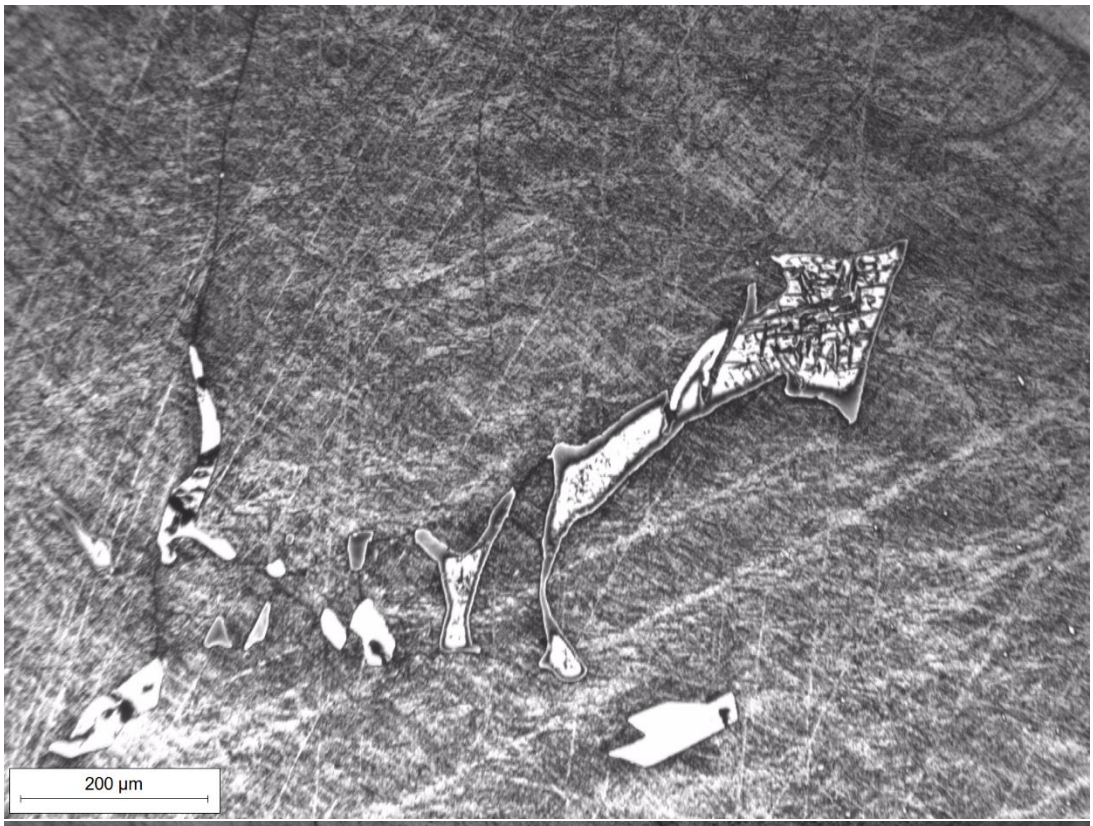
200 µm

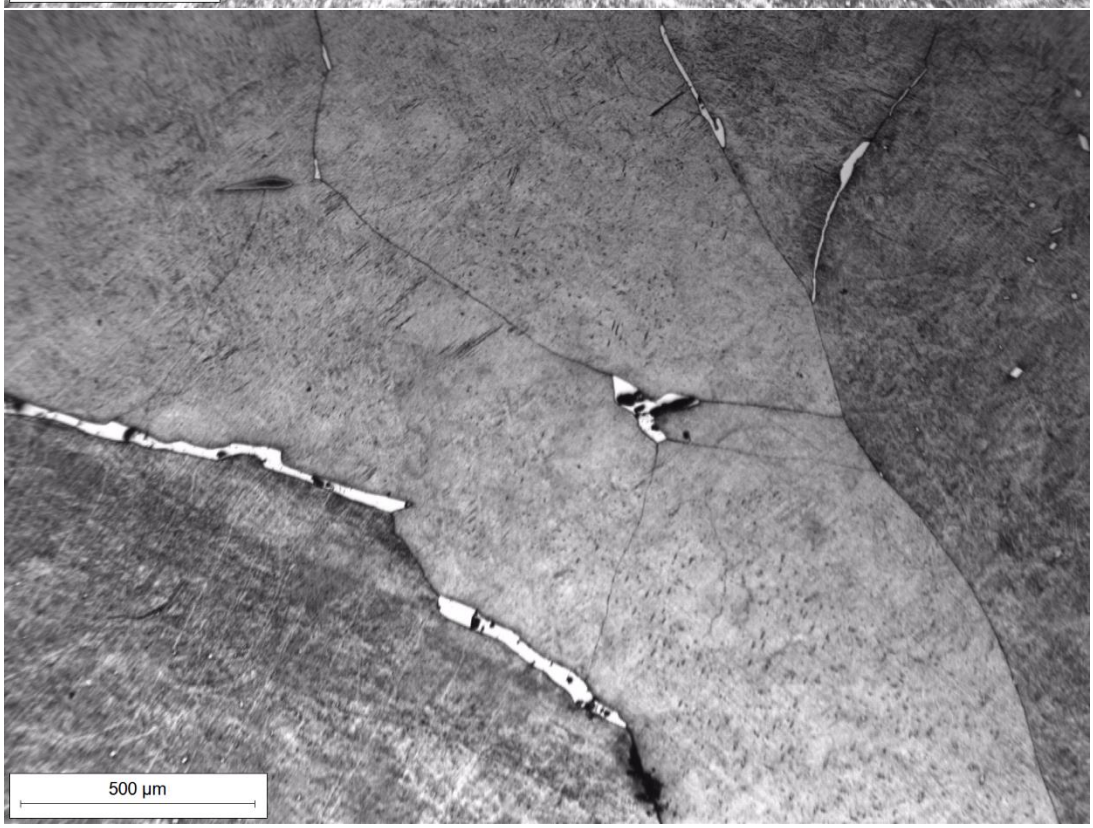
500 µm

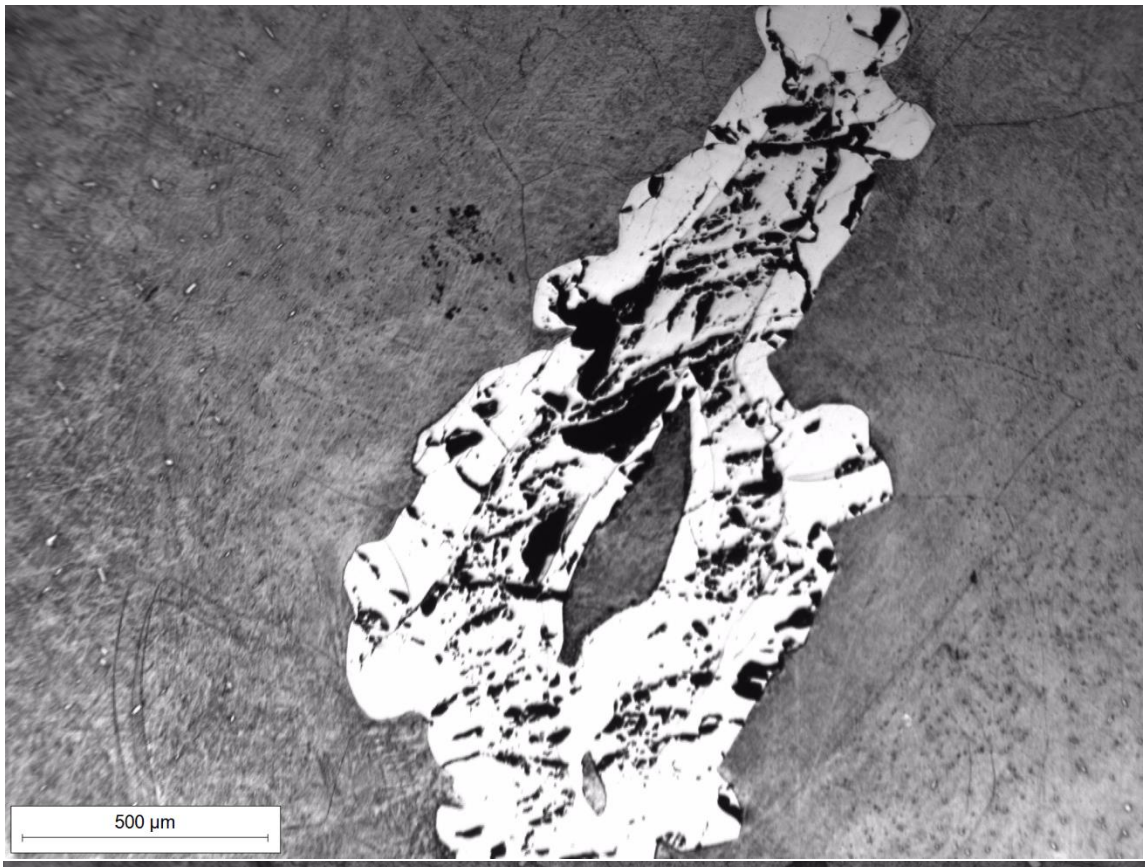
500 µm

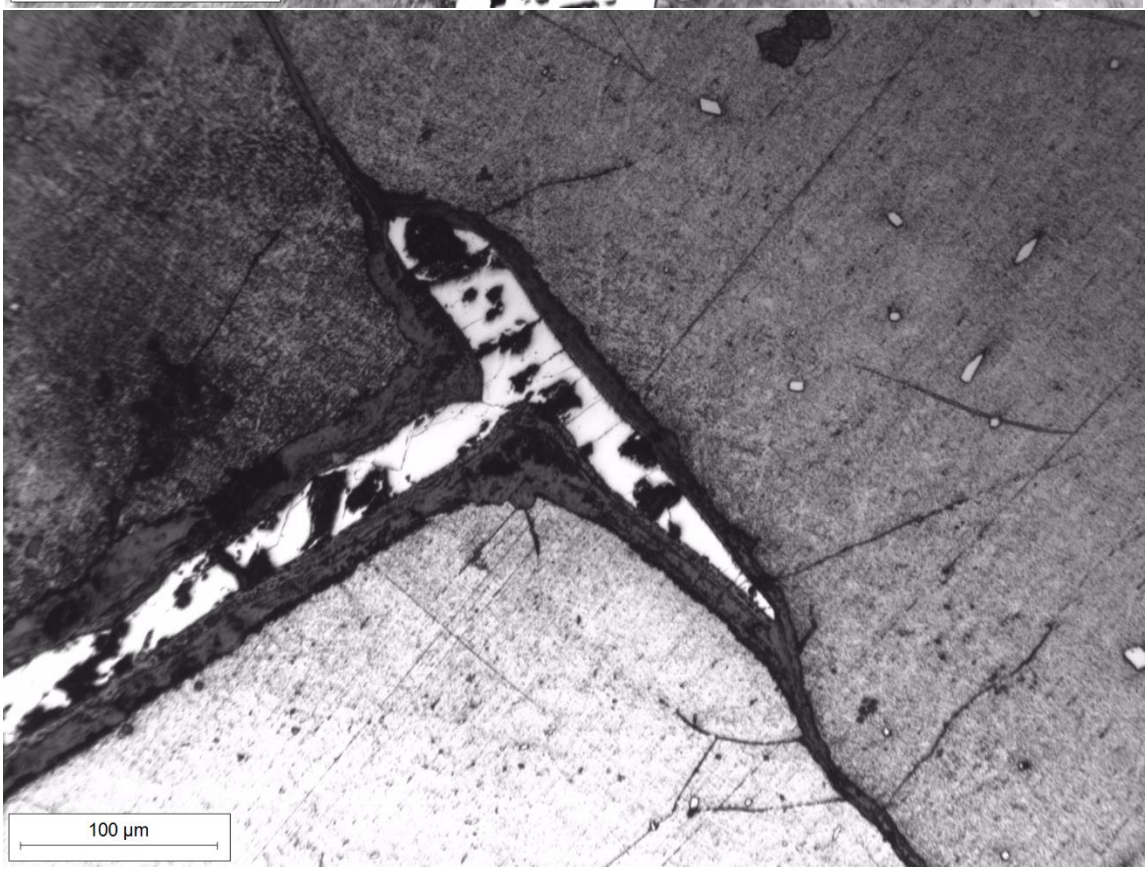
100 µm

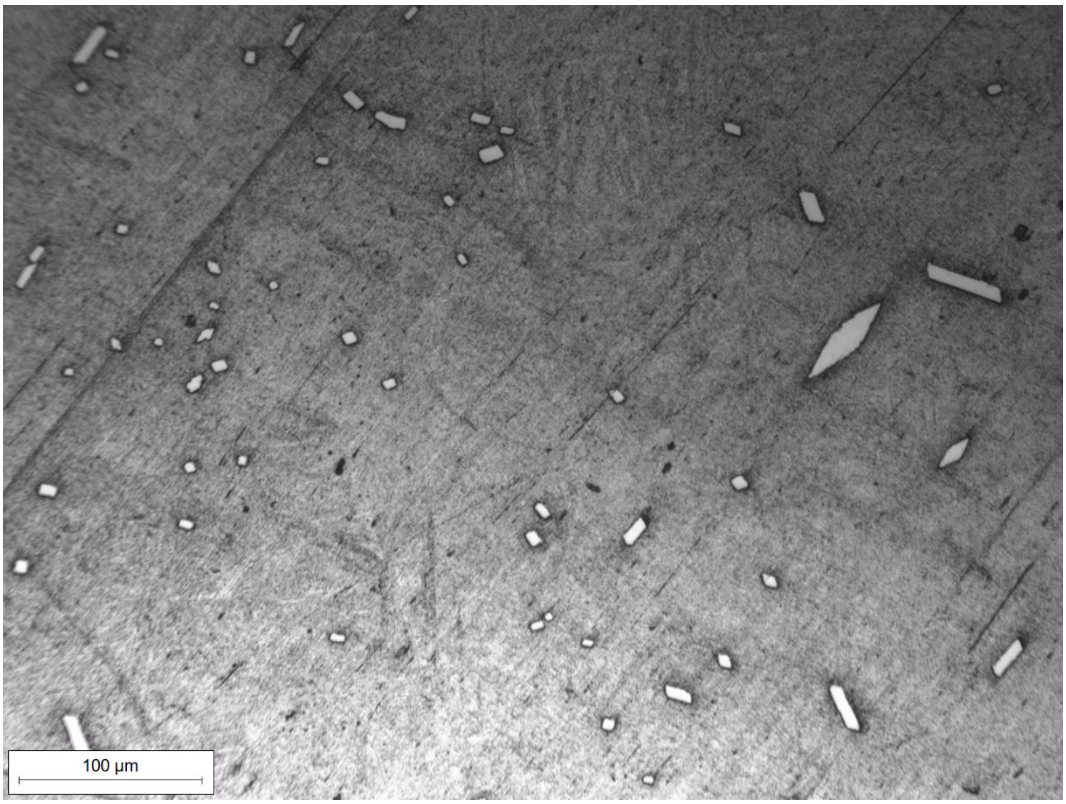
100 µm

Zone II

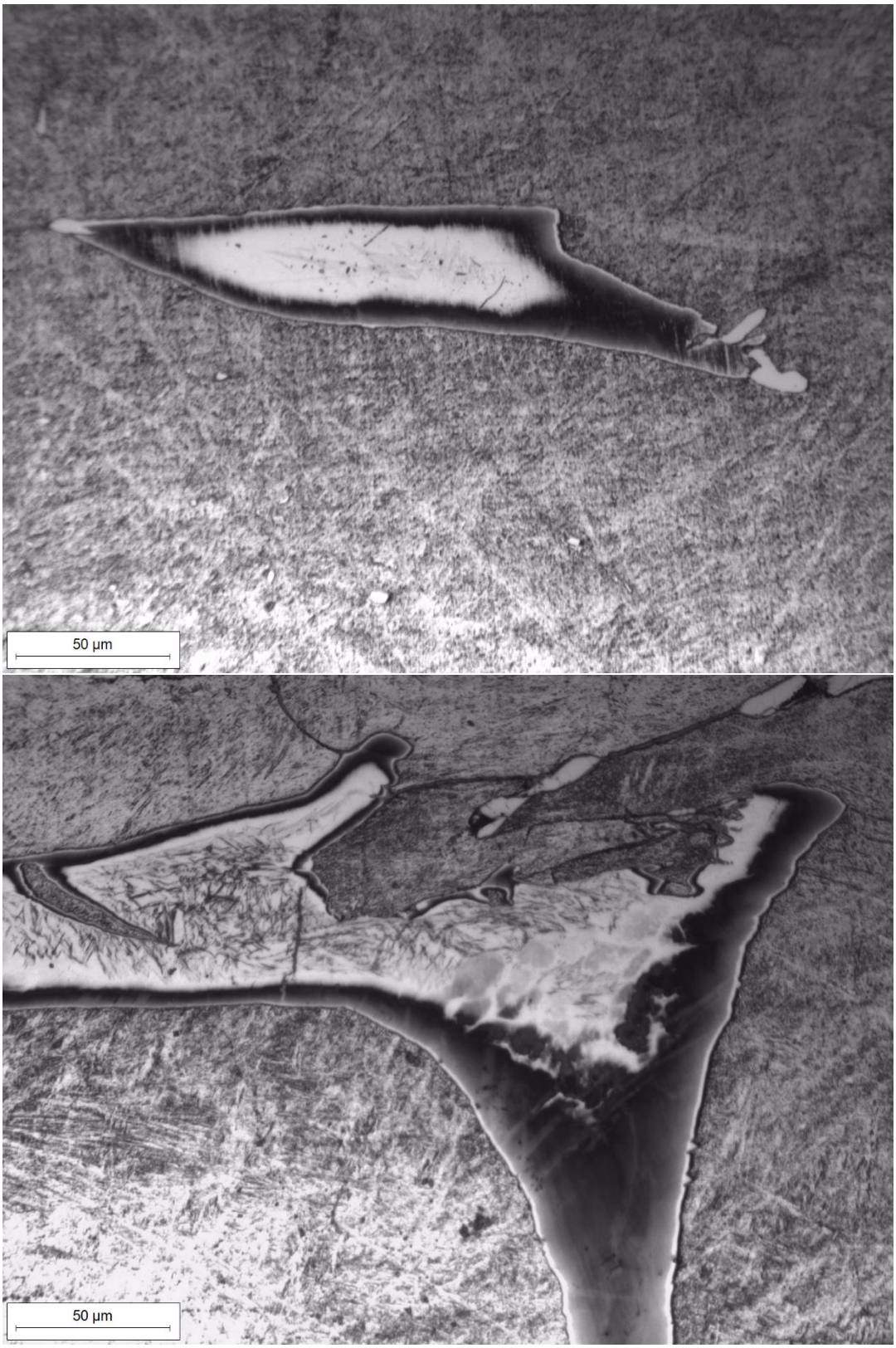

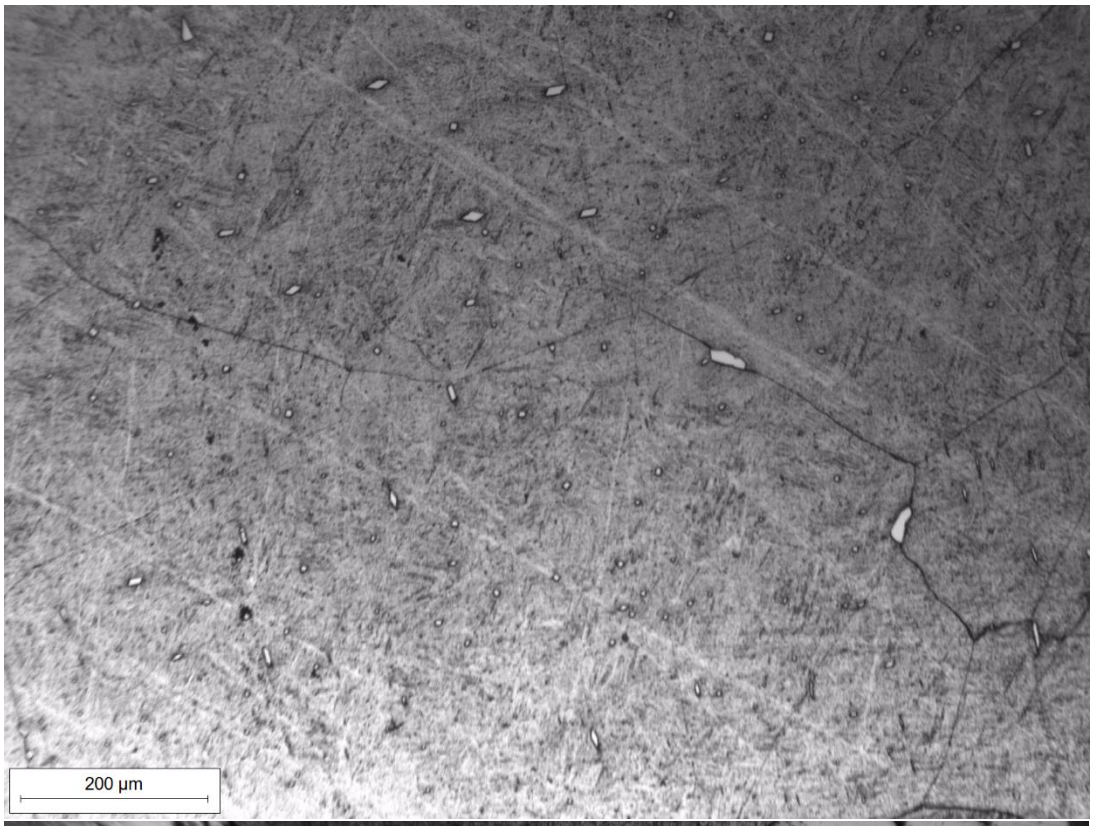
200 µm


500 µm

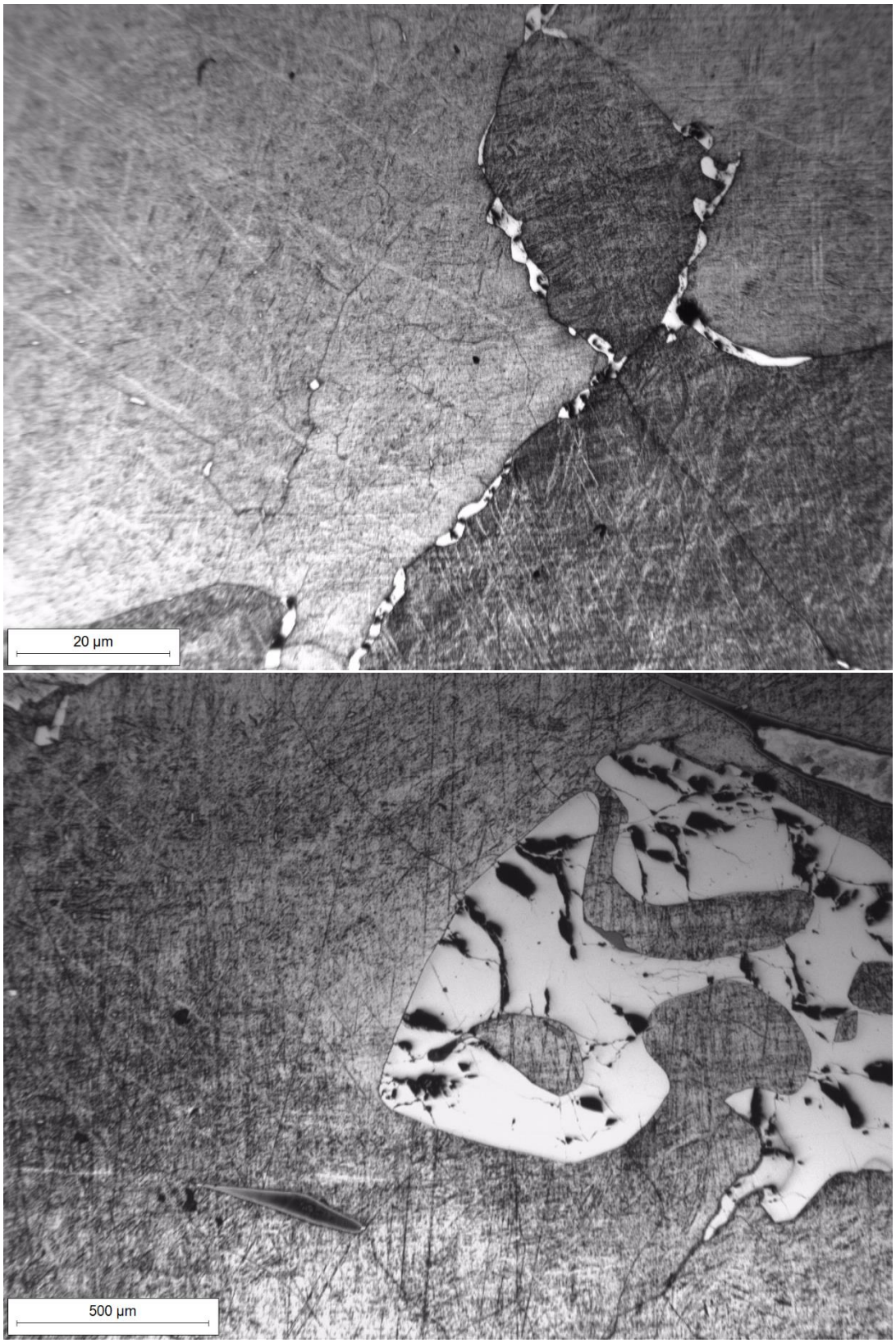
20 µm
500 µm


500 µm

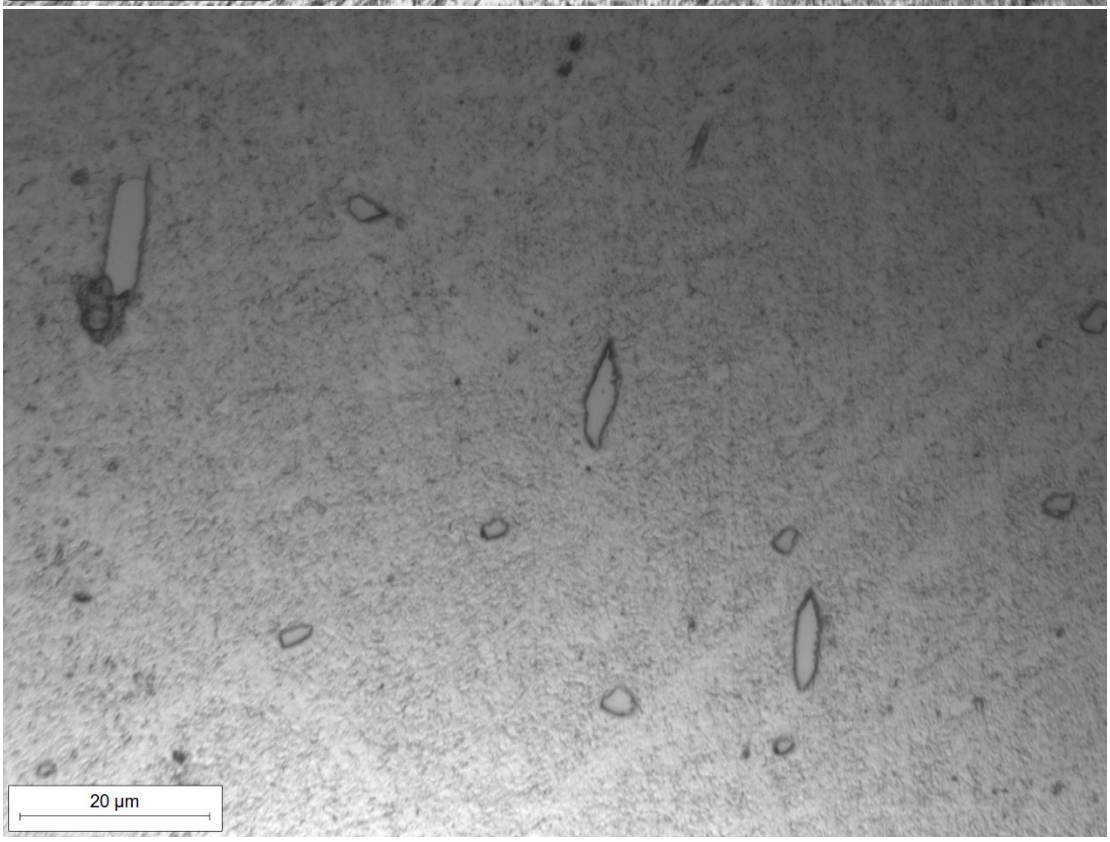
20 µm

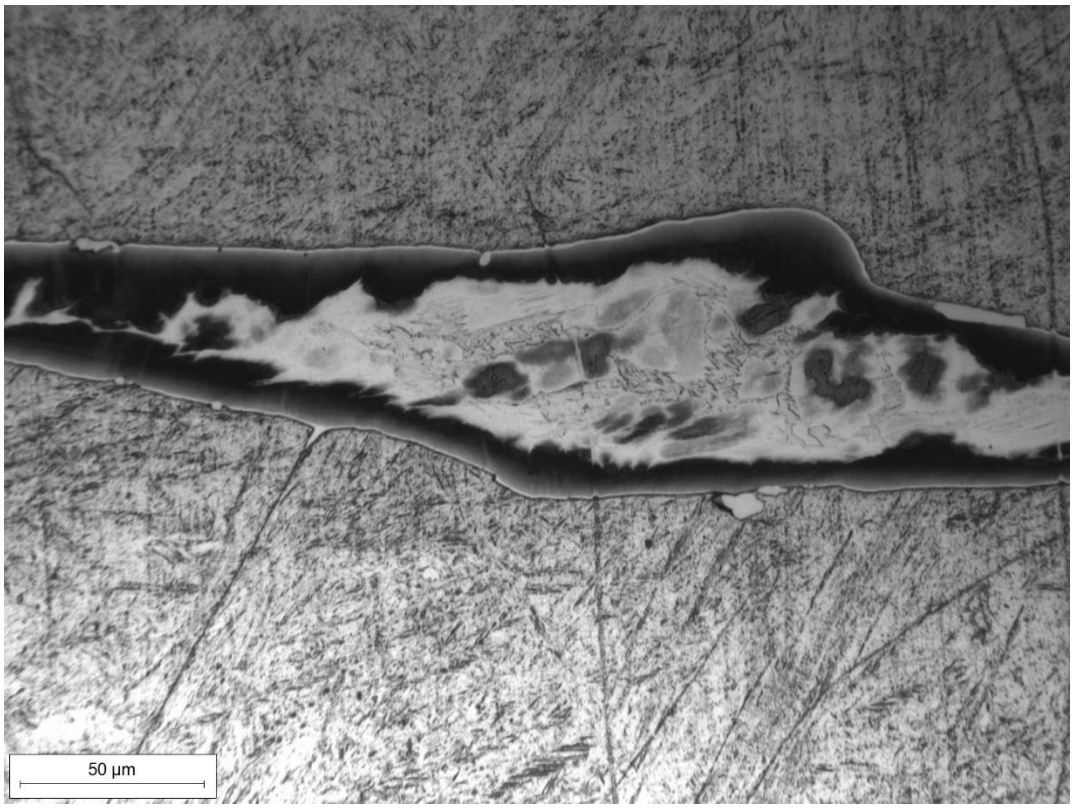
50 µm

Zone III

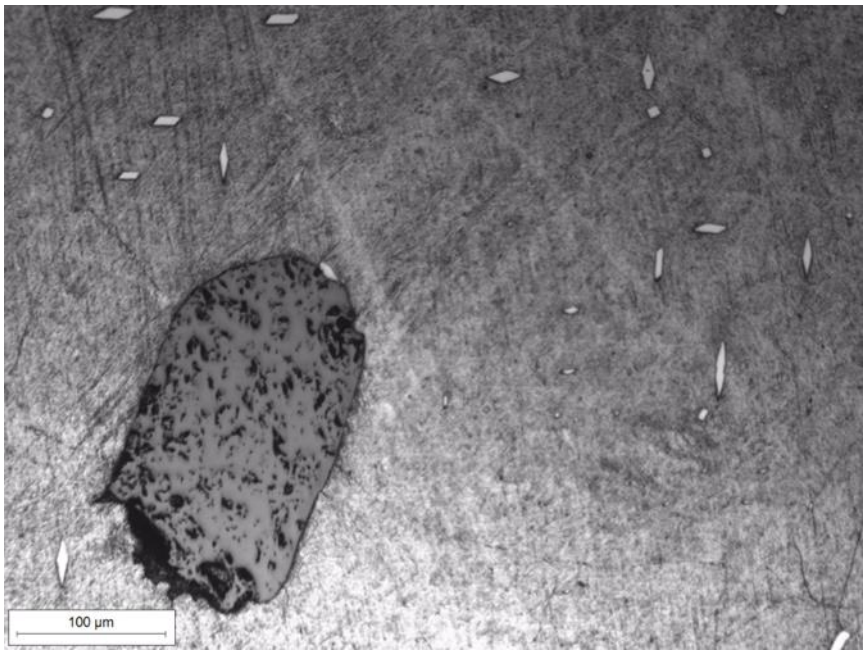

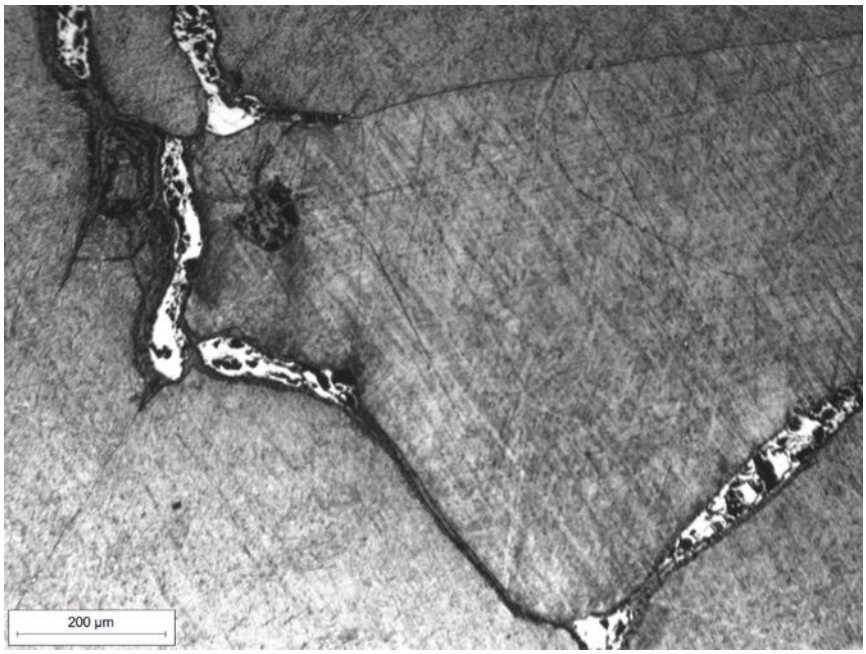

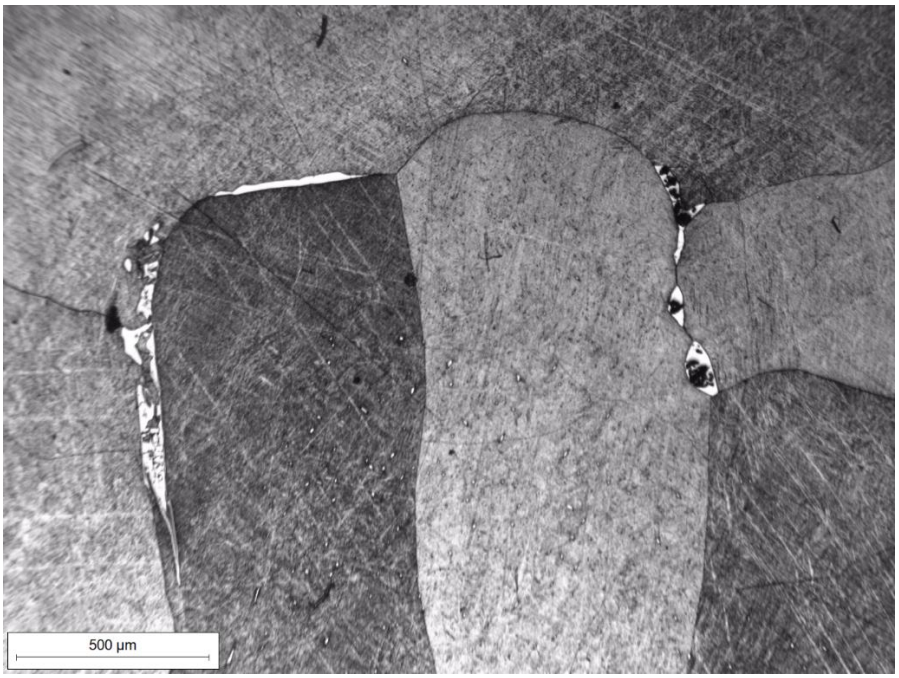
500 µm

CARLTOWN

Pre-M.A. observation

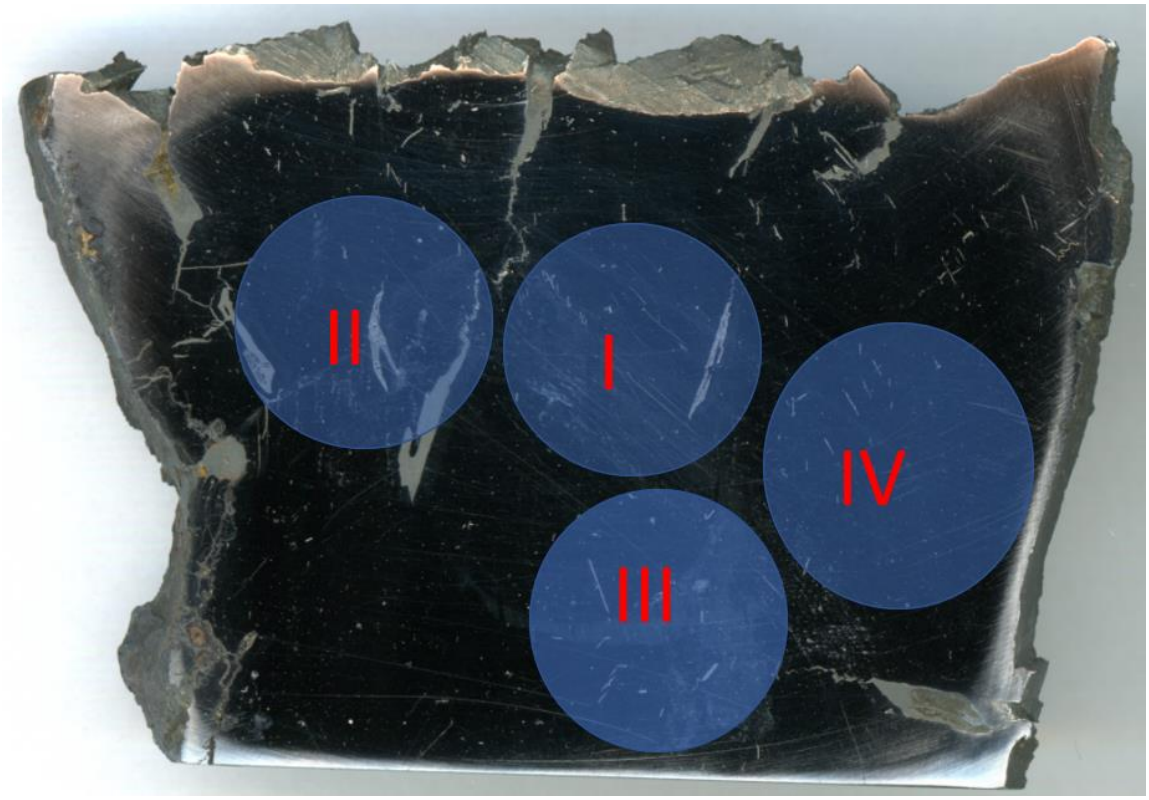

Zone I

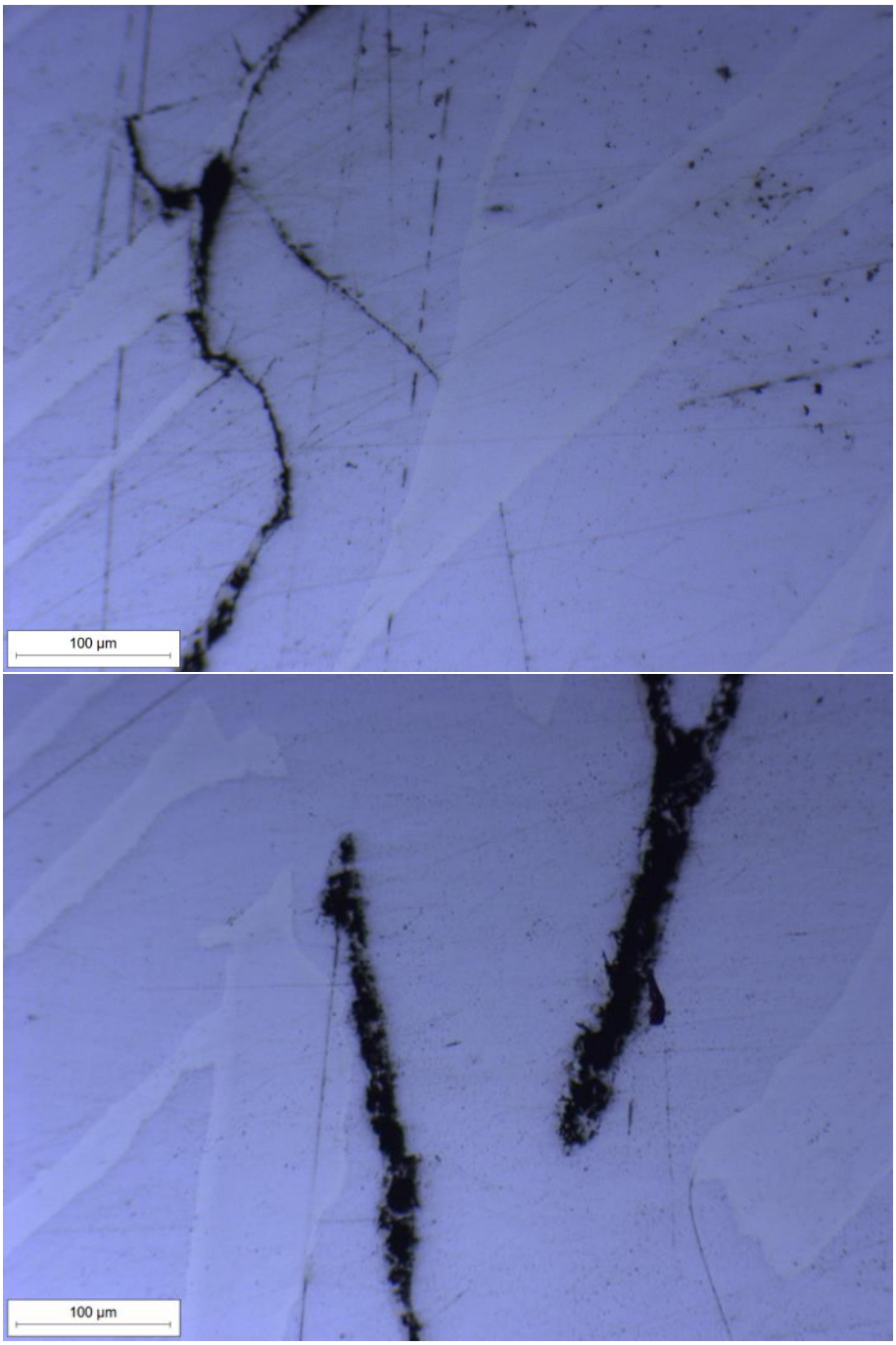

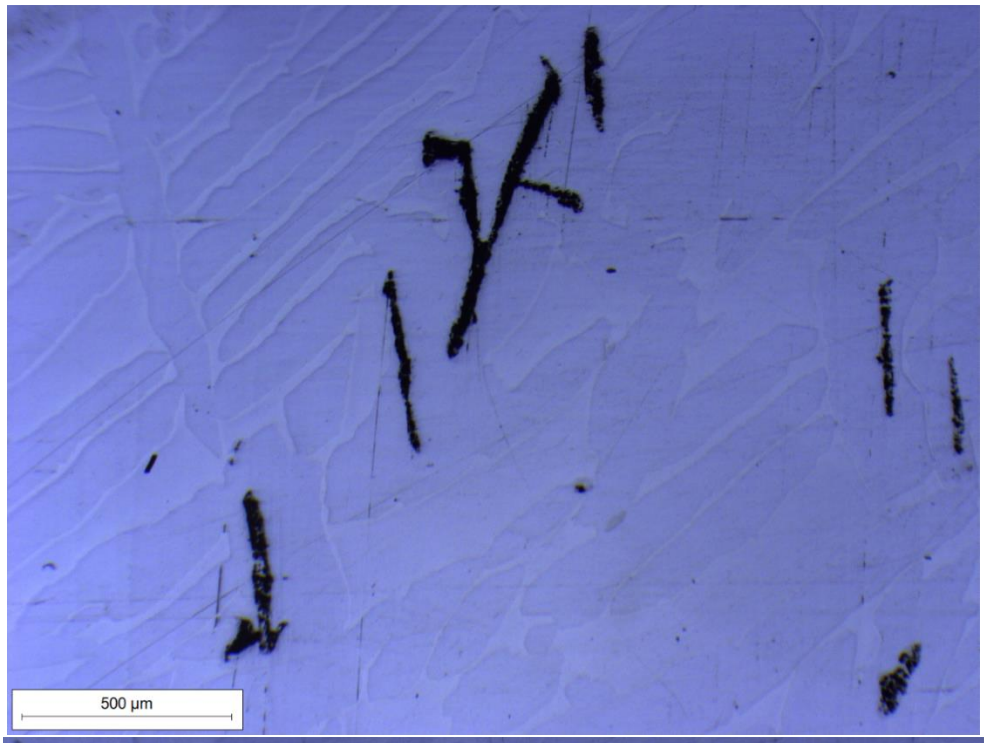
500 µm

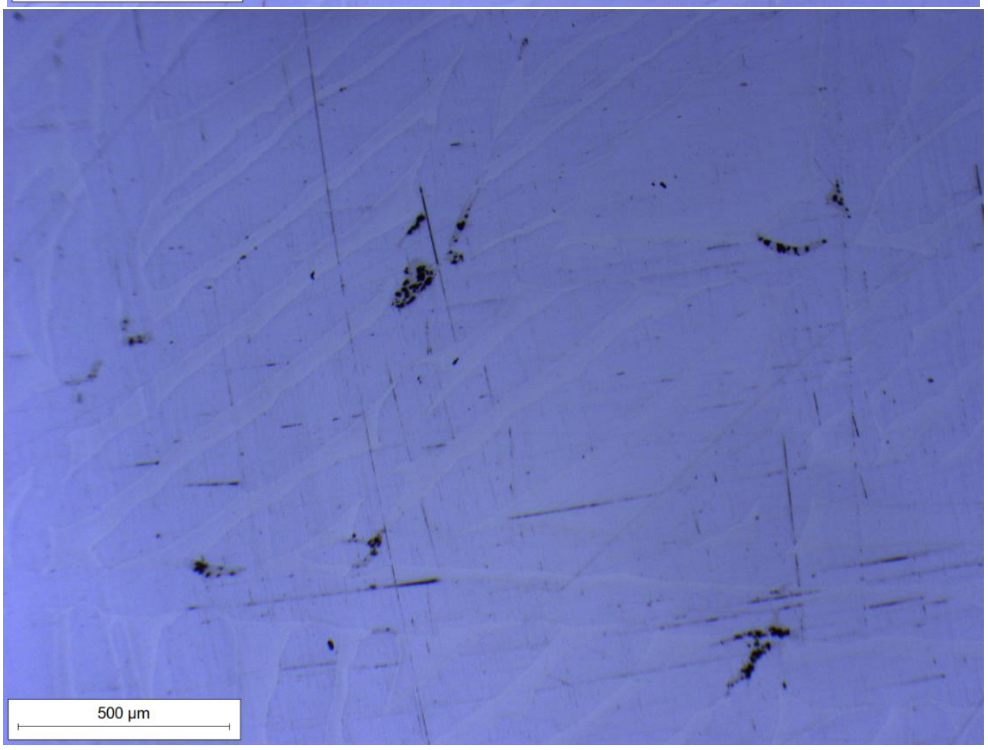
500 µm

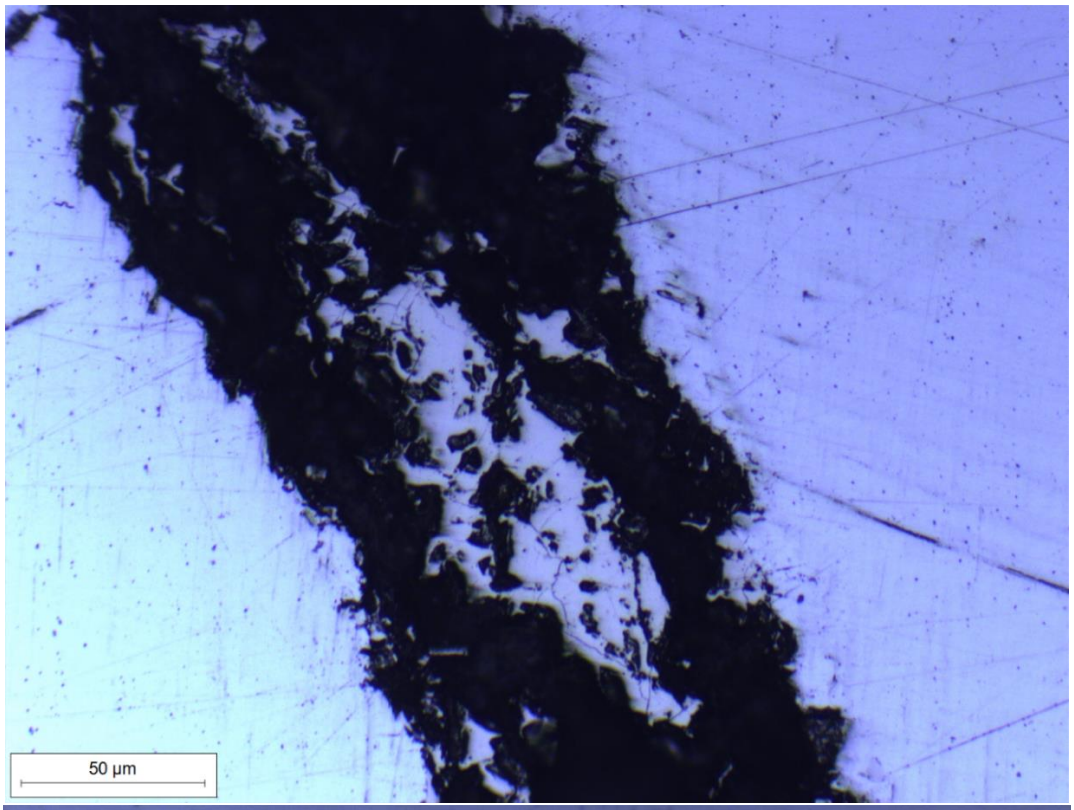
50 µm

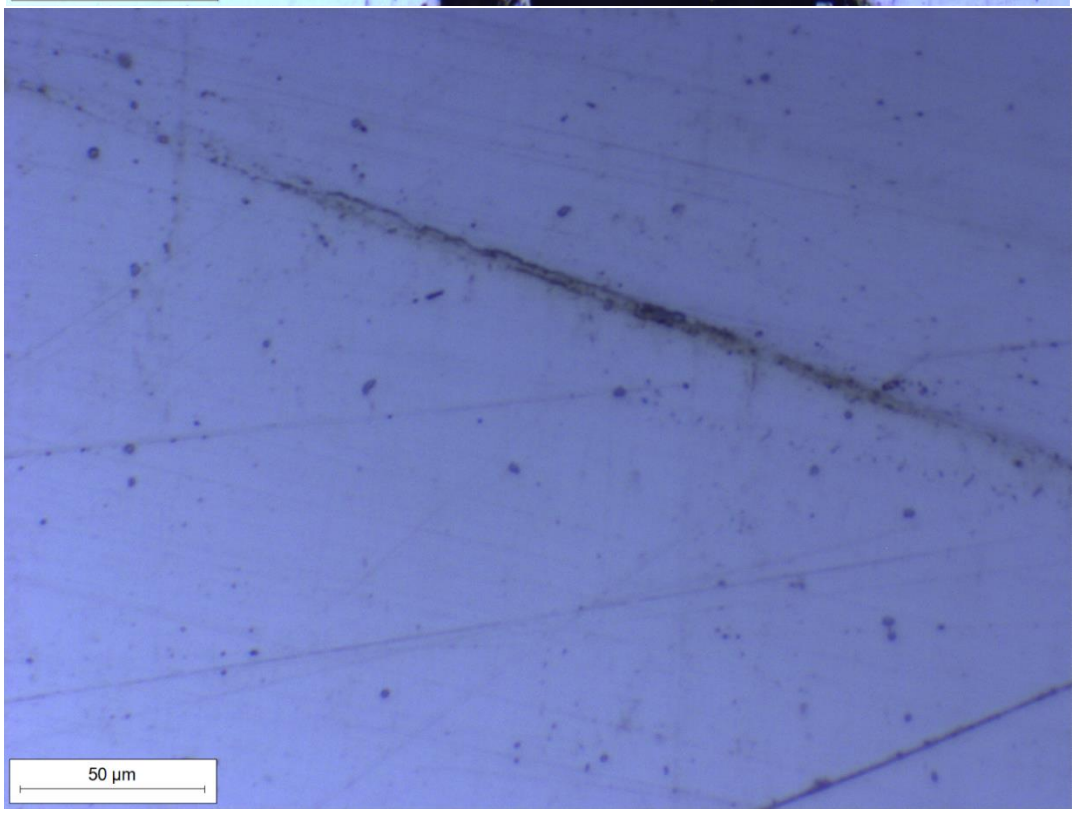
50 µm

Zone II

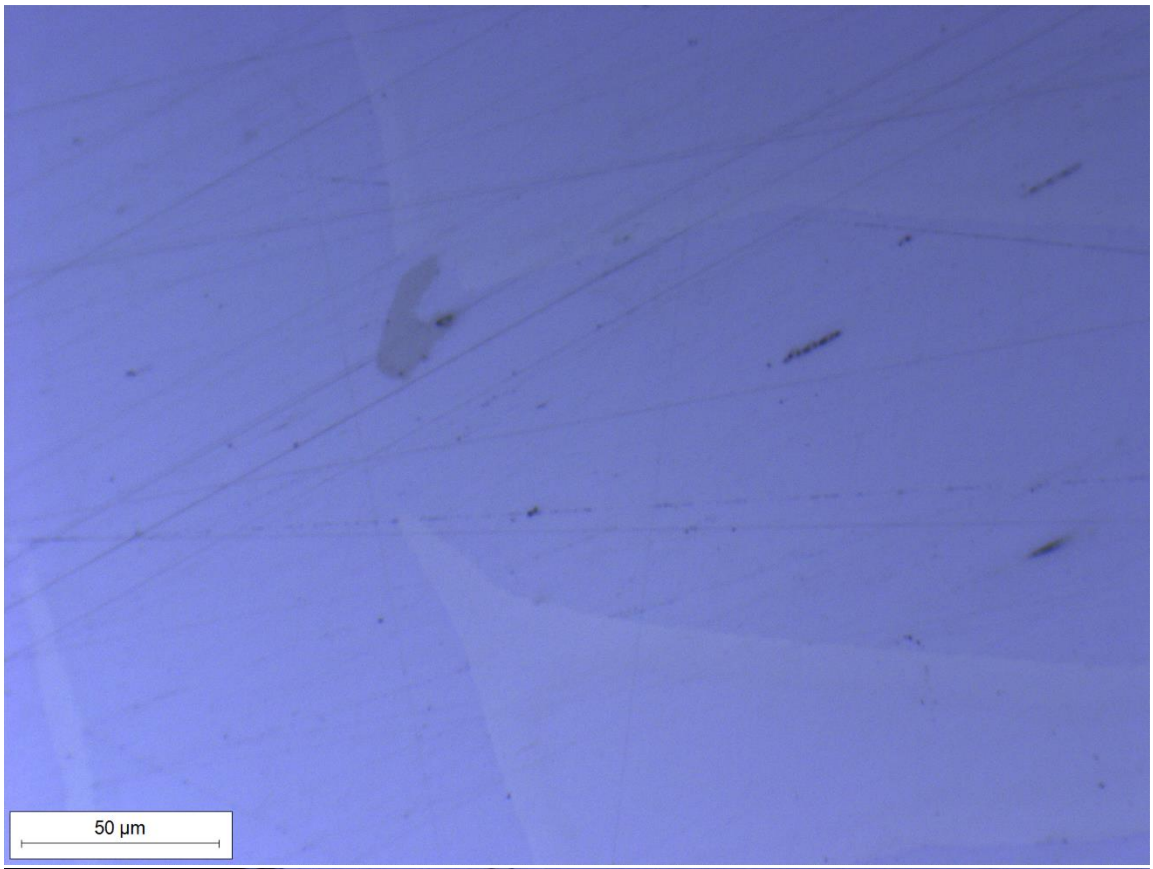

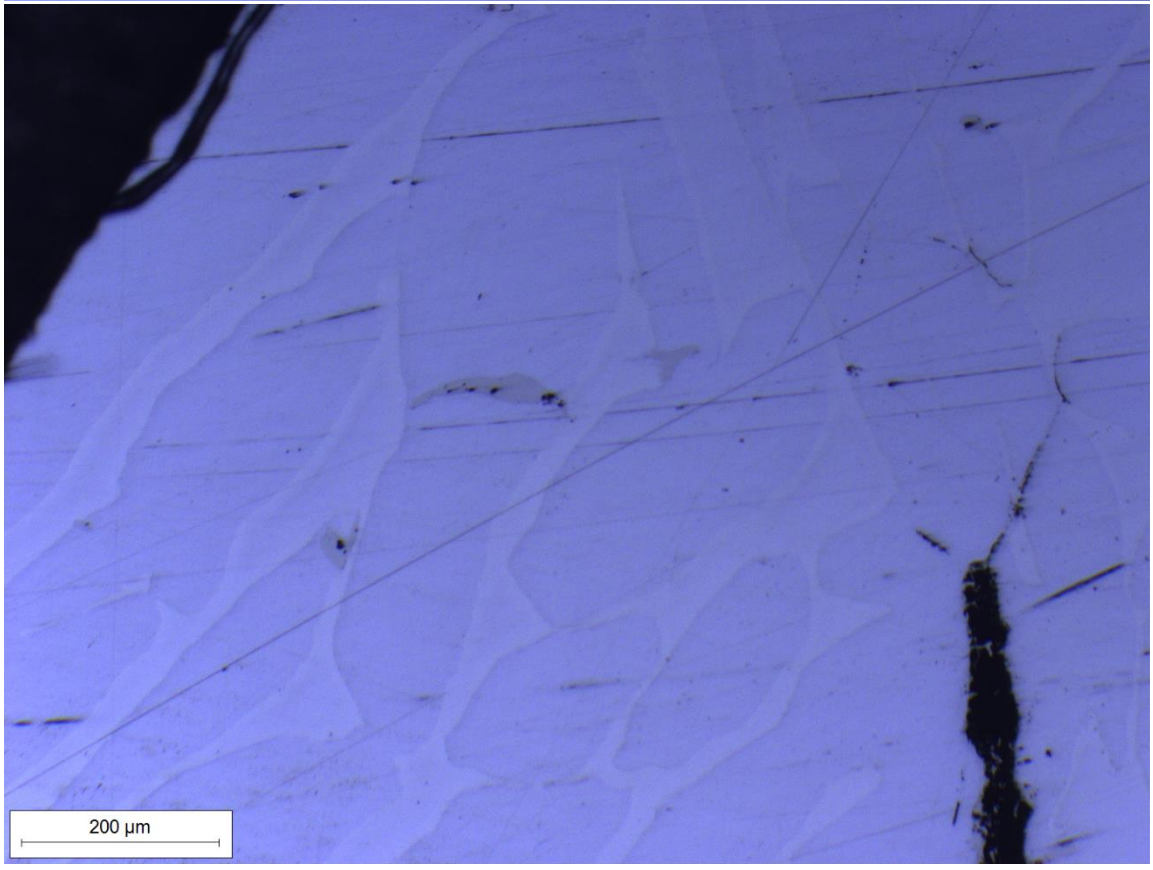

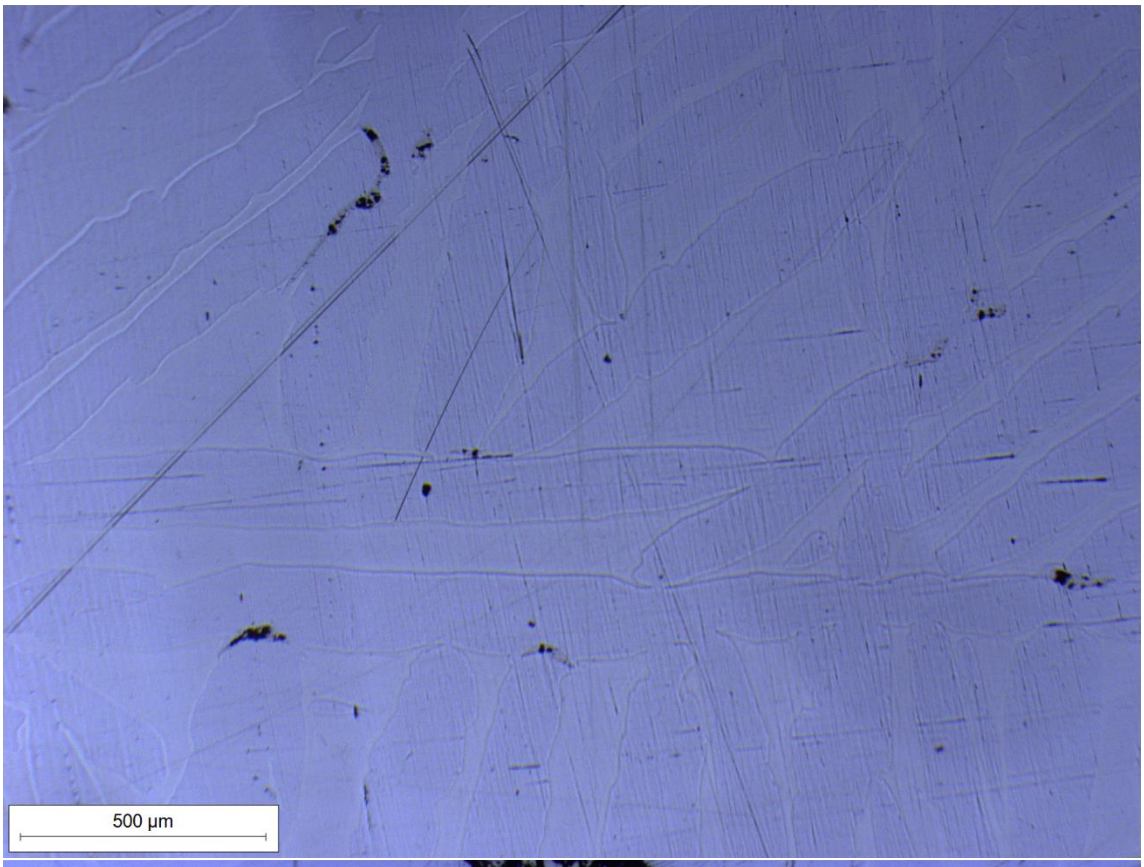
500 µm

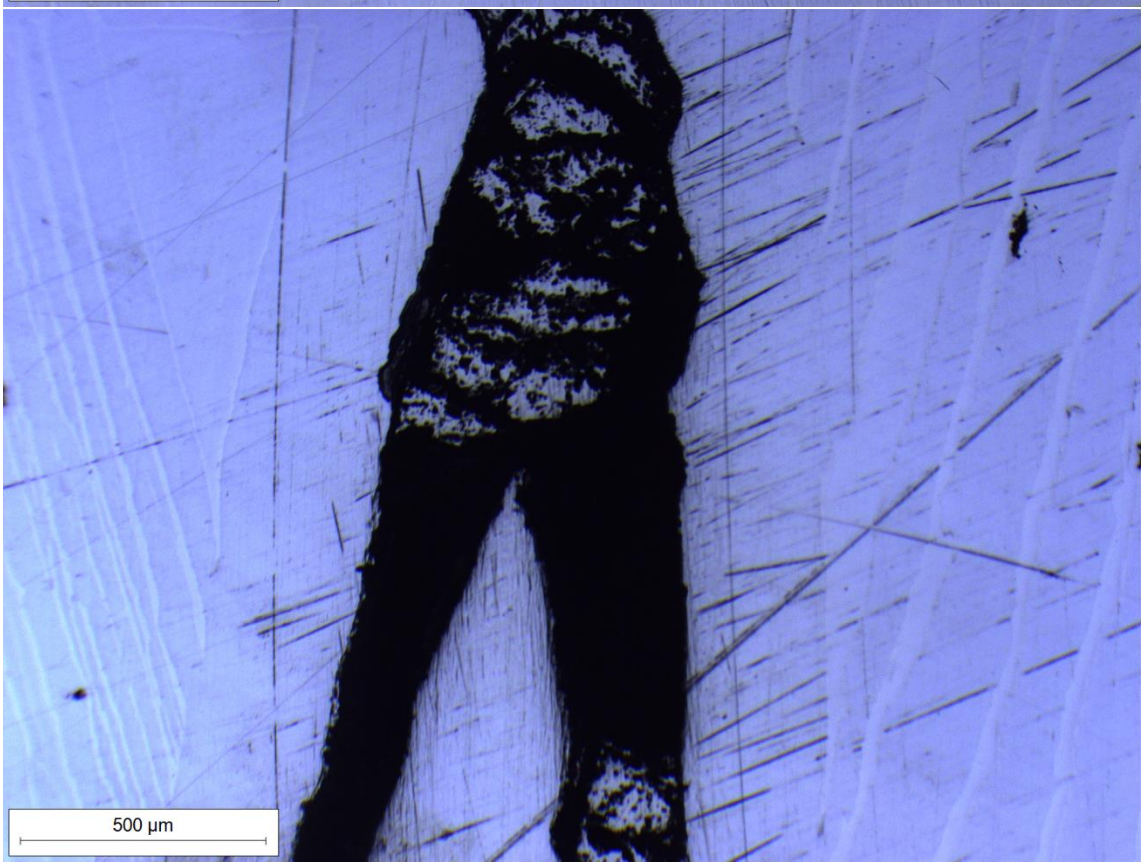
500 µm

Zone III

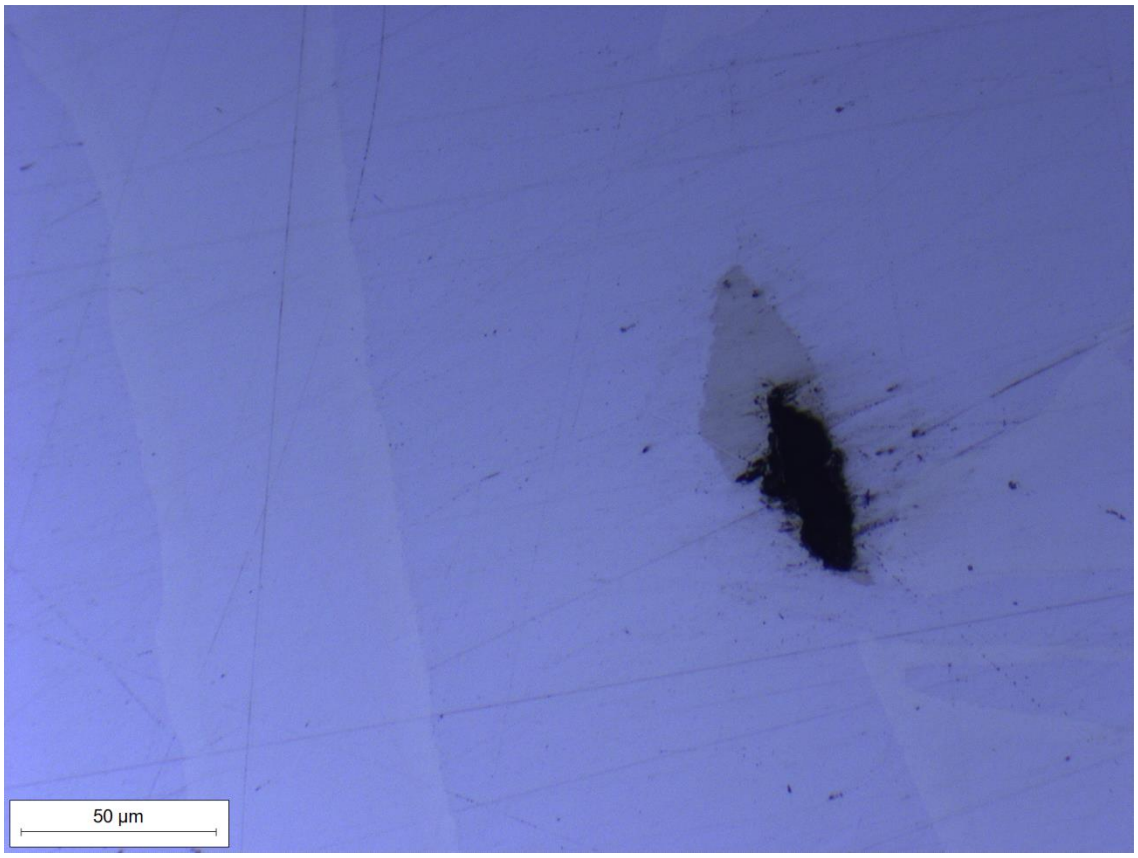

Zone IV

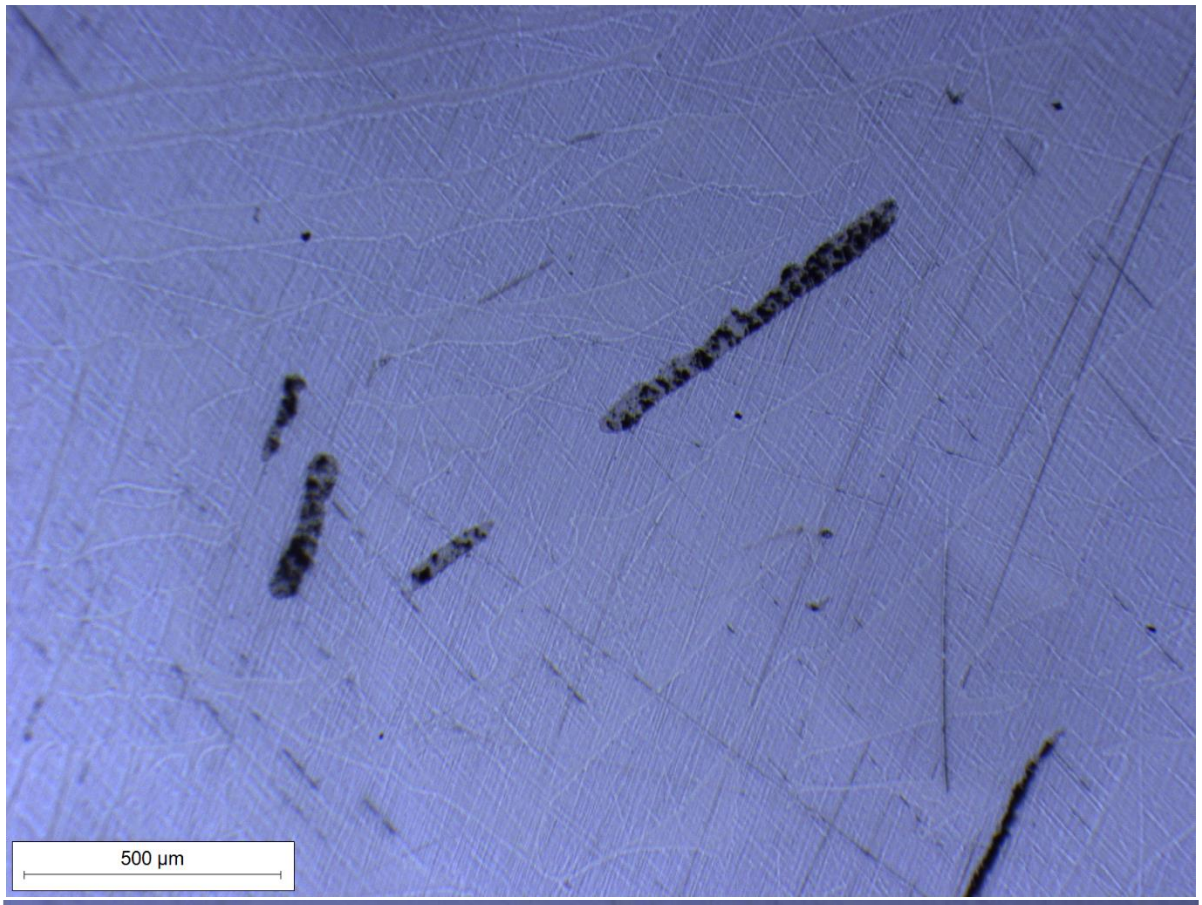

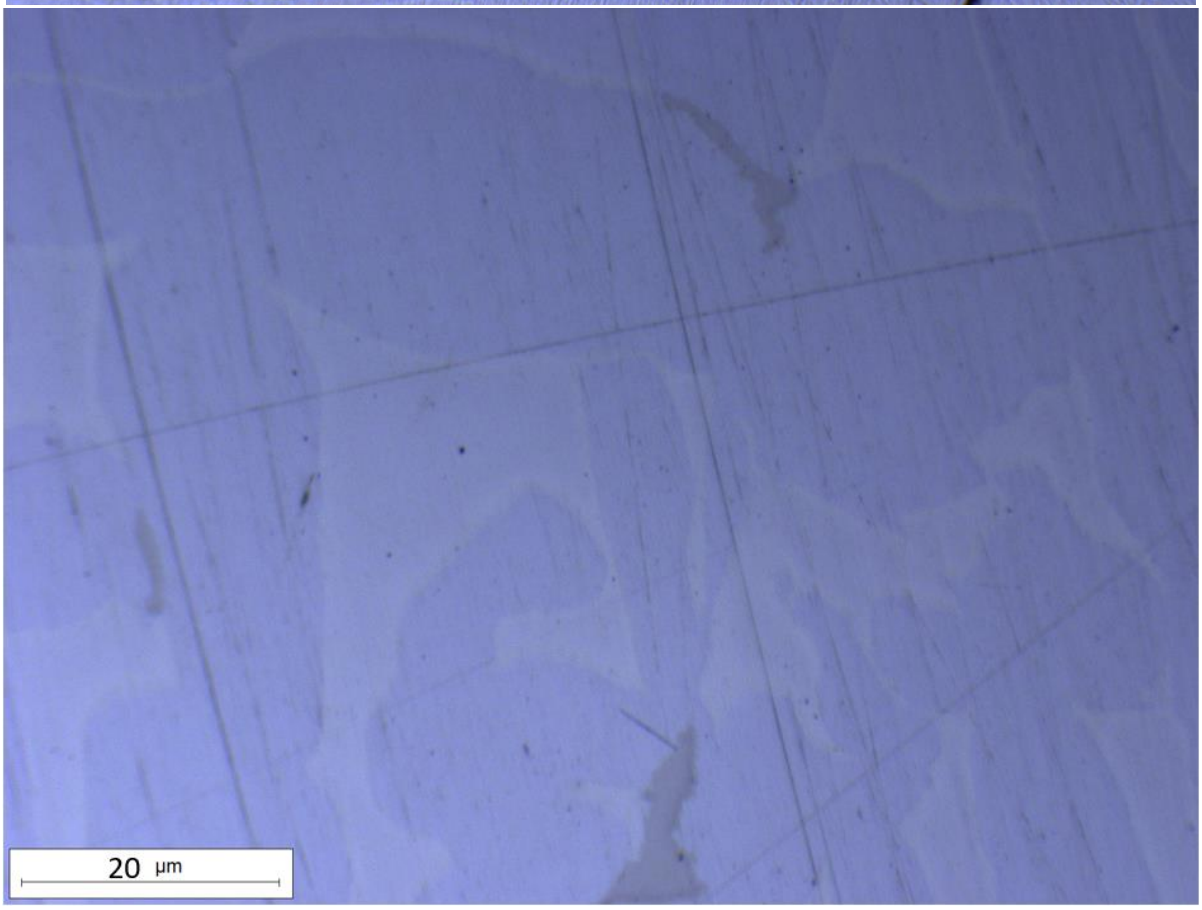

Post-M.A. observation

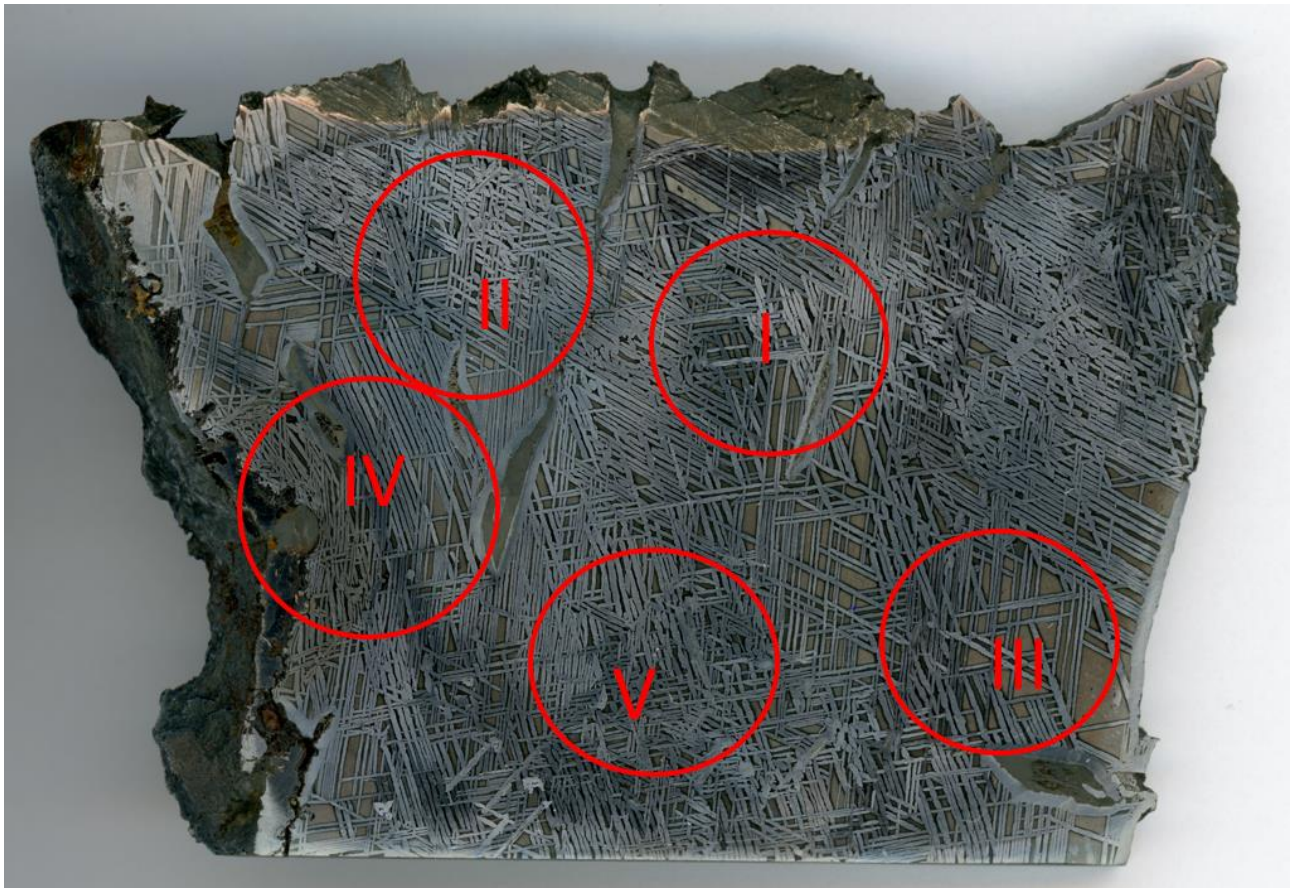

Zone I

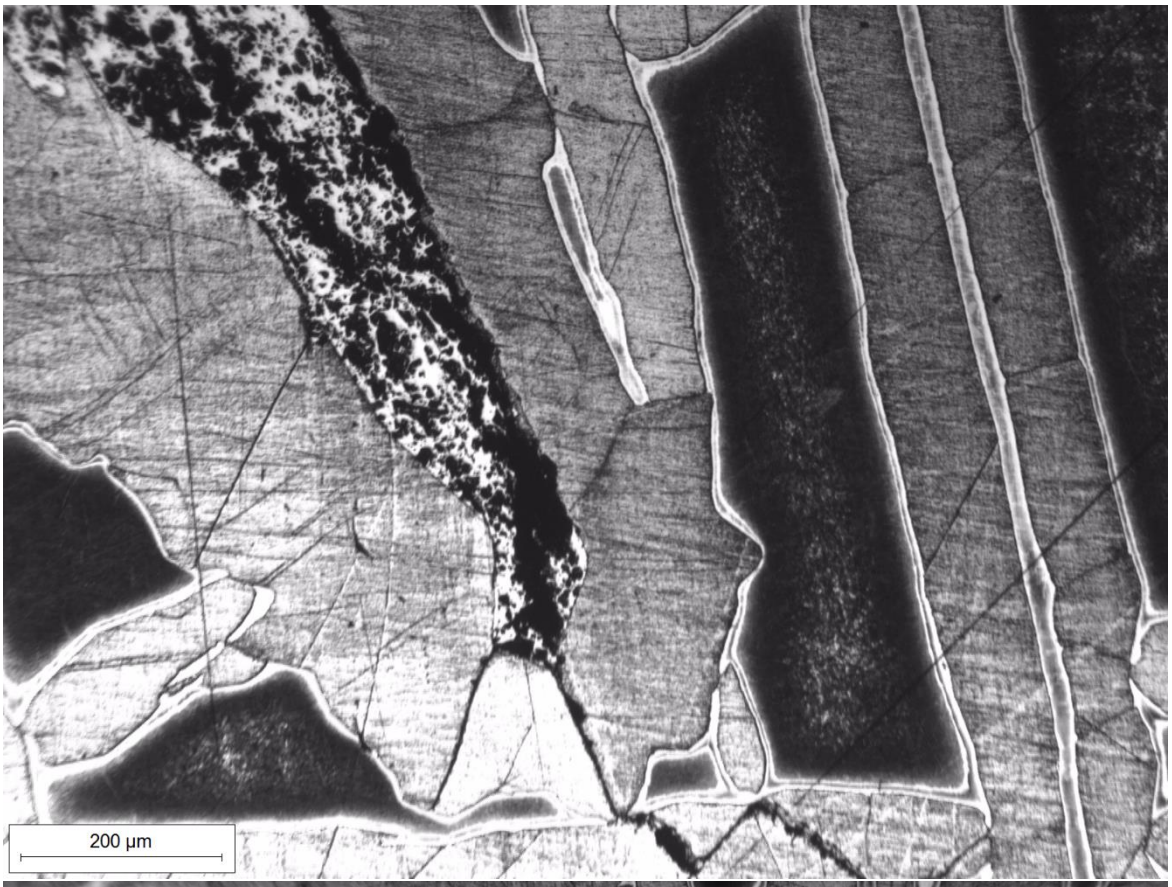
200 µm

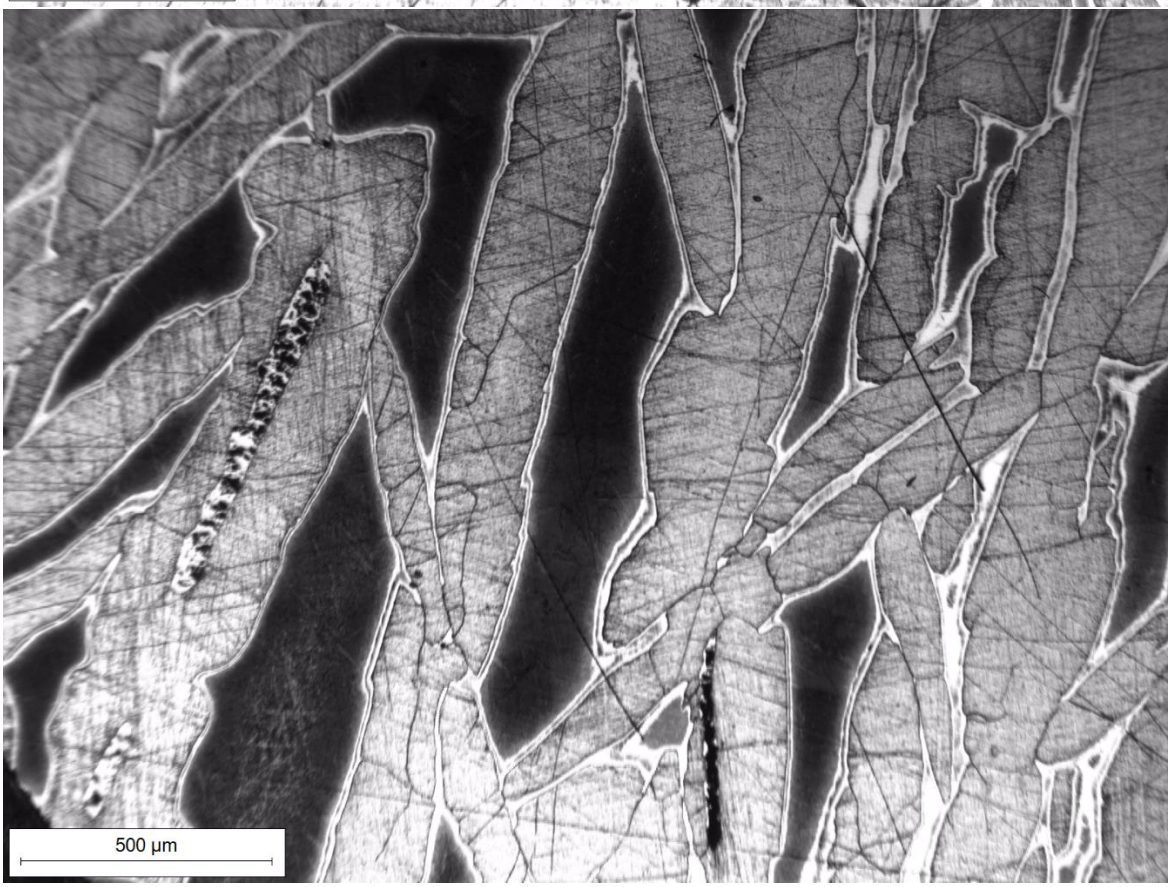
500 µm

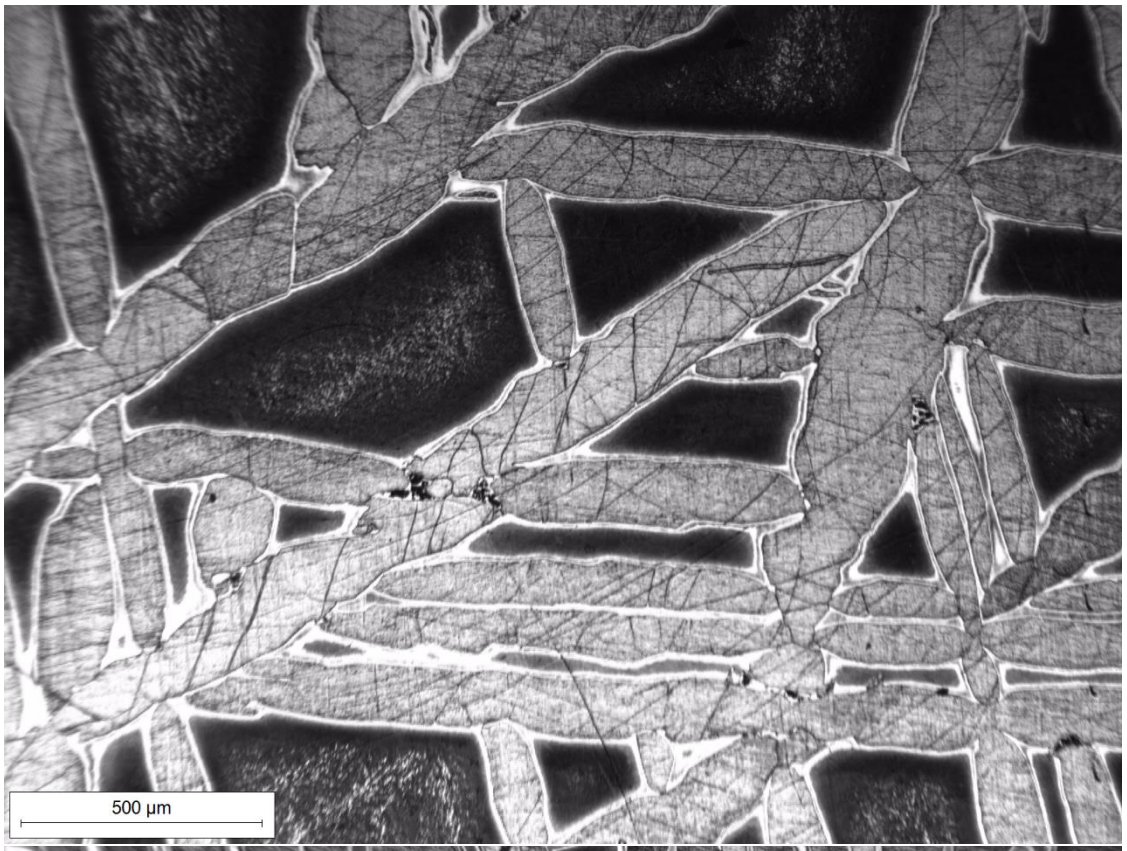
500 µm

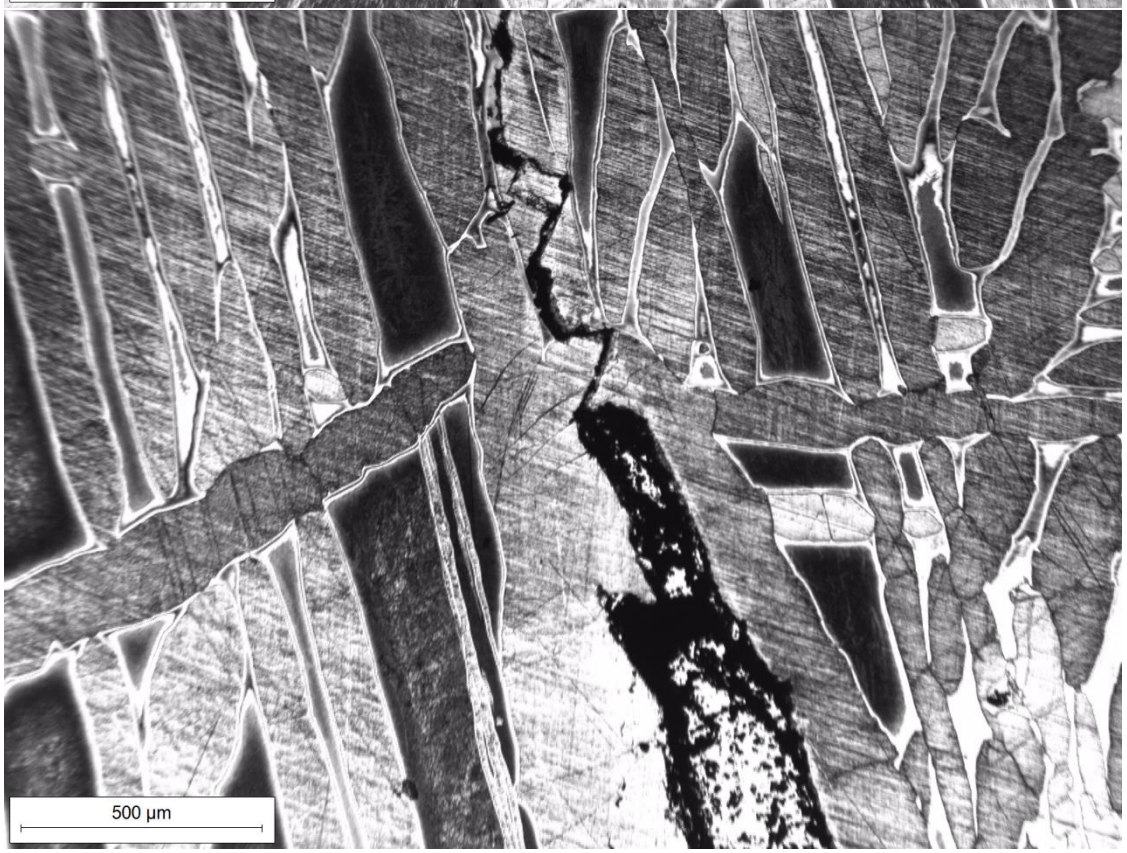
500 µm

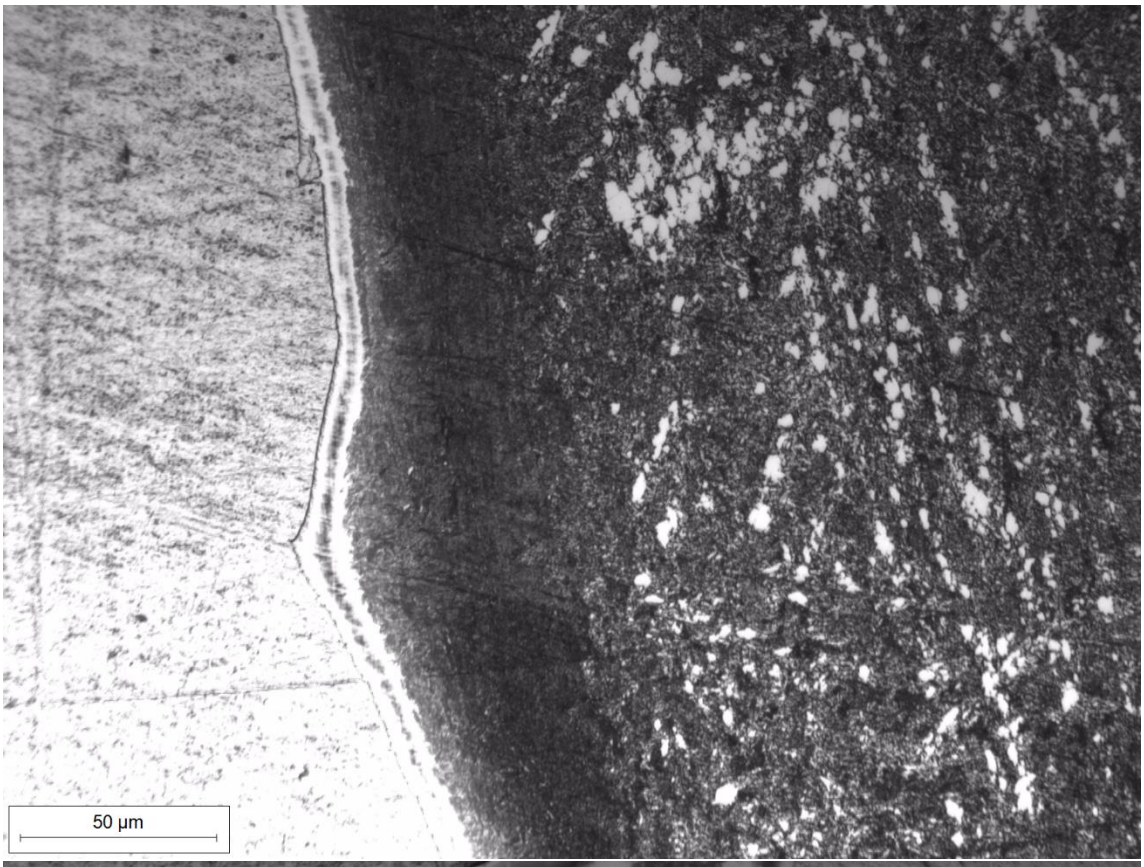
50 µm

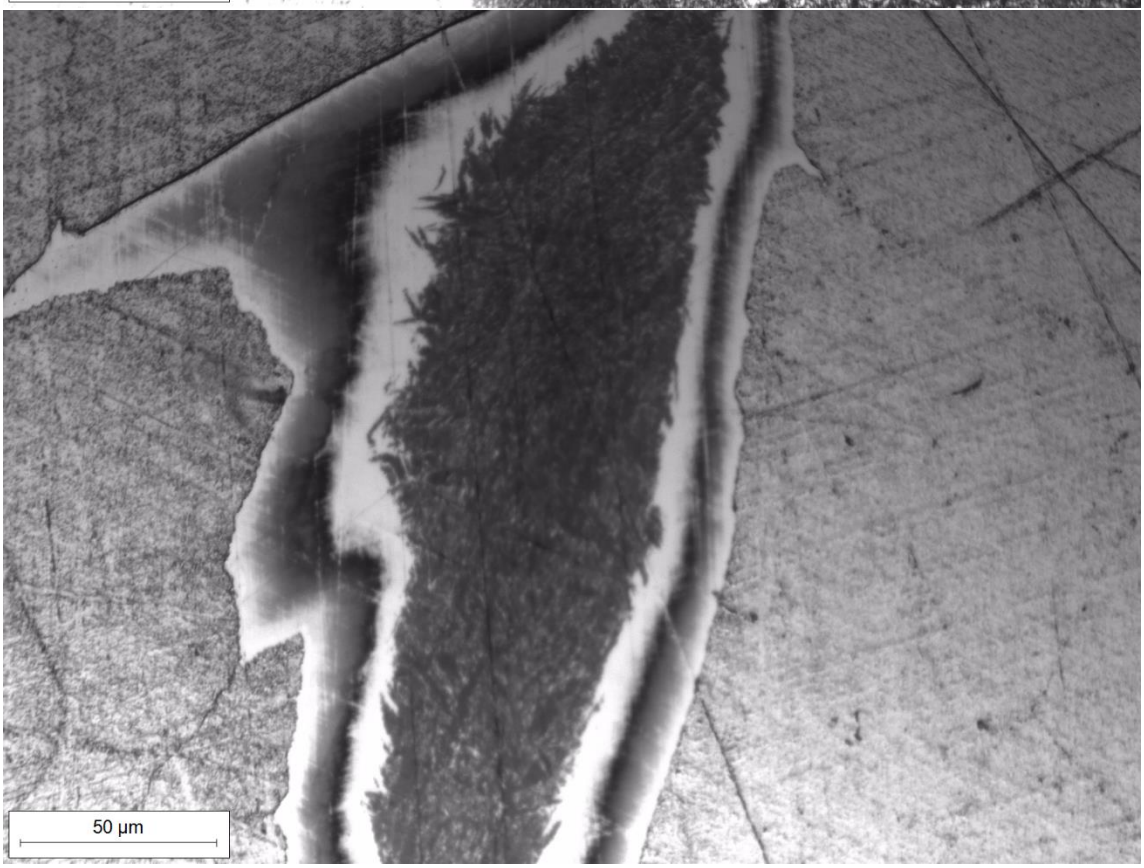
50 µm

Zone II

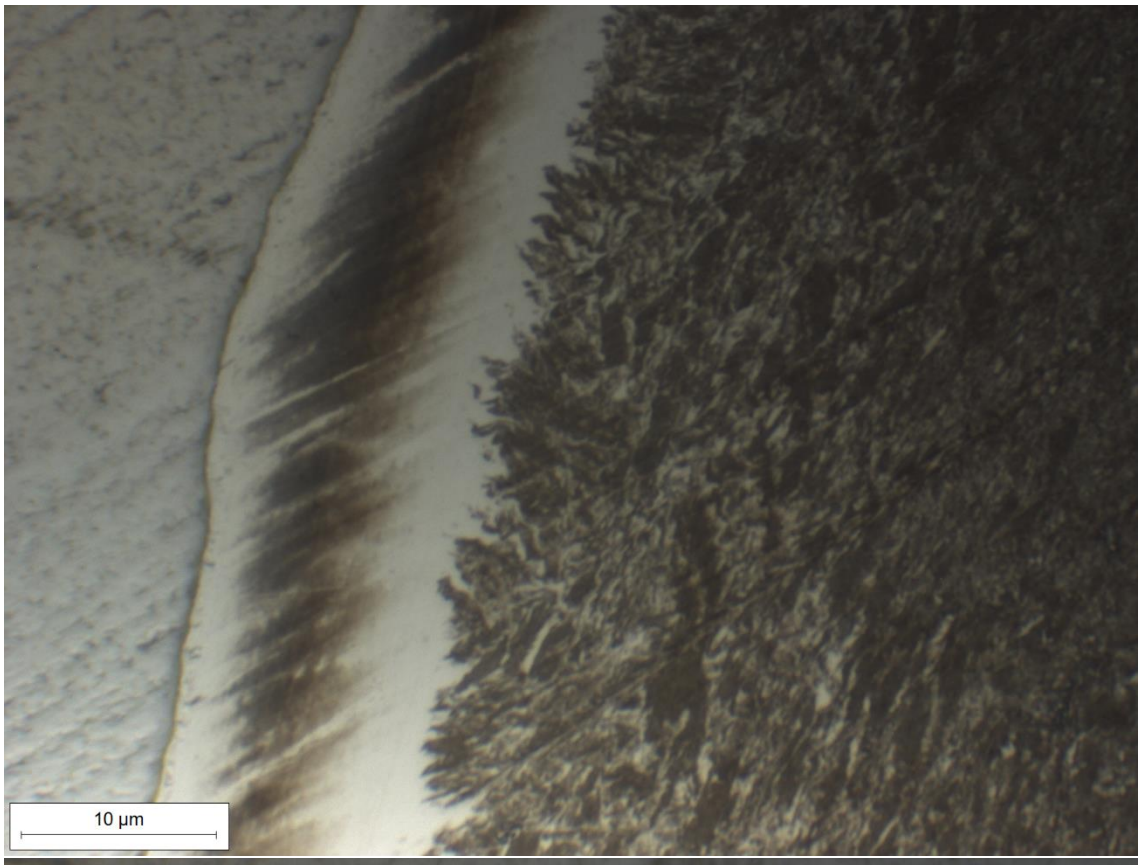

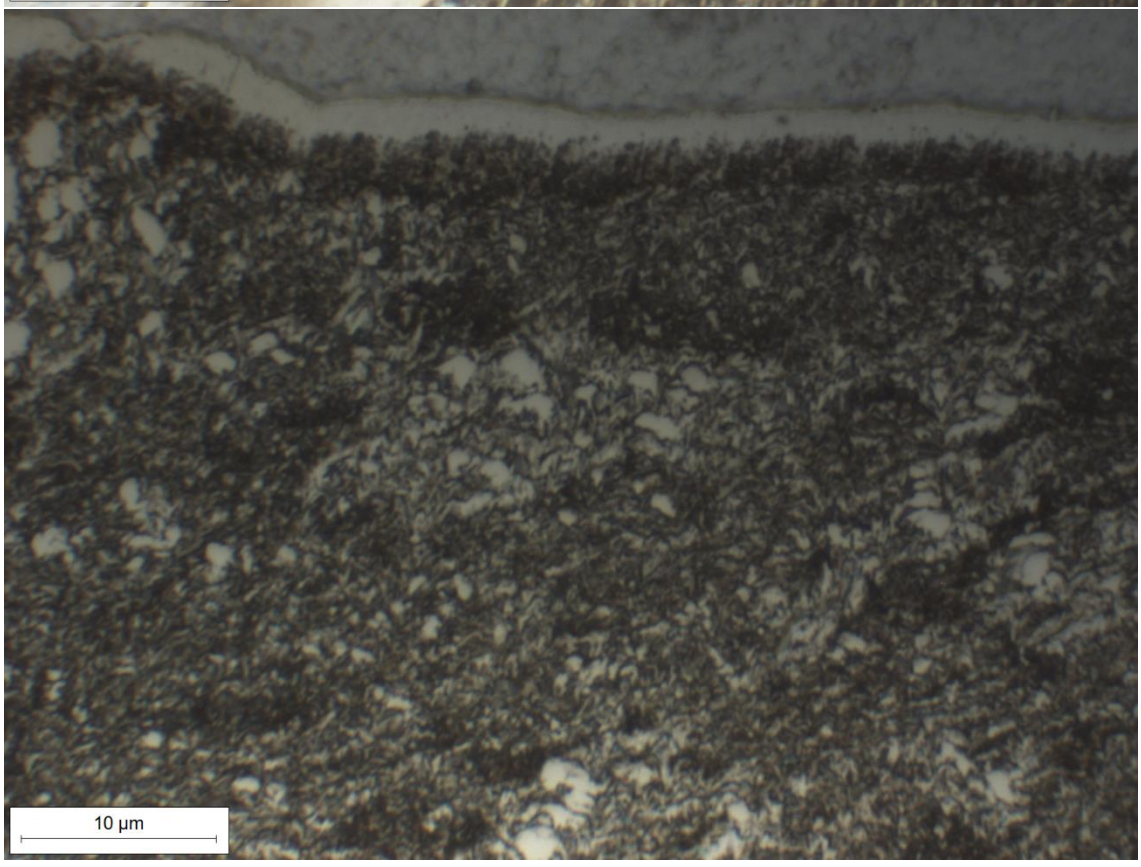

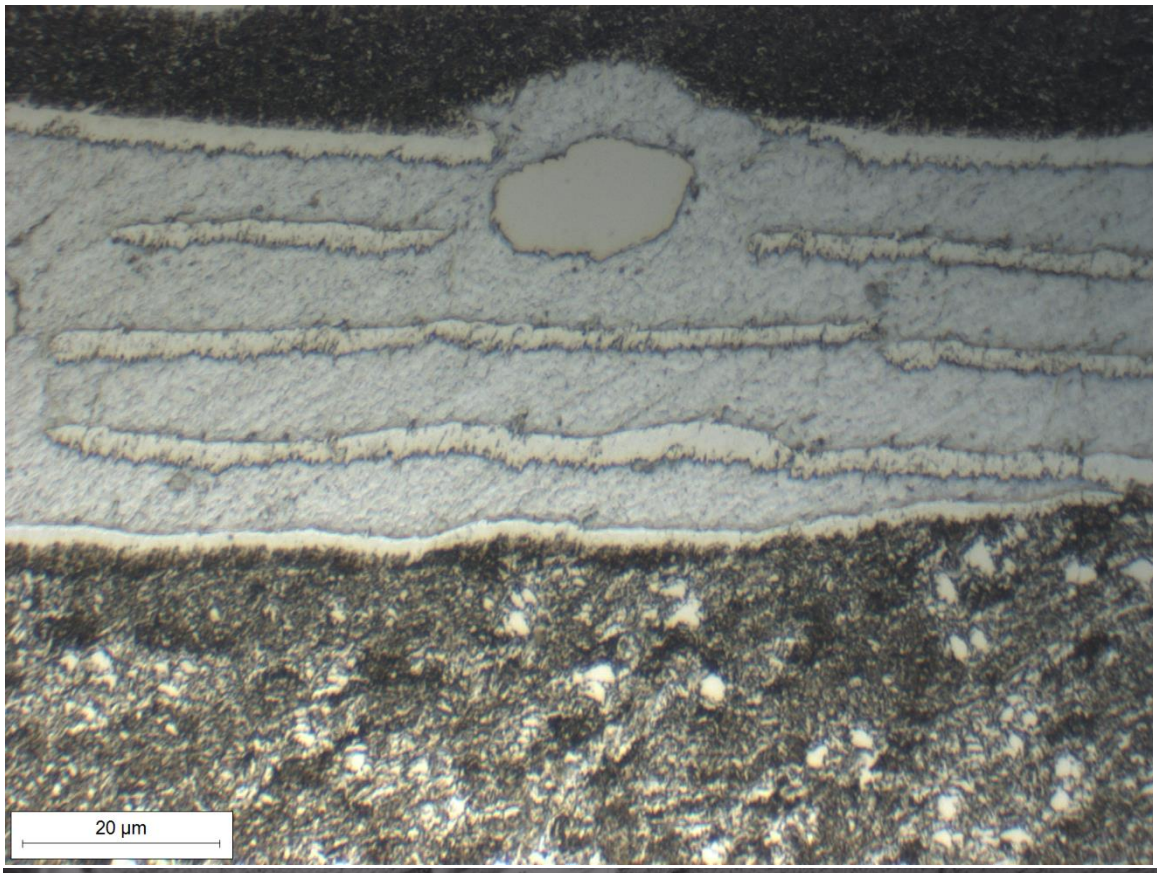
20 µm

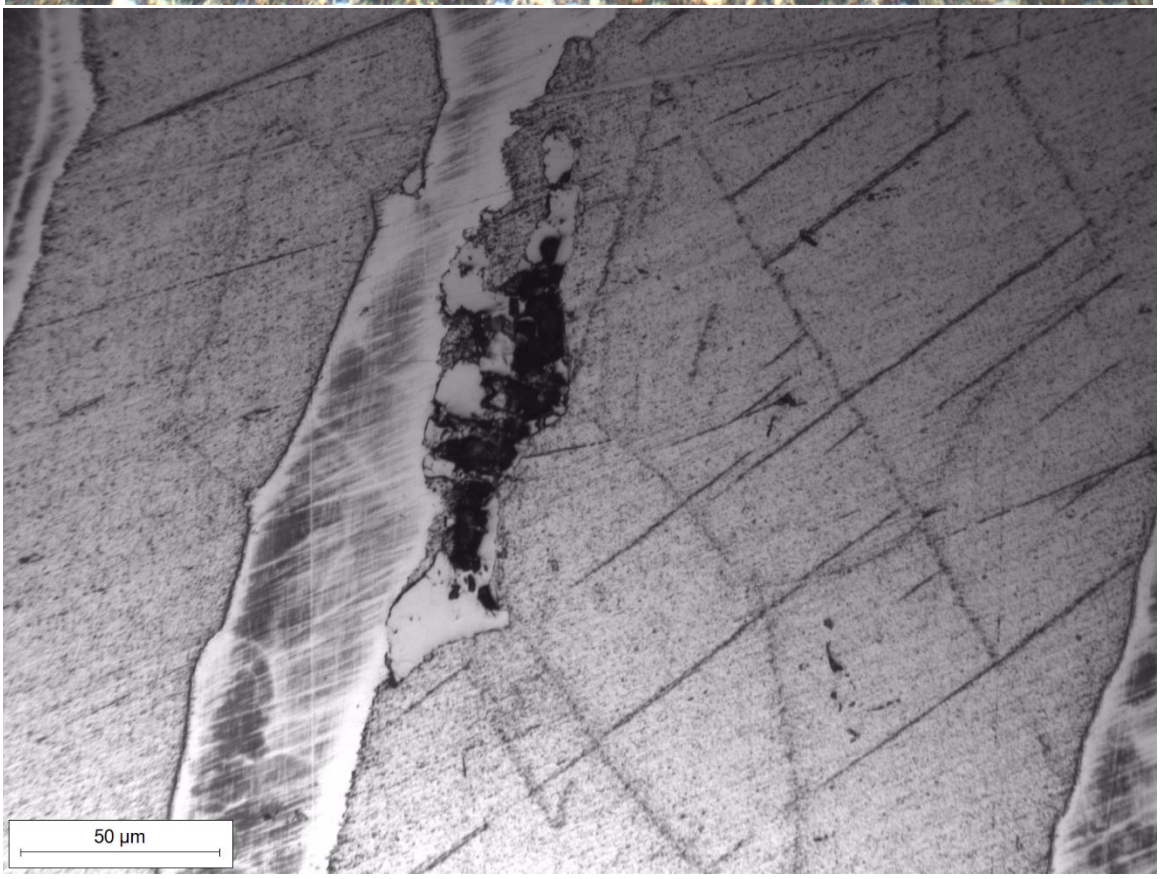
50 µm

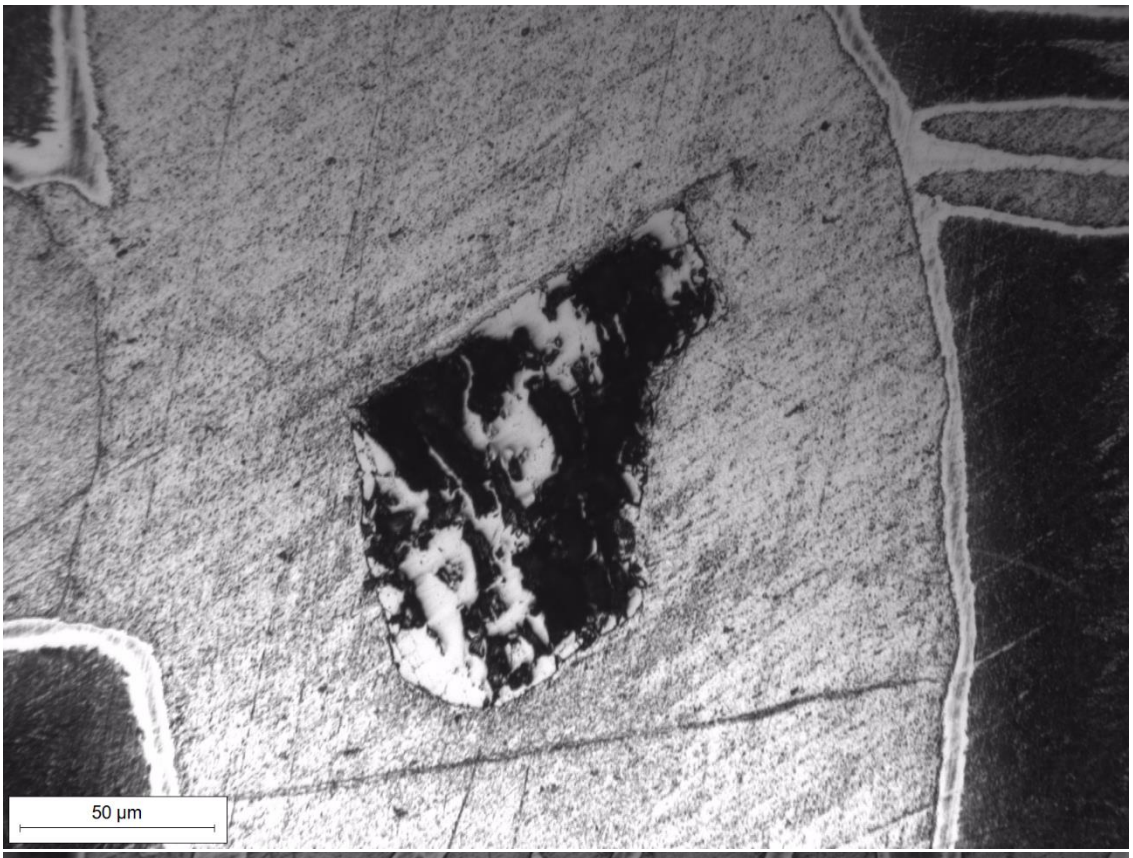
50 µm

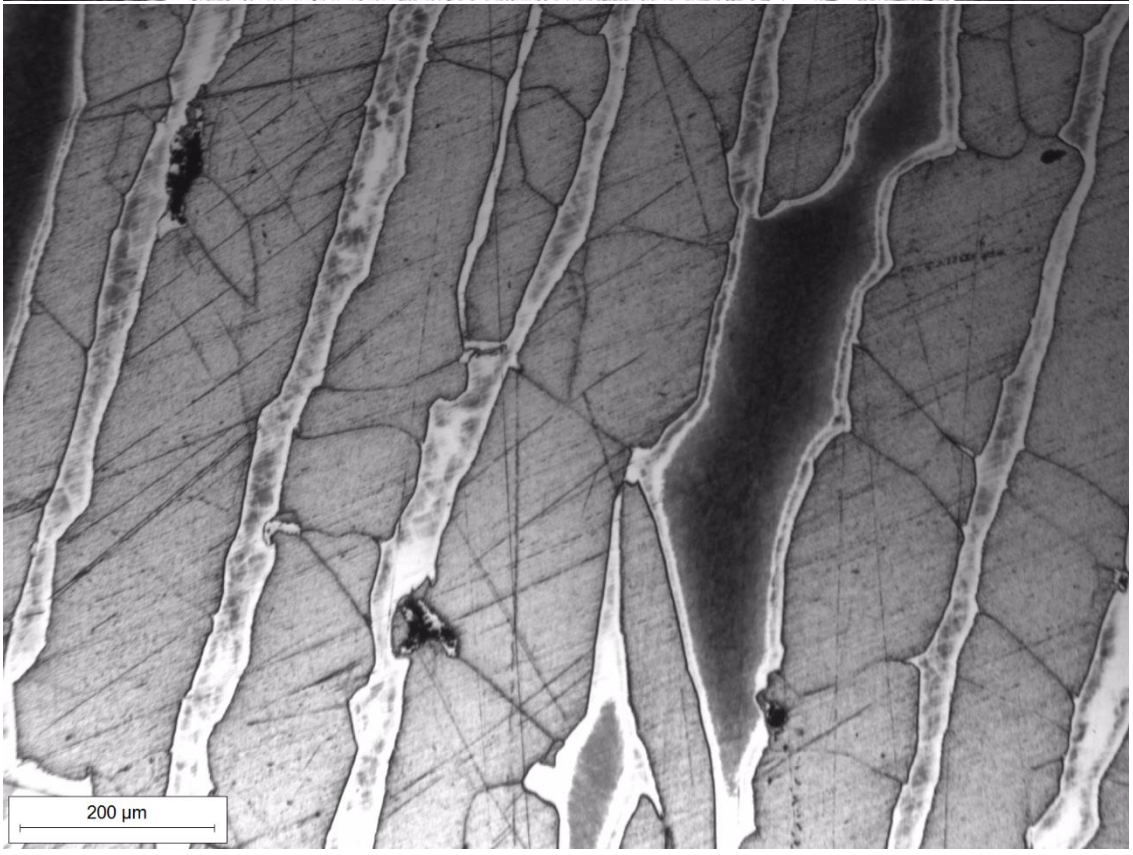
200 µm

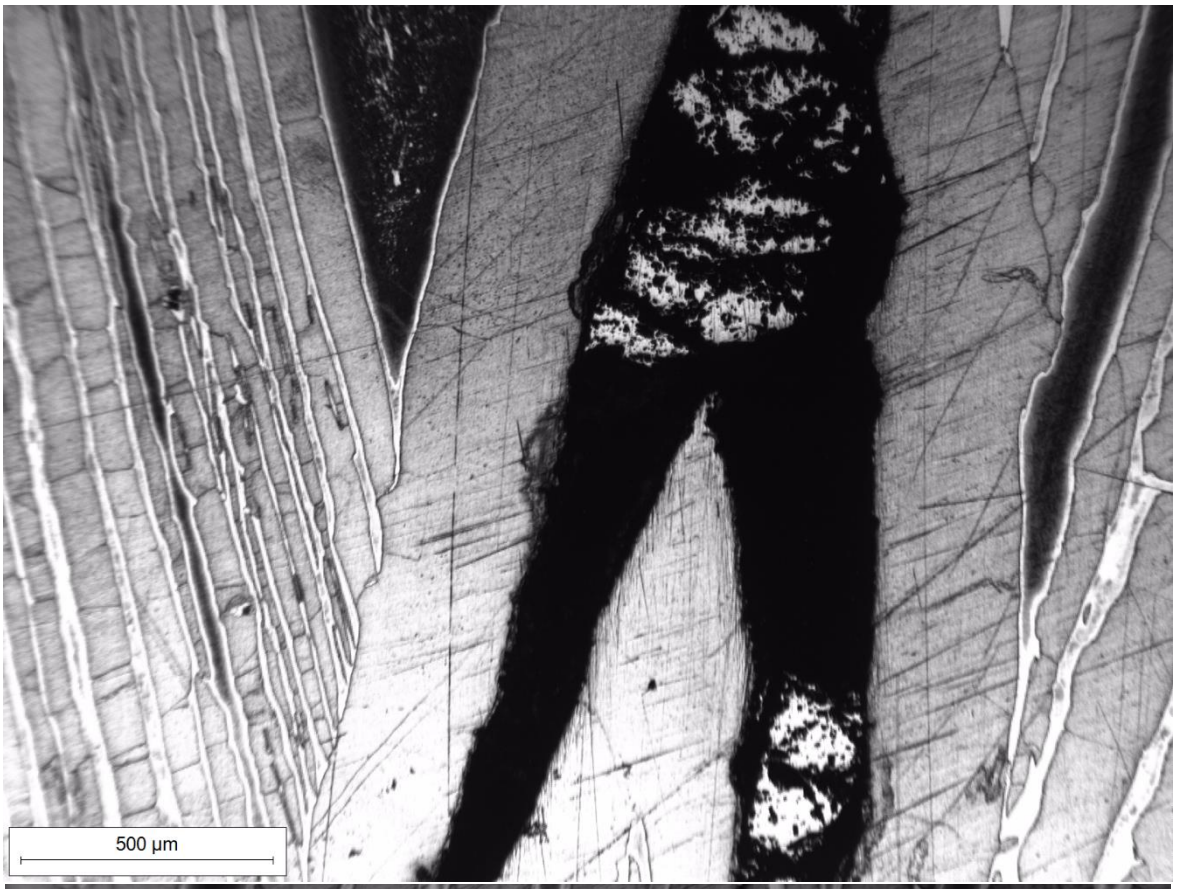
500 µm

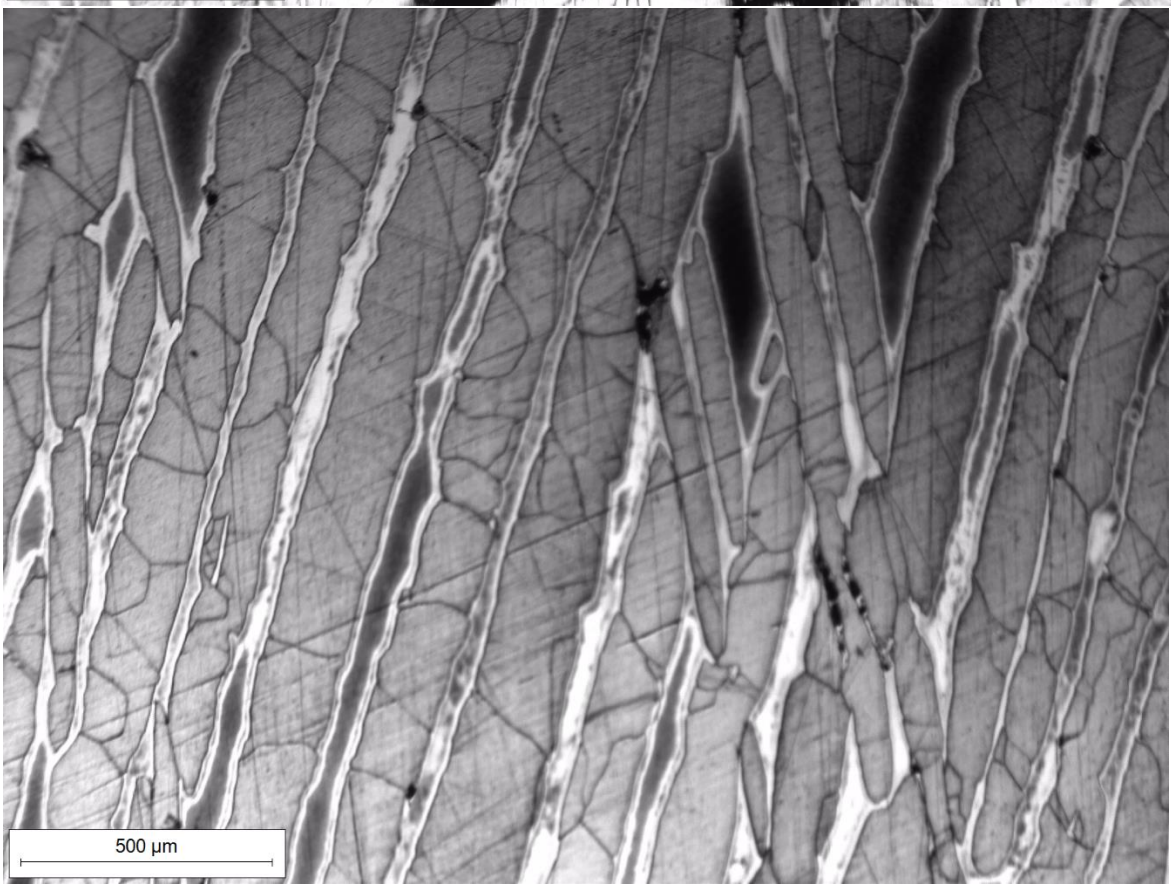
500 µm

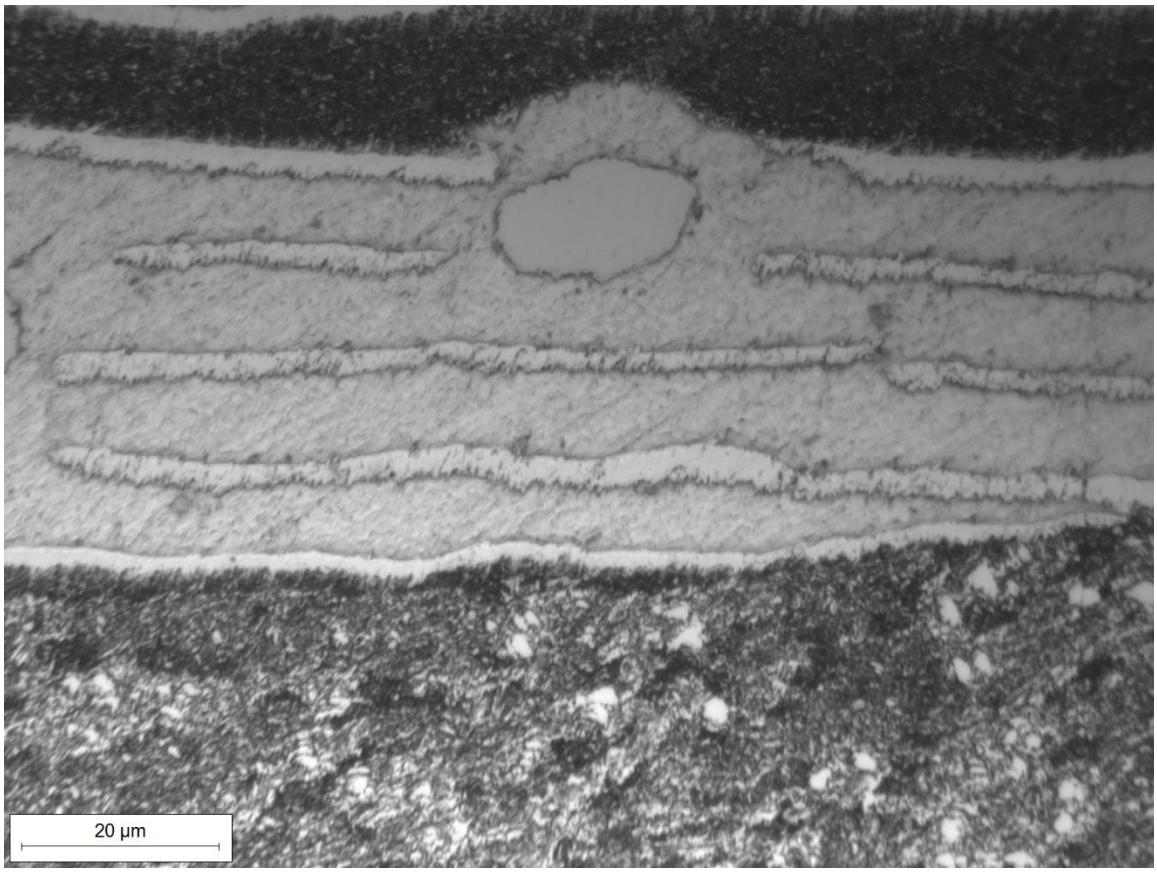
20 µm

Zone III

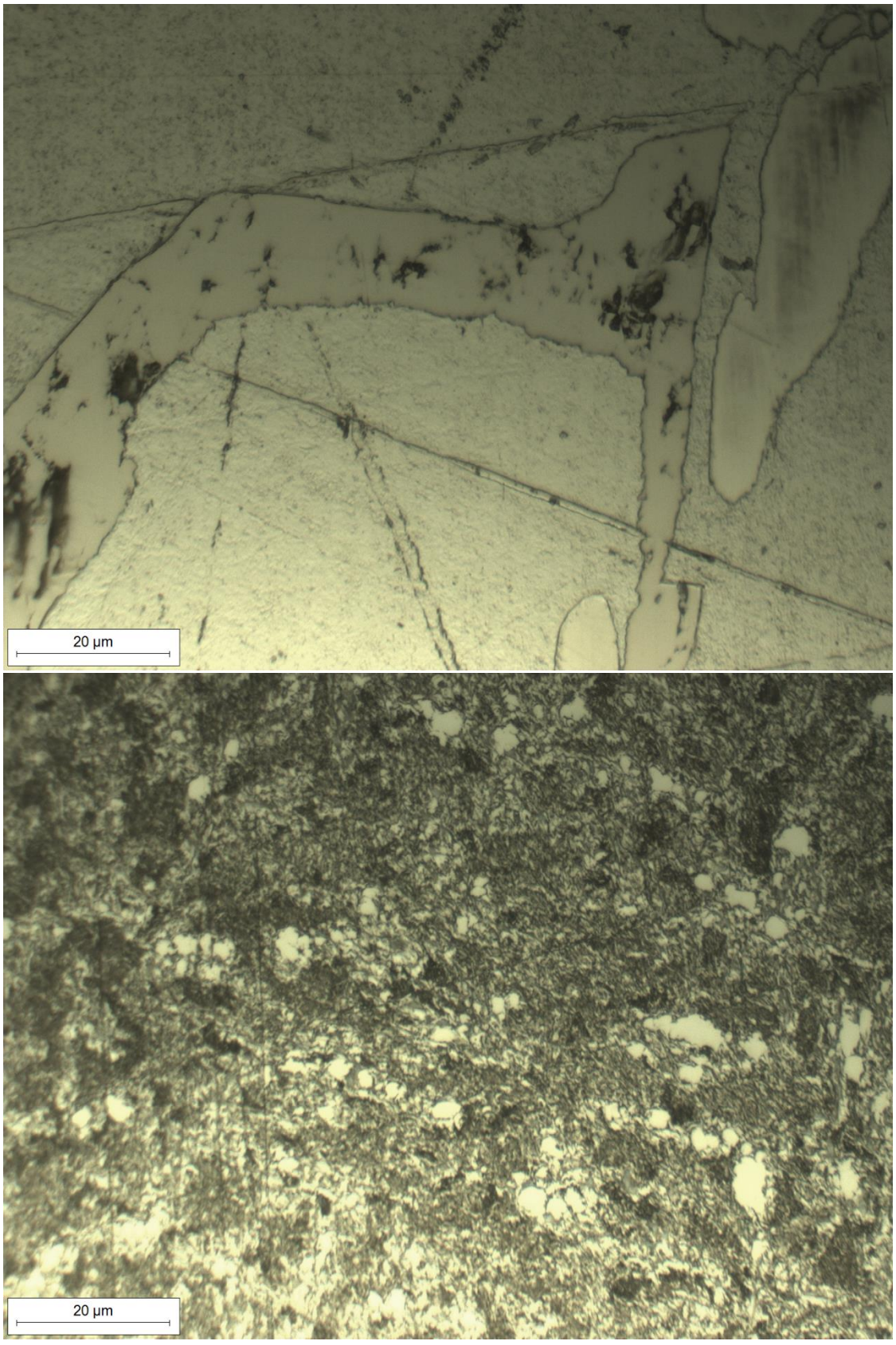

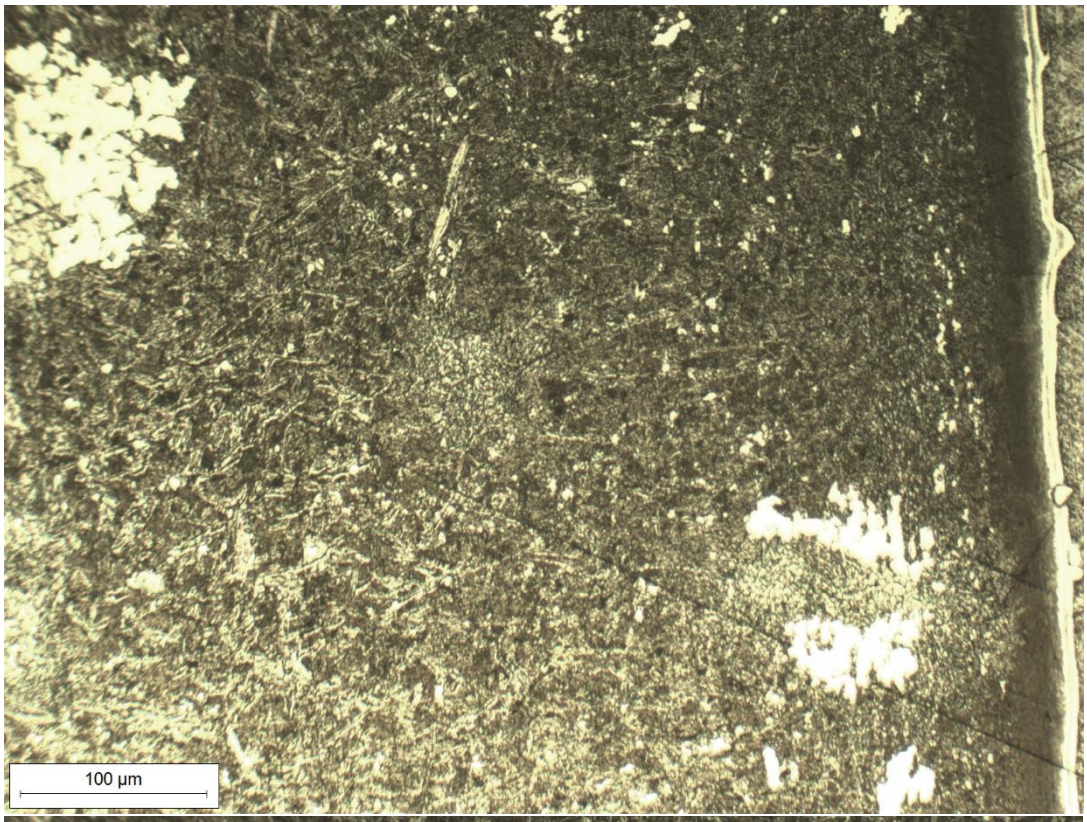
100 µm

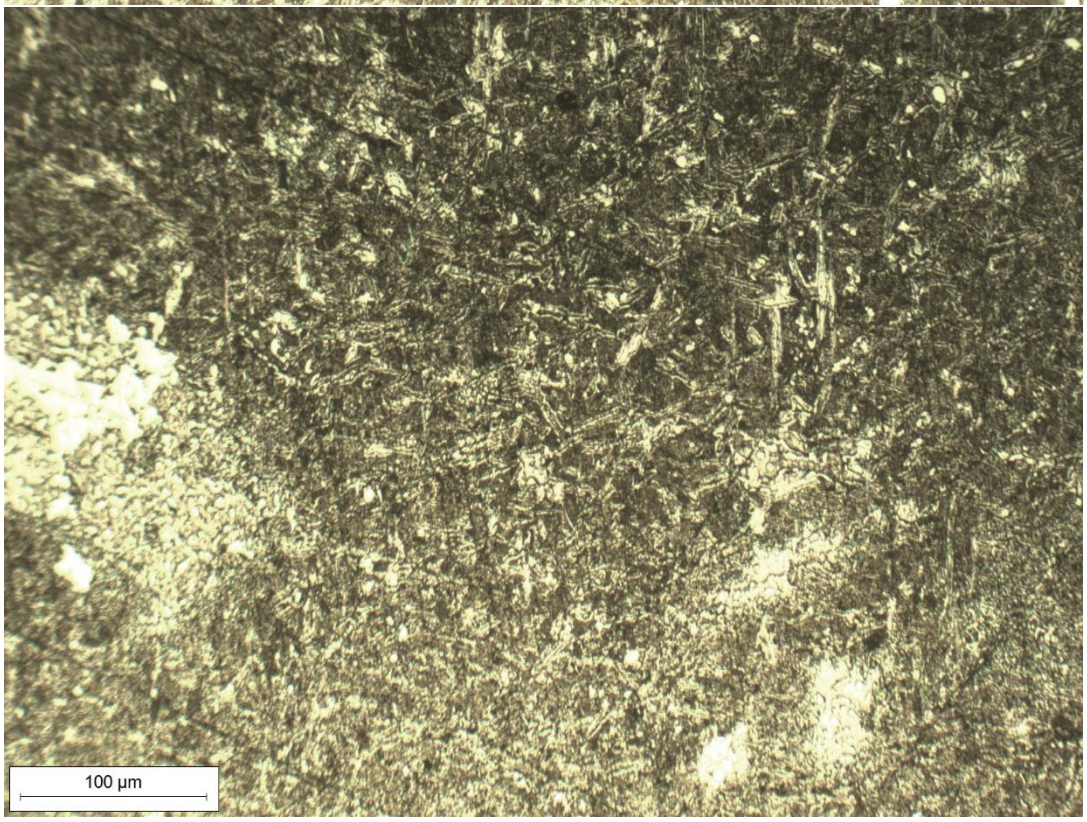
100 µm

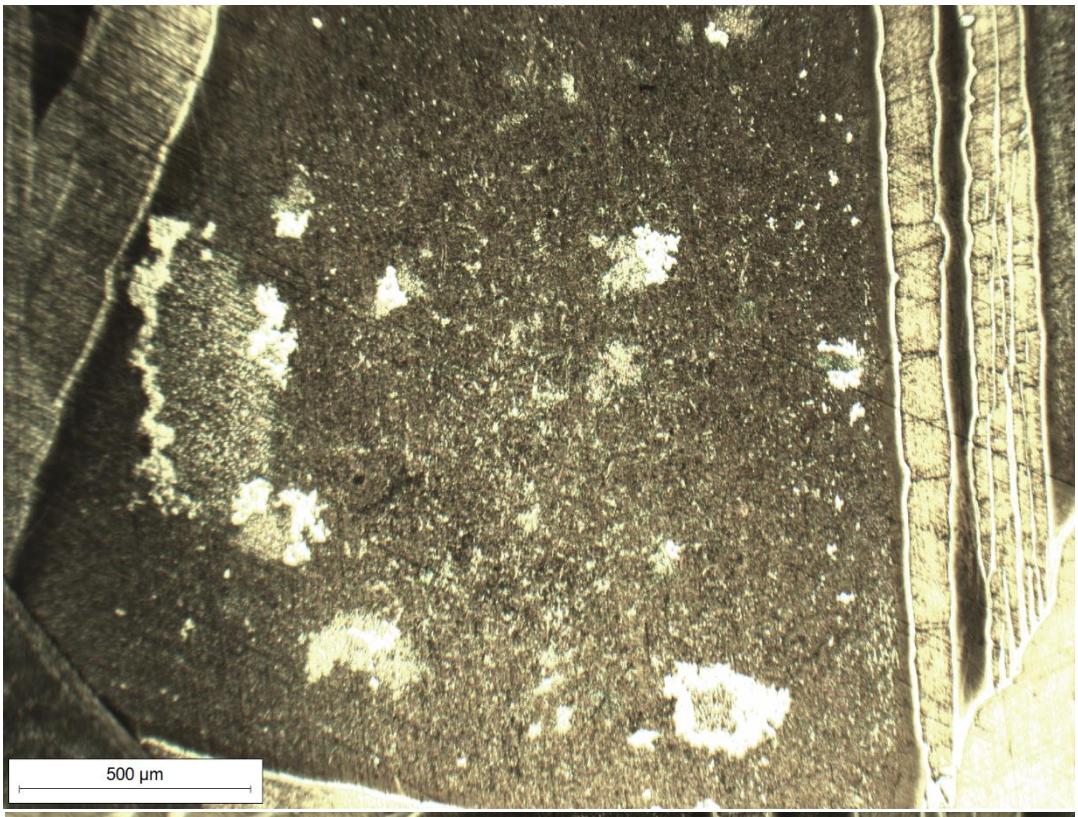
500 µm

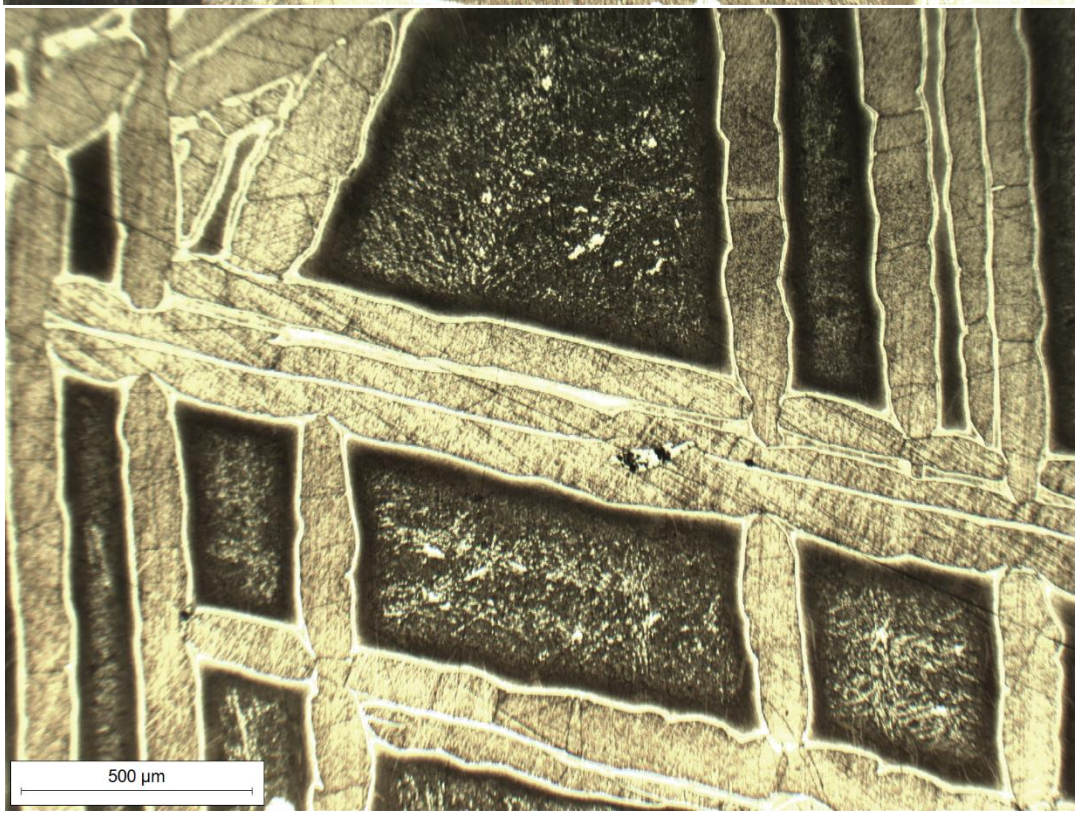
500 µm

Zone IV

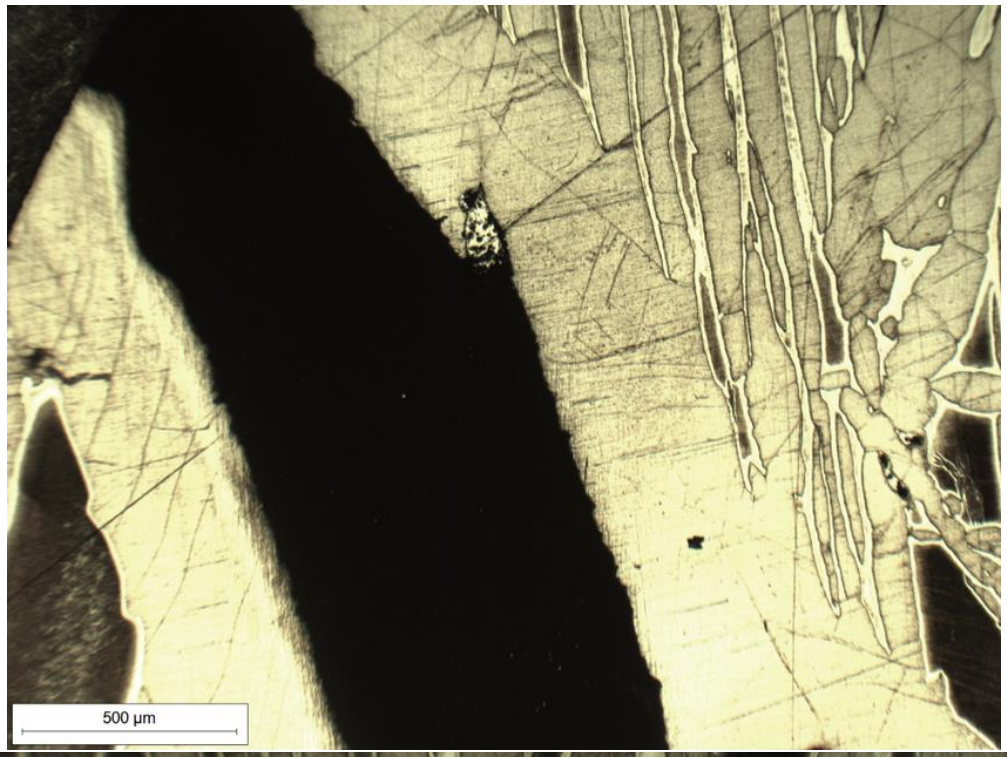

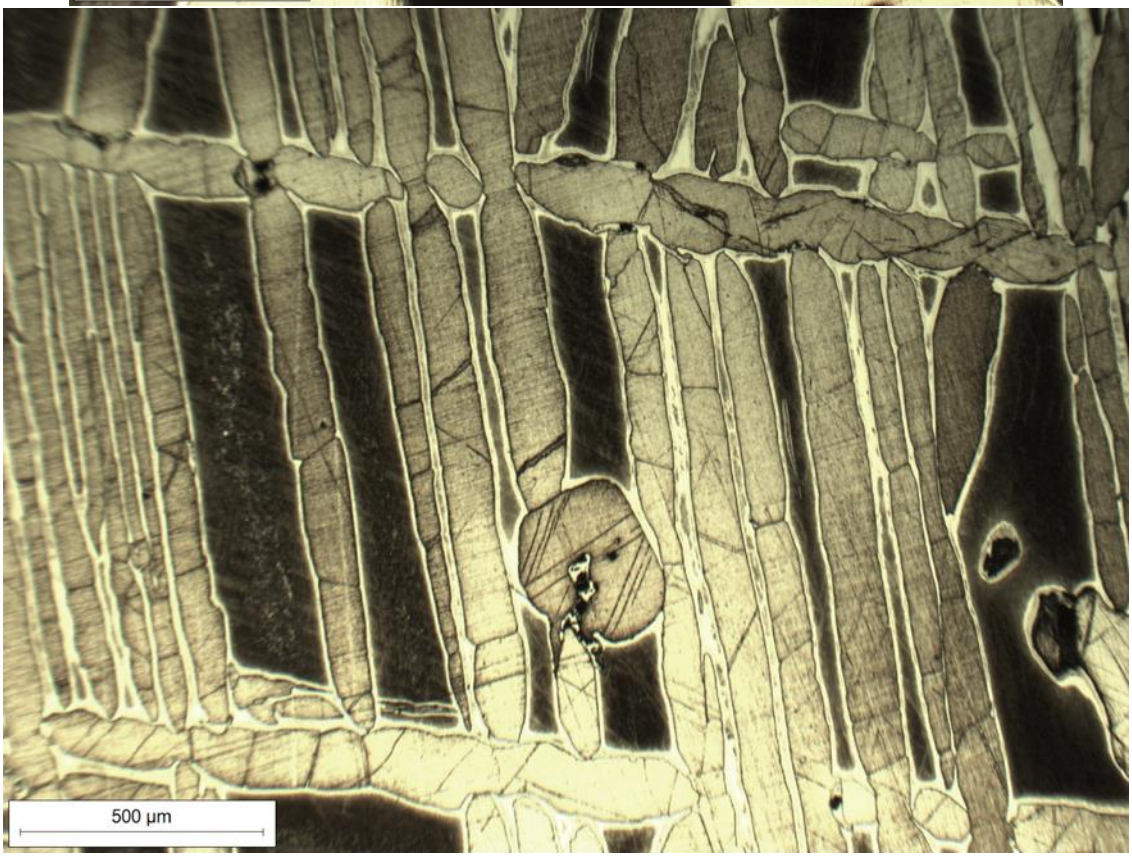

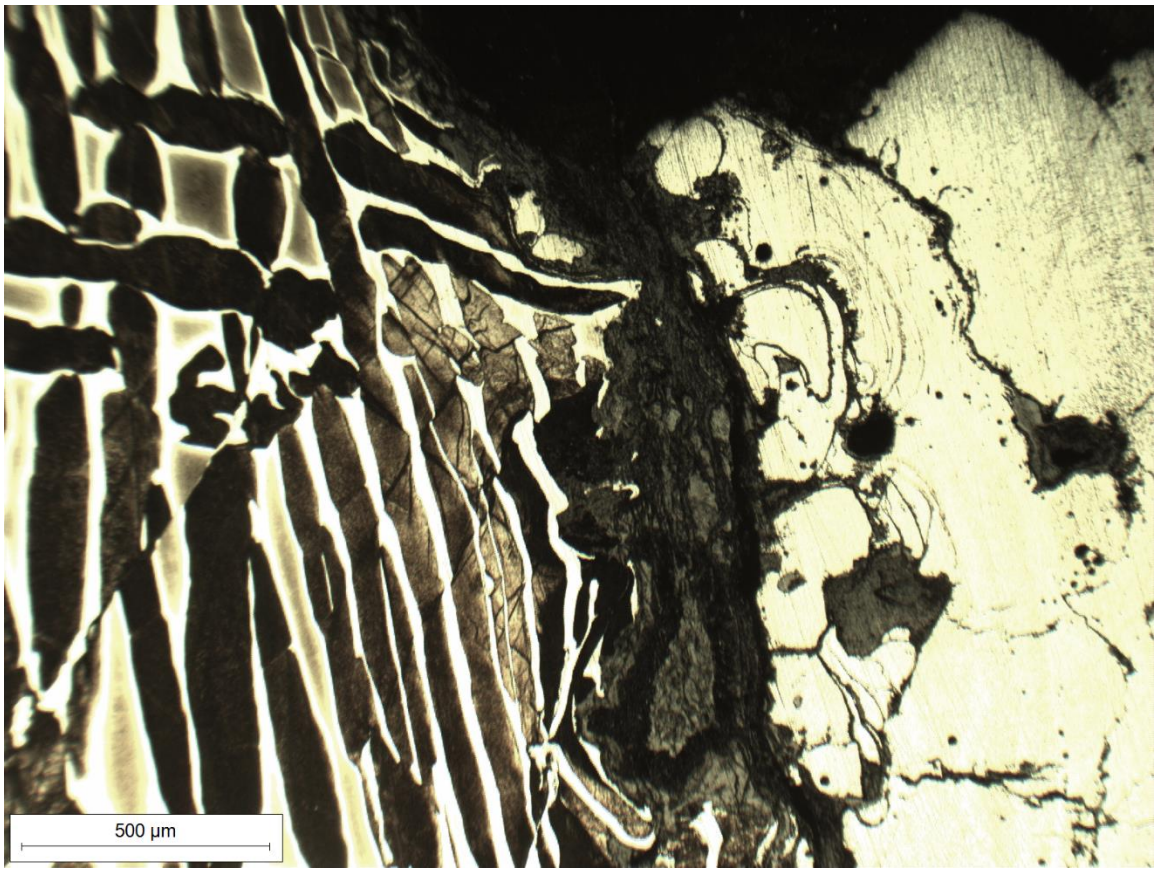
500 µm

Zone V

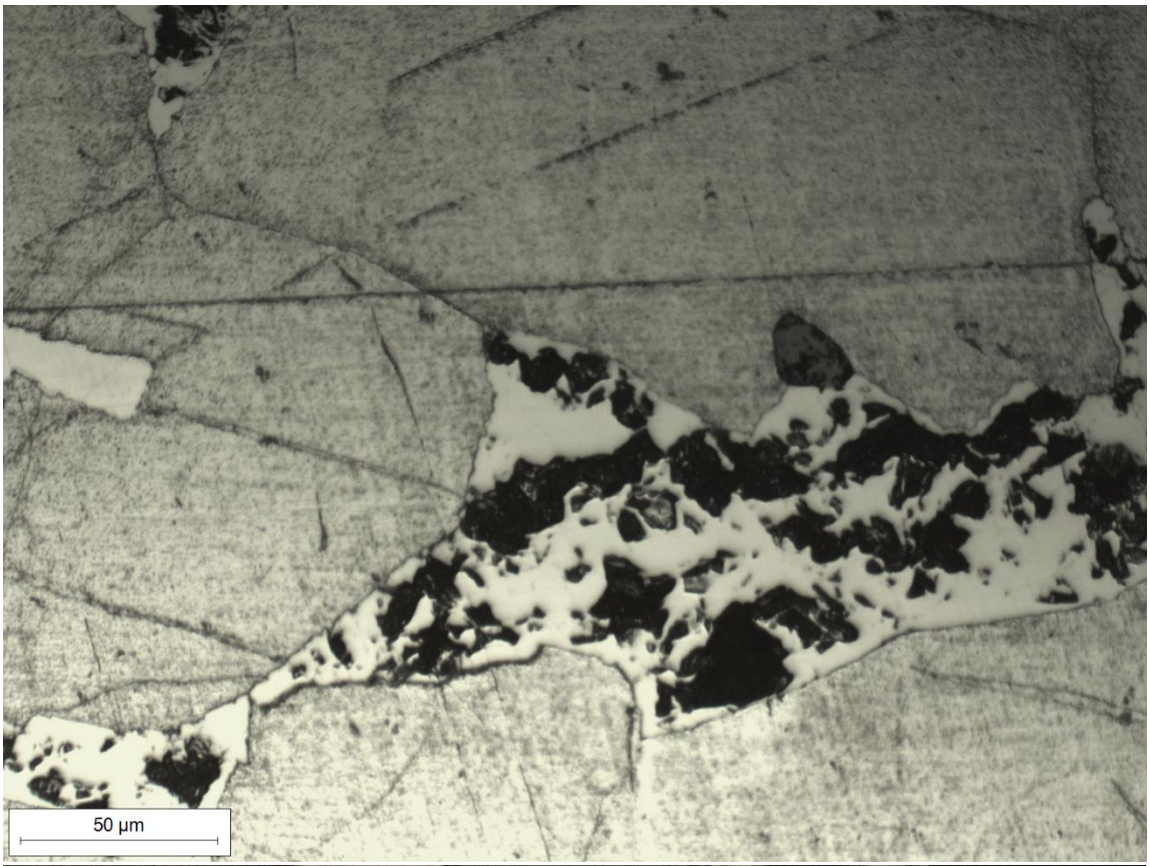

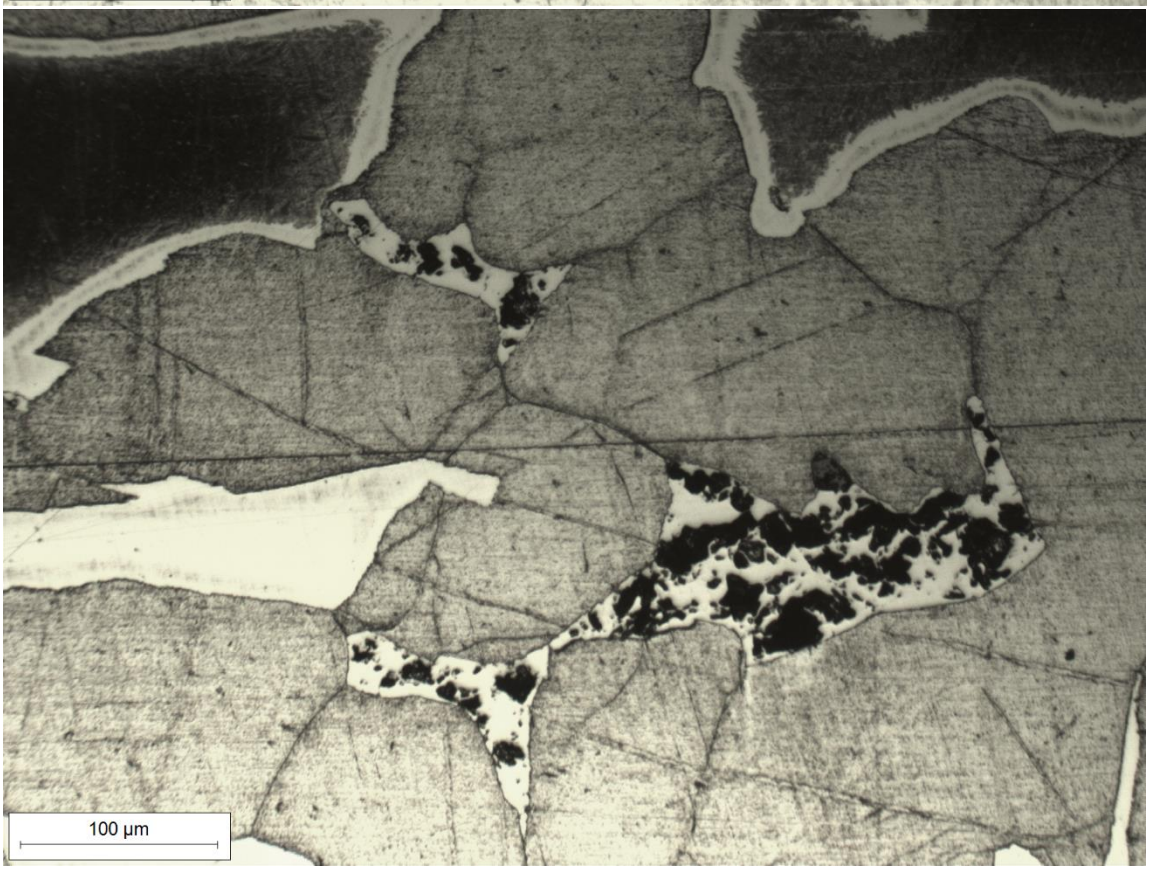


500 µm

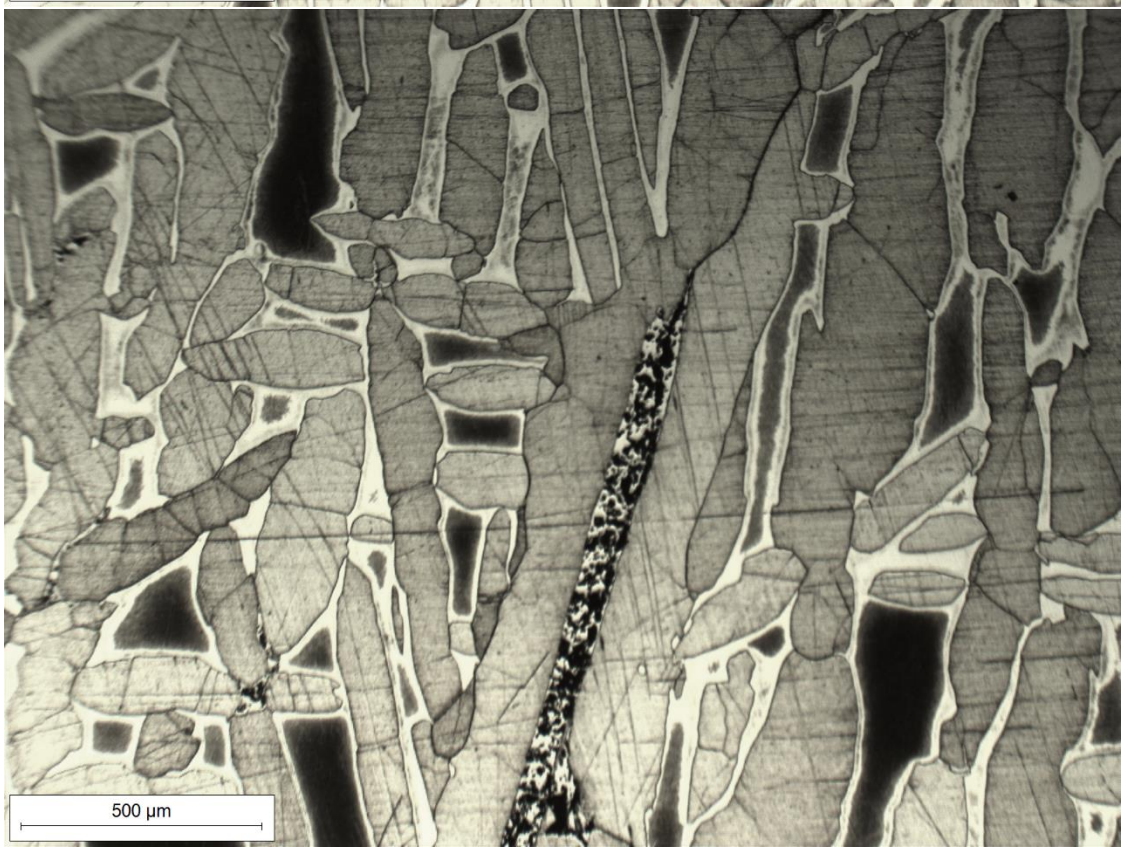
500 µm

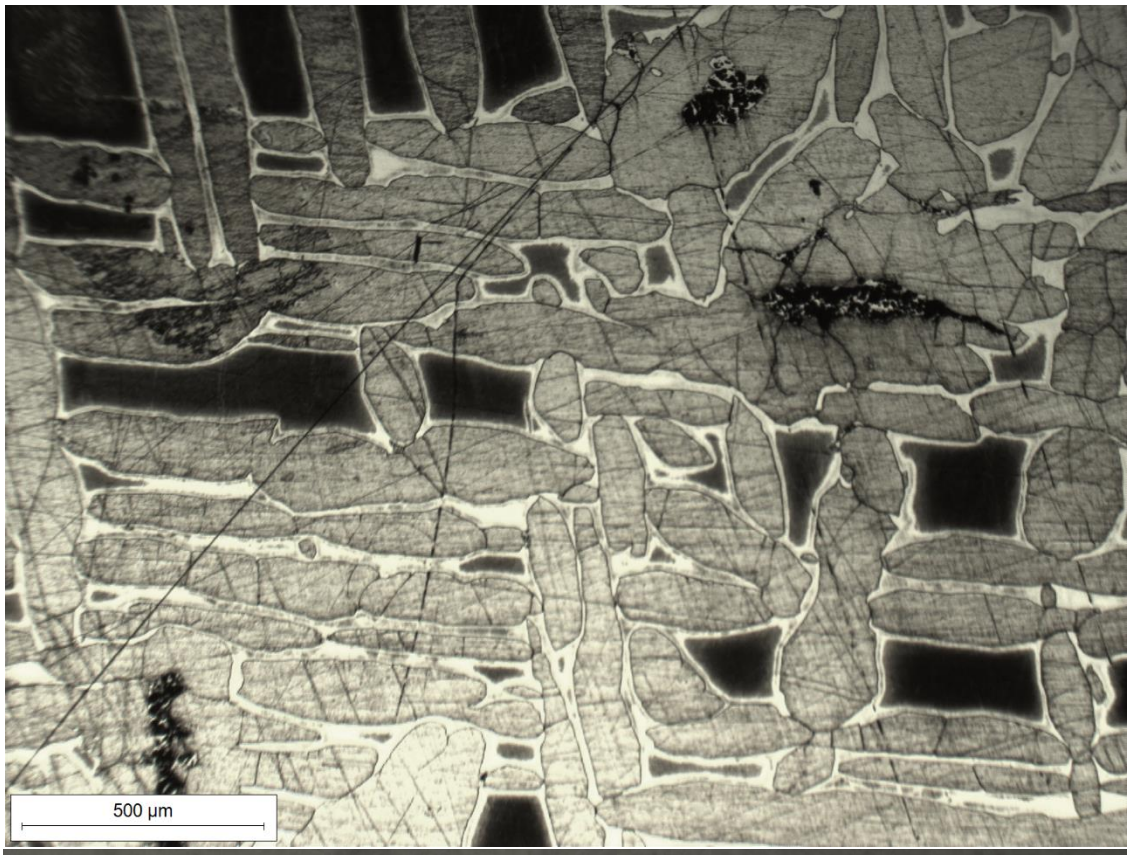
500 µm

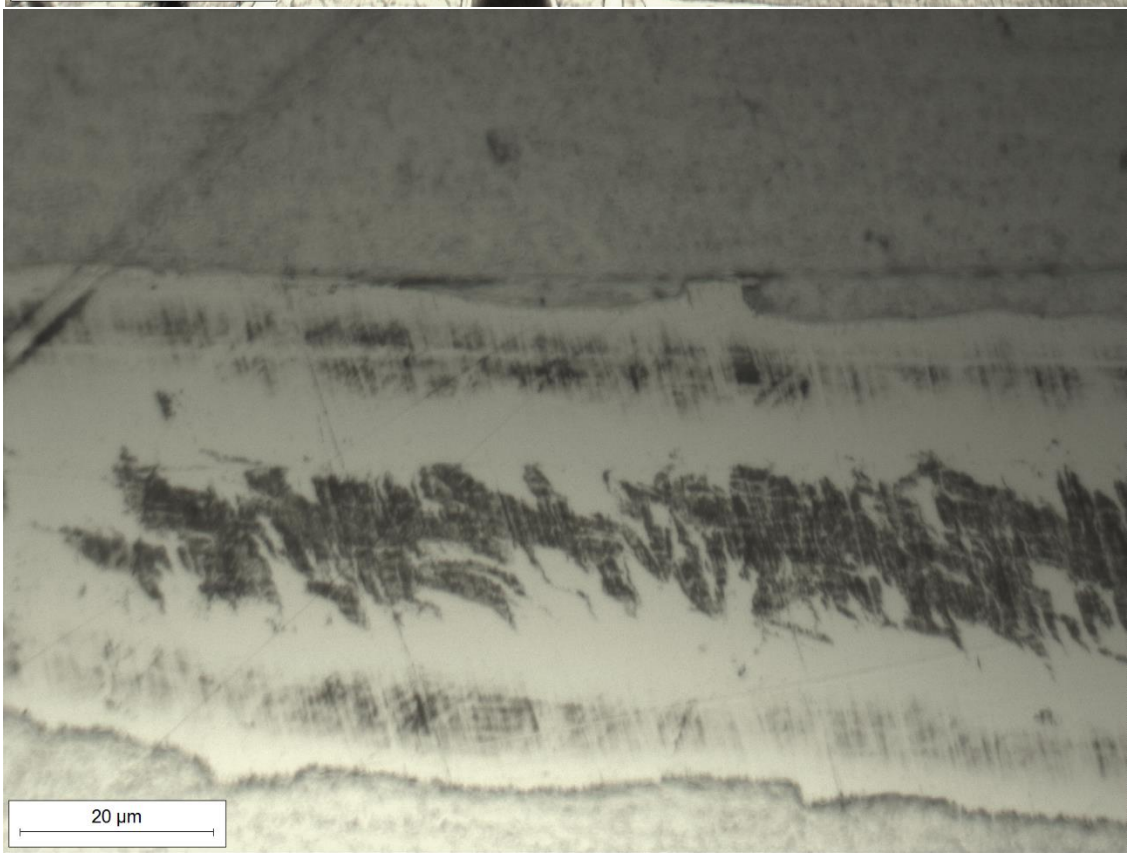
20 µm

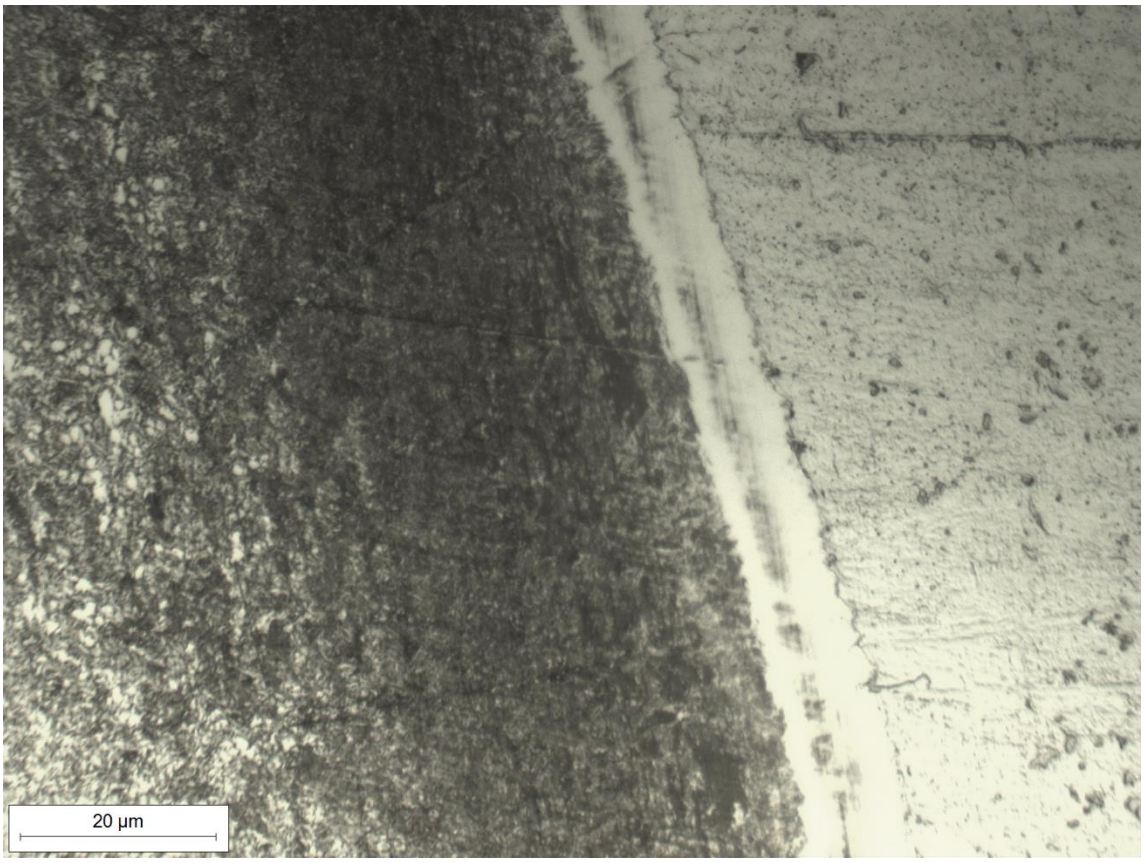
20 µm

HV tests

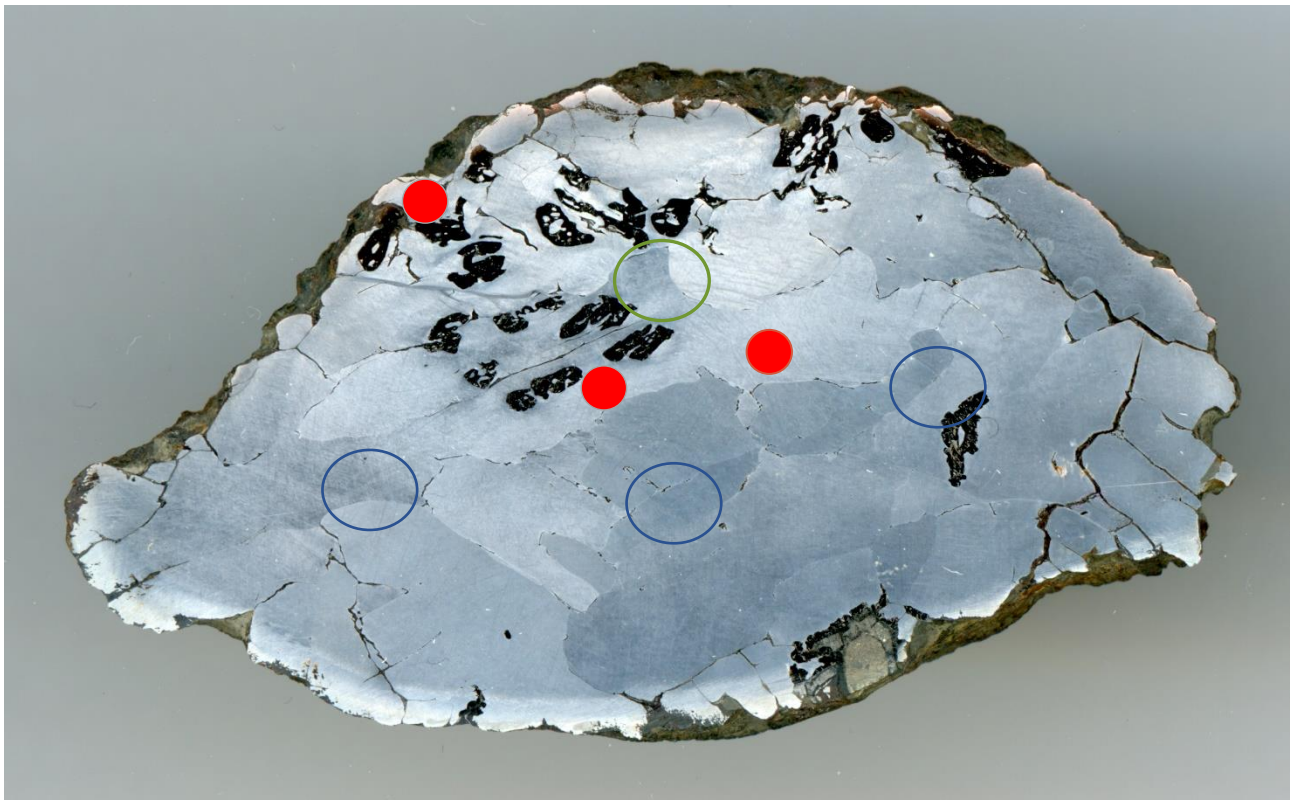

Figura 1 Red spots: tests on Taenite, from left to right 1st, 2nd, 3rd. Hollow blue circles: tests on ferrite.

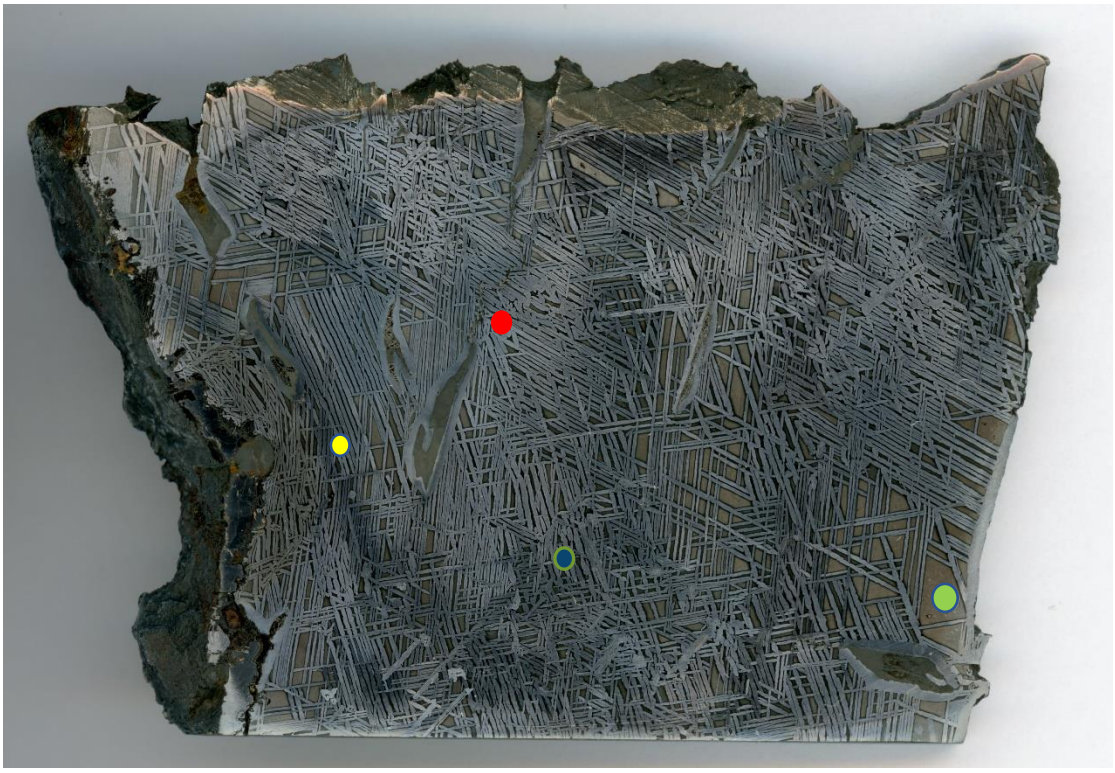

Figura 2 red spot: serie 1, blue spot: serie 2, yellow spot: serie 3, green spot: big taenite with inclusions